

Residential Microgrids for Disaster Recovery Operations

James W. Hurtt

Thesis submitted to the Faculty of the
Virginia Polytechnic Institute and State University
in partial fulfillment of the requirements for the degree of

Master of Science

in

Electrical Engineering

Lamine Mili, Chair

Jason Lai

C. Yaman Evrenosoglu

November 15, 2012

Falls Church, Virginia

Keywords: Microgrids, Distributed Generation, Modeling, Disaster Recovery

© Copyright 2012, James Hurtt

Abstract

The need for a continuous supply of electric power is vital to providing the basic services of modern life. The energy infrastructure that the vast majority of the world depends on, while very reliable, is also very vulnerable. This infrastructure is particularly vulnerable to disruptions caused by natural disasters. Interruptions of electric service can bring an end to virtually all the basic services that people are dependent on. Recent natural disasters have highlighted the vulnerabilities of large, economically developed, regions to disruptions to their supply of electricity. The widespread devastation from the 2011 Japanese Tsunami and Hurricane Irene in North America, have demonstrated both the vulnerability of the contemporary power grids to long term interruption of service and also the potential of microgrids to ride through these interruptions. Microgrids can be used before, during, and after a major natural disaster to supply electricity, after the main grid source has been interrupted. This thesis researches the potential of clean energy microgrids for disaster recovery. Also a model of a proposed residential microgrid for transient analysis is developed. As the world demands more energy at increasingly higher levels of reliability, the role of microgrids is expected to grow aggressively to meet these new requirements. This thesis will look at one potential application for a microgrid in a residential community for the purpose of operating in an independent island mode operation.

Acknowledgements

I would first like to thank my friends, family, and colleagues for giving support over the years to reach this level of academic achievement. In particular, my wife Anna, who has been an endless source of strength and encouragement. As well as my parents who have nurtured me from a young age to be hard working and be curious. My brother, for always being there and always knowing more about the world than I ever will. I am especially grateful for my colleagues at work who have given me the support I needed to work and achieve my academic goals simultaneously. A special thanks to the late Louis Larkin, for whom I worked with for many years. He taught me the value of engineering excellence.

My development as a researcher would not be possible without the support of my advisor, Dr. Lamine Mili. His guidance and patience with me as my thesis slipped further behind schedule is much appreciated. I am also very grateful for my committee members Dr. Lai and Dr. Evrenosoglu for agreeing to sit on my committee and giving me very constructive feedback. Finally, I would like to acknowledge my good friend, Ibrahima Diagne. Ibrahima has been an invaluable friend and colleague over the past several years. He has helped me out on numerous occasions. I would not be where I am today without his support. Thank you.

This thesis is dedicated to my son Daniel.

Contents

1	Research Introduction	1
1.1	Microgrid Definition	2
1.2	Research Motivation	3
1.3	Microgrid Concept and Scope of Study	4
1.4	Contributions	6
1.5	Thesis Overview	6
2	Literature Review	8
2.1	Microgrid History	9
2.2	Microgrids in Contemporary Application	11
2.2.1	Microgrids for Disaster Recovery	11
2.3	Clean Energy and Fuel Independent Microgrids	12
2.4	Trends in Microgrid Research and Development	13
3	Hurricane Occurrence and Impact	14
3.1	Brief Overview of Atlantic Hurricanes	14
3.2	Hurricane Impact to Electricity Delivery	16
3.2.1	Case Studies: Katrina, Wilma, Ike	16
3.2.1.1	Hurricane Katrina	17
3.2.1.2	Hurricane Wilma	18
3.2.1.3	Hurricane Ike	19
3.2.2	Summary of Case Studies	19
4	Modeling Overview	21
4.1	Environmental Characteristics Model	21
4.1.1	Wind Resource Environmental Model	21
4.1.2	Solar Resource Environmental Model	24
4.2	Battery Storage Model	26
4.2.1	Battery Voltage Source Model	27
4.2.2	Battery Array Model and Implementation	30
4.2.3	PSCAD Implementation and Verification	32
4.3	Photovoltaic (PV) Model	35
4.3.1	Current Source Diode Model	35
4.3.2	Photovoltaic Sizing	39
4.3.3	PSCAD Implementation and Verification	40
4.4	Wind Turbine Model	45
4.4.1	Wind Turbine Transient Model	46
4.4.1.1	Wind Turbine Approximate Model	46
4.4.1.2	Permanent Magnet Machine Model	48
4.4.1.3	Three Phase Rectifier Model	49
4.4.2	PSCAD Implementation and Verification	51
4.5	Residential Load Model	55
5	Microgrid Control System	60
5.1	Concept of Operation	60
5.2	Inverter Model	63
5.2.1	Inverter Design	63

5.2.2	LC Filter Design	66
5.2.3	Inverter PQ Controller	68
5.2.4	PSCAD Implementation	72
5.3	Power Management Controller	75
5.3.1	Island Mode Power Flow Balancing	77
5.3.2	Environmental Resource Monitor	78
5.3.3	Emergency Load Control	79
5.4	Island-mode Droop Control	80
6	Integrated Microgrid Model and Steady-State Verification Results	84
6.1	Microgrid Implementation in PSCAD	84
6.1.1	Transformer and Line-Loss Consolidation	84
6.1.2	PSCAD Microgrid Model	85
6.2	Microgrid Steady-State Performance	86
6.2.1	Grid-Connected Steady-State Operation	86
6.2.2	Island-Mode Steady-State Operation	88
7	Transient-Simulation Scenarios and Results	91
7.1	Scenario 1: Loss of Grid, Transition to Island Mode Operation	92
7.2	Scenario 2: Island Mode - Interconnecting PV Microsources	94
7.3	Scenario 3: Island Mode Operation-Variability of Microsources with a Constant Load	99
7.4	Scenario 4: Island Mode-Wind Gust Ride Through	102
7.5	Scenario 5: Island Mode-PMC Battery Management	105
7.6	Scenario 6: Island Mode-PMC Source Curtailment	107
7.7	Scenario 7: Island Mode-Wind Turbine Fault Isolation	110
7.8	Scenario 8: Microgrid Resynchronization with the Grid	113
8	Conclusions and Future Work	116
8.1	Research Summary	116
8.2	Recommended Future Work	117
8.2.1	Communications Future Work	117
8.2.2	Controller Future Work	116
8.2.3	Economic Analysis Future Work	118
8.2.4	Proposed Pilot Implementation	119
	References	120

List of Figures

1.1: Microgrid Concept for Residential Distribution	3
1.2: Conceptualization of Proposed Residential Microgrid	4
1.3: One-line Diagram for the Single Phase Microgrid	5
2.1: Microgrid Concept for Remote Military Installations	10
2.2: Microgrid Megawatt Capacity Growth Projections	13
3.1: Hurricane Cyclone Formation	15
3.2: Major Landfall Hurricanes in 2005 and 2008	16
3.3: New Orleans and Surrounding Vicinity Power Outage Map	18
3.4: Power Outage Map in the Houston Metro	19
3.5: Number of Customers Without Power vs. Number of Weeks Since Landfall	20
4.1: Annual Average Wind Resource for the State of Florida	22
4.2: Average South Florida Wind Speed Sample Near Sea-Level	23
4.3: Average South Florida Wind Speed Sample at 30 feet Height	24
4.4: Average Solar Energy Resource for the Continental United States	25
4.5: Average Hourly Solar Irradiation for September in South Florida	26
4.6: Typical Battery Discharge Curve of a 1.2 V Lead Acid Cell	28
4.7: Equivalent circuit of a battery cell	30
4.8: PSCAD Implementation of the Battery Model Control	33
4.9: PSCAD Implementation of Battery System Equivalent Circuit	33
4.10: Response of Battery System from Discharging to Charging State	34
4.11: Battery System Efficiency at Nominal Discharge	34
4.12: The I-V curve for a BP 220 Watt module	35
4.13: PV cell equivalent circuit model	36
4.14: PV Array Equivalent Circuit Implemented in PSCAD	41
4.15: Calculation of the Maximum Power Point Implemented in PSCAD	41
4.16: Short Circuit Current and Open Circuit Voltage Calculation in PSCAD	42
4.17: Fill Factor Calculation for the PV Array	42
4.18: Calculation of the Series and Shunt Resistance of the PV Array	43
4.19: The Power Output Response to a Change in Solar Irradiance	44
4.20: Efficiency of the PV Array System (Includes Inverter Losses)	44
4.21: Block Diagram of the Wind Turbine Transient Model	45
4.22: The Power Curve of the Hummer Power Unit	48
4.23: The Effect of a 3-Phase Full Wave Rectifier	50
4.24: Wind Turbine Approximation Model	52
4.25: Existing PSCAD PM Machine Model	52
4.26: 3-Phase Rectifier Bridge for Wind Turbine Model	53
4.27: Wind Turbine Response to a Change in Wind Speed	54
4.28: Efficiency of the Wind turbine System (Includes Mechanical, Generator, Rectifier, and Inverter Losses)	55
4.29: Hourly Energy Consumption Profile of a Standard Home and Home with PV and High Efficiency Appliances	56
4.30: Hourly Demand Curve for High Efficiency Microgrid Home	57
4.31: Single Residence Average Hourly Generation and Demand Profile	58
4.32: Total Average Energy Generated and Consumed in a Single Residence	59

5.1: Top-Level Controller Hierarchy	61
5.2: Microgrid Operation and Reference Points	62
5.3: Battery Inverter Control Concept of Operation	62
5.4: H-Bridge Inverter with Filtering and Grid Connection	63
5.5: Power Semiconductor Capability Chart	65
5.6: General Control Loop for Real Power Control	70
5.7: General Control Loop for Reactive Power Control	70
5.8: PWM Train Generated from Carrier Signal	71
5.9: PWM Generator for PQ Controller	72
5.10: H-Bridge, LC Filter, and Isolation Transformer for the Inverter Circuit	72
5.11: Control Loop for Real Power/Angle Control	73
5.12: Control Loop for Reactive Power/Voltage Control	73
5.13: Verification of Voltage Output from the Inverter against Grid Voltage	74
5.14: Current Harmonic Spectrum for Inverter at Full Load	74
5.15: Voltage Harmonic Spectrum for Inverter at Full Load	75
5.16: PMC Top-Level Control Diagram	76
5.17: Power Balancing Function Implementation in PSCAD	78
5.18: Wind/Solar Resource Monitor Implementation in PSCAD	79
5.19: PMC Emergency Load Control Implementation in PSCAD	80
5.20: Droop Characteristics for Frequency and Voltage	81
5.21: Droop Controller Implementation for Phase Control on the Battery Inverter	82
5.22: Droop Controller Implementation for Voltage Control on the Battery Inverter	82
5.23: Voltage Transient Response with Droop Control	83
5.24: Phase Transient Response with Droop Control	83
6.1: Microgrid Implemented in PSCAD	85
6.2: Grid Connected Steady State Power	87
6.3: Grid Connected Steady State Voltage	87
6.4: Grid Connected Steady State Frequency	88
6.5: Island Mode Steady State Power	89
6.6: Island Mode Steady State Voltage	89
6.7: Island Mode Steady State Frequency	90
7.1: One-line Diagram of the Microgrid with Measurement Points	92
7.2: Power Load Demand and Supply from PV, Batt, and WTG	95
7.3: System Voltages for the Common Bus, Residence Bus, and Battery Bus	94
7.4: Battery Phase Angle Change (w.r.t. to Residence Bus)	95
7.5: System Frequency Response during Transition	95
7.6: Change in Power Output during Transition	97
7.7: Change in PV and Battery Output during Transition	97
7.8: Voltage Response during Transition	98
7.9: Frequency Response during Transition	98
7.10: Battery Phase Angle (w.r.t. to Load Bus) during Transition	99
7.11: Worst Case Solar Irradiance Variation Frequency	100
7.12: Worst Case Wind Speed Variation Frequency	100
7.13: Power Output Resulting From Resource Variation	101
7.14: Voltage Response to Changing Renewable Sources Variation	101
7.15: Battery Phase Angle Response to Changing Renewable Sources Output	102

7.16: Worst Case Wind Gust	104
7.17: Power Output during Wind Gust	104
7.18: Power Output during Wind Gust	105
7.19: Battery Phase Angle Response during Wind Gust	105
7.20: Worst Case Battery Discharge Rate	106
7.21: PMC Reducing Curtailing Demand from Residences during Battery Discharge	107
7.22: Battery Phase Angle Response to Rapid Discharging	107
7.23: PMC Source Curtailment Due to High Battery SOC	108
7.24: WTG 1 Breaker Initialized by PMC	109
7.25: Battery SOC Change during Curtailment	109
7.26: Battery SOC Change during Curtailment	110
7.27: Battery and WT Contribution to Fault Event	111
7.28: System Voltage Response to Fault Event	112
7.29: WTG Inverter Fault Current Contribution and Isolation (after 3 cycles)	112
7.30: WTG PM Generator Fault Current Contribution and Isolation (after 3 cycles)	112
7.31: Change in Power Output during Resynchronization	114
7.32: System Voltage Change during Resynchronization	114
7.33: Battery Phase Angle Change during Resynchronization	115

List of Tables

3.1: Electrical Infrastructure Impact from Major Hurricanes	20
4.1: Electrical Characteristics of the BP 3220 Panel	39
5.1: Inverter Hardware Specification	65
5.2: LC Filter Specification	68
5.3: Truth Table for the H-Bridge Inverter	71
5.4: PMC Load Balancing Truth Table	76
6.1: Grid-Connected Mode Steady State Operation Unit Status	86
6.2: Island Mode Steady State Operation Unit Status	88
7.1: System Configuration for Scenario 1	93
7.2: System Configuration for Scenario 2	96
7.3: System Configuration for Scenario 3	100
7.4: System Configuration for Scenario 4	103
7.5: System Configuration for Scenario 5	106
7.6: System Configuration for Scenario 6	108
7.7: System Configuration for Scenario 7	111
7.8: System Configuration for Scenario 8	113

Chapter 1

Research Introduction

Natural disasters have a devastating impact on people, the environment, and everyday way of life. Virtually no place on earth is spared from natural disasters such as floods, hurricanes, earthquakes, tsunami's, drought, tornados, blizzards, and many other events. On the southeastern seaboard of the United States, the primary threat is from hurricanes. In particular, the state of Florida bears the brunt of many tropical systems. Between the years 1851-2004, 110 hurricanes impacted the state [1]. This accounted for 40% of all hurricanes that have struck the eastern seaboard of the United States during that time [1]. By the same margins, 35 major hurricanes (category 3 and higher) have made landfall during this time in Florida [1]. Hurricane impacts often result in extensive damage to local infrastructure. Electric service can quickly be interrupted for millions of customers and in some cases, remain offline for weeks afterwards [2]. The growing development of microgrids has the potential to provide continuous power to these affected communities during an outage of indefinite duration. Currently, a large number of residences use emergency gasoline/diesel generators during outages. Drawbacks to the current implementation of these generators are that they are isolated, typically non-redundant, produce dangerous emissions, and are dependent on a large fuel supply during extended outages. The safety concerns with emergency generators are of particular concern. According to [3], between 1999-2011, 755 people died in the United States from carbon monoxide poisoning from emergency generators. Microgrids with "green" sources of energy generation can reduce dependence on these gas generators while reducing emissions without heavy reliance on inefficient emergency gasoline generators. Another consideration is the large number of injuries

that occur after a hurricane has past that are related to improper use and handling of gasoline generators with injuries ranging from electric shock, carbon monoxide poisoning, and physical injury. From this, it can be seen how an autonomous microgrid can provide additional safety over existing technology.

1.1 Microgrid Definition

Microgrids have the potential to drastically alter the infrastructure and nature of power generation on a global scale. While the formal definition of a microgrid varies by audience, a common definition is an integrated energy system consisting of distributed energy resources and multiple electrical loads operating as a single, autonomous grid either in parallel to or “islanded” from the existing utility power grid [4]. The key distinguishing feature between a microgrid and the classical macrogrid is the collocation of generation and load centers. The network minimizes the burden of large transmission and distribution networks. Only a small, local, distribution system is needed to interconnect generation and load centers. Figure 1.1 shows a conceptual architecture for a microgrid, intertie with an existing radial distribution system.

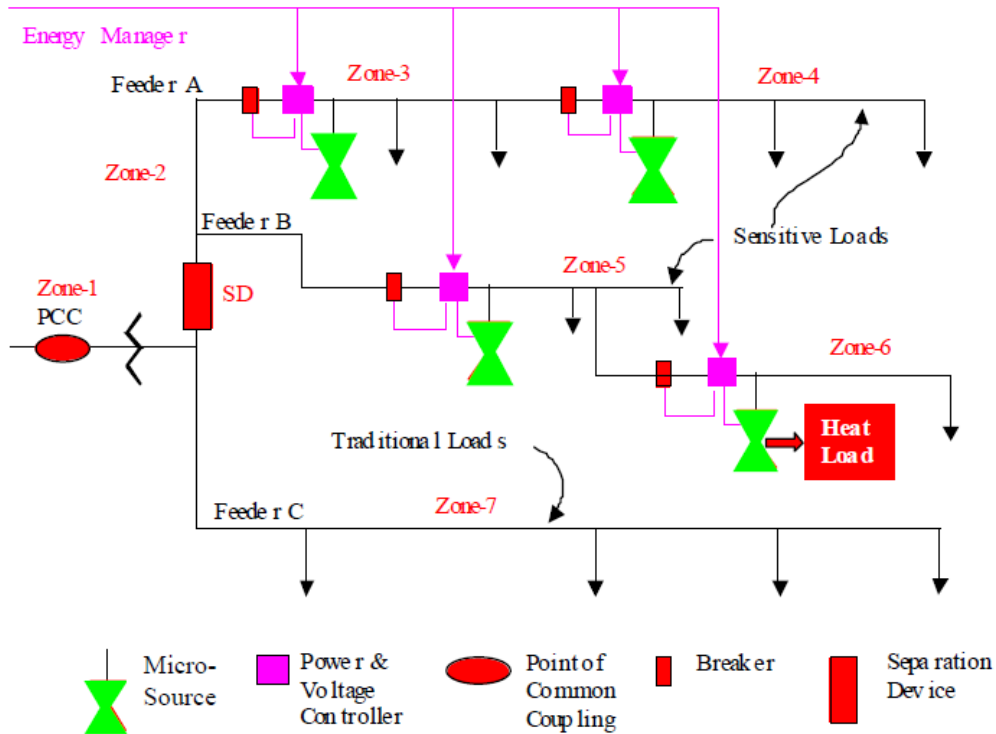


Figure 1.1: Microgrid Concept for Residential Distribution [5]

1.2 Research Motivation

The primary motivation for pursuing this research topic is to highlight the key features that a microgrid can provide to power system networks that the contemporary electric grid cannot achieve. This includes greater reliability, resilience, emissions reduction, and rapid demand management. In particular, in the event of large scale natural disasters, the limitations of the existing grid are apparent. Dependence on high voltage transmission and distribution lines, predominantly routed overhead, often result in widespread outages during and immediately following a natural disaster. Customers in small towns and rural areas are generally given lower priority to restoring service than the population centers in larger cities. Customers without emergency generators or inadequate fuel supplies, face a prolonged outage. This research will

emphasize clean and sustainable microgrids as an alternative to the traditional emergency gasoline generators. The robustness of the system to transients that occur during and after a storm will also be evaluated.

1.3 Microgrid Concept and Scope of Study

The concept for this microgrid is 3 small residences, adjacent to each other, with renewable sources installed on each property. One wind turbine and one PV array is connected to each residence. The residences are tied back to a local substation on a single phase where they connect to the local distribution substation. A battery storage bank is tied in to the substation at another location to provide backup for the renewable devices. A notional concept for the microgrid is captured using Google sketch-up and shown in Figure 1.2.

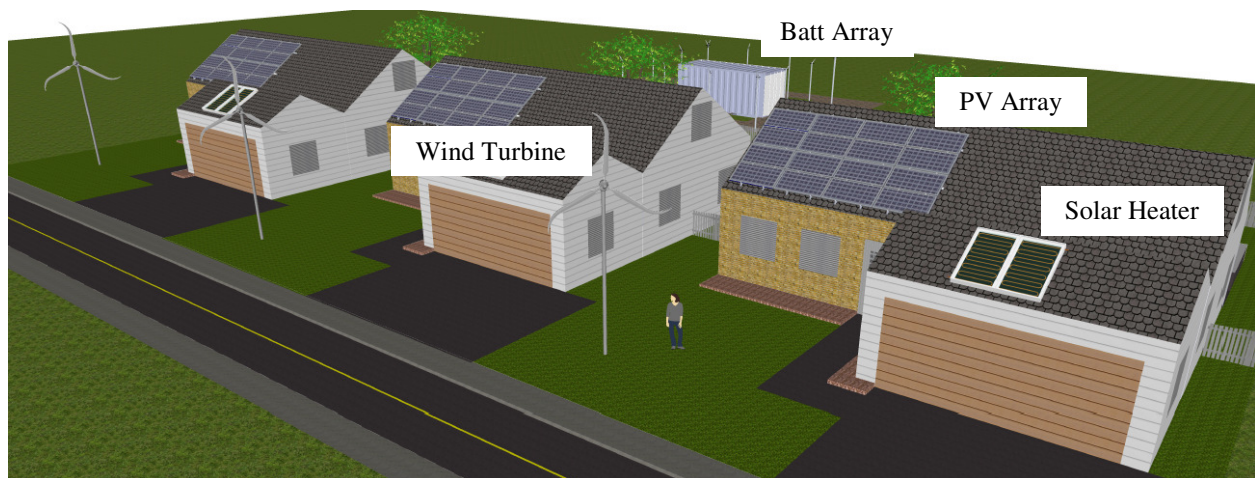


Figure 1.2: Conceptualization of Proposed Residential Microgrid

It can be seen that the proposed microgrid fits within the boundaries of the referenced residence without an excessive amount of real estate required. In a practical system, the turbine would likely be located further away from the residences to provide better airflow around the blades,

but this is shown for visualization purposes. The residences are tied to the same single phase feeder from the residential distribution source. It is also assumed that a small amount of real estate is required for the battery storage module shown in Figure 1.2. The details of the physical layout are not covered in this thesis, but rather notionally given as a reference to the feasibility of the proposed microgrid. The one-line diagram for the microgrid is shown in Figure 1.3. This one-line is not representative of all residential distribution layouts. There are numerous variations of residential distribution schemes that exist.

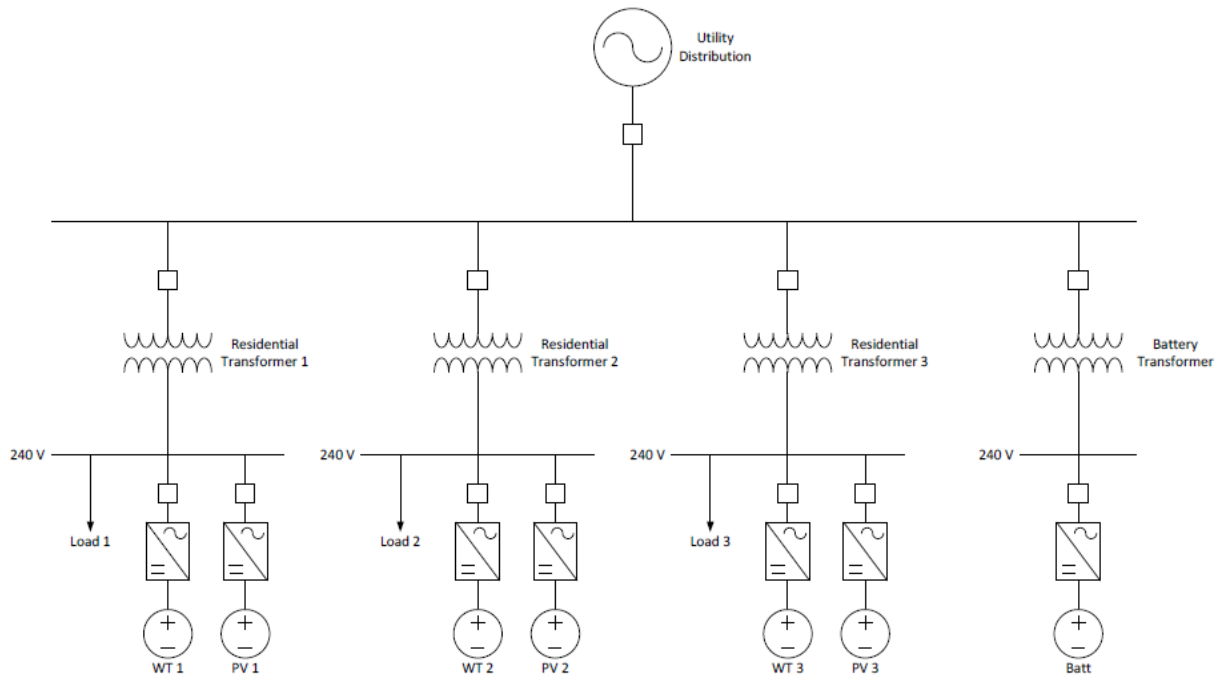


Figure 1.3: One-line Diagram for the Single Phase Microgrid

While the proposed model is limited to 3 residences and a small number of generation sources, it is important to note that this system is highly scalable. The size of the microgrid for this research is limited to reduce simulation time and provided more detailed results for a smaller network. Future study into this system should consider a much larger number of nodes and is proposed in Chapter 8. The proposed system can be implemented in a variety of network schemes that do not

alter the operation of the microgrid. The operation of the system is focused on island mode generation and maintaining voltage and frequency stability with the residences. Grid-connected mode is investigated for steady-state verification, as well as disconnecting and reconnecting to the macrogrid, but is not the emphasis of this research. Scenarios to be investigated will be focused on changing system conditions and how the microgrid responds.

1.4 Contributions

This research proposes a novel microgrid that is capable of being islanded from the main grid and free of fuel source generations (namely gas generators and/or fuel cells). While significant research is being performed in microgrids and disaster recovery currently (see Chapter 2), there is limited research on microgrid systems for clean, sustainable electricity delivery. This novel system architecture also produces novel solutions for power flow and system stability. The constraints of this novel approach also leads to new challenges. For instance, control of power output through phase angle droop control, rather than classical frequency control, is presented in this research. Utilizing a battery array, rather than fossil system, for a reference point and for stabilizing the microgrid power production is also discussed. Novel modeling and control schemes for an islanded microgrid are also presented that allow for greater energy utilization and demand side management. This work sets the foundation for further investigation and implementation for future research studies.

1.5 Thesis Overview

This thesis is divided into 8 chapters. Chapter 1 provides an introduction to the topic and the scope of the research. Chapter 2 covers the literature review of previous research efforts and

similar efforts performed on microgrid research. Chapter 3 provides motivation for this specific research topic through reviewing hurricanes and impact on electric power delivery. Chapter 4 covers in detail the various sub-models that make up the generation sources, environmental model, and residential loads. Chapter 5 goes over the control system and hierarchy of the microgrid. Chapter 6 covers the interconnection of the sub-models from chapter 4 and control system from chapter 5 together into an integration microgrid model along with steady state results. Chapter 7 covers the results of various dynamic scenarios for the consolidated microgrid. Chapter 8 concludes the thesis with final results and recommendations for future expansion of the research topic.

Chapter 2

Literature Review

Recent natural disasters such as the 2011 Japanese Tsunami and Hurricane Irene (U.S. 2011) have demonstrated the potential of microgrids for disaster recovery. In particular, university research microgrids have made their way into the spotlight after these two events. During the Japanese tsunami, the city of Sendai, which is located on the Northeastern coast of Japan, was directly in the path of the major tsunami [6]. Hundreds of residents perished as catastrophic damage occurred to buildings and infrastructure as far as 8 miles inland [6]. One surprising success story from this devastation, was the resilience of the Tohoku Fukushi University microgrid. This system supplied 1 megawatt of uninterrupted power to the university buildings and hospital for several days until power was restored [6]. Through a combination of fuel cells, photovoltaic panels, and natural gas microturbines the university was able to keep the lights on while much of the city was left in the dark. A similar operational success story occurred when Hurricane Irene struck the U.S. Northeast coast in 2011 [7]. Three university microgrids located at Cornell University (38 MW microgrid), New York University-Washington Square Park (13.4 MW), and Utica College (3.6 MW) were able to supply uninterrupted power immediately following the storm [7]. Overall, interest in microgrids for emergency events is growing and accelerating by each new natural disaster.

2.1 Microgrid History

Basic microgrids have been around since the early days of electrification. Early generation facilities, such as Thomas Edison's generating stations in New York City, were located very close to customer lighting loads. These systems were isolated where a few string of lights would intertie to a single generator. As demand for lighting grew and the advent of alternating current, the nature of electricity changed. Generation units grew larger, more interconnected, and located further away from load centers. Large scale transmission lines interconnected the electrical grids of multiple utilities together. From this growing interconnection, the macrogrid was formed and individual microgrids became uneconomical compared with the larger economy of scale networks [4]. Microgrids have held on in some key markets over the years where connection to a macrogrid was either unreliable or unavailable for local demand. These include remote communities, factories with large industrial loads, and critical infrastructure (i.e. hospitals, emergency responders, military installations, etc...) [4]. In particular, the U.S. Department of Defense (DoD) has been on the forefront of recent microgrid development projects for remote military bases. Microgrid technology for the defense industry is being driven by the need to reduce fuel convoys to forward operating bases [8]. These convoys traverse very dangerous remote regions with heavy casualties by military personnel and contractors. Figure 2.1 show a proposed microgrid for defense application developed by the Lockheed Martin Corporation.



Figure 2.1: Microgrid Concept for Remote Military Installations [8]

While microgrids have found a niche in defense and critical infrastructure markets, they are also growing in distributed generation as well. With increasing demand for electricity, competitive electricity markets, and greater reliability concerns, they are making a significant comeback. New projects offer isolated, clean, and reliable power production for an adjacent customer demand. Most major commercial buildings are now equipped with some form of emergency power, typically a diesel generator with a short duration battery backup system [9]. In addition, numerous universities are investing in microgrids for research opportunities and to meet local demand. Residential communities have the potential for multiple homes with distributed resources attached to them to work in concert to deliver cost effective, reliable, energy to homes. While the residential market for microgrids is currently just beginning to emerge, it does offer the largest market potential for growth. New pilot projects for microgrids are being developed at numerous research universities, like the 4 referenced in Chapter 1, as well national laboratories. The national renewable energy laboratory (NREL) in Golden, CO is developing a test microgrid to test the many variations of the system configuration that can be utilized [9]. This project along

with others signals a are large shift in research and new product development into the area of microgrid development.

2.2 Microgrids in Contemporary Application

There are several power operations where microgrids have a practical application. Common implementations include peak load shaving for demand side management. In this situation, dispatchable units such as a diesel generators, microturbines, fuel cell stacks, or battery array come online to supply part of the load to a customer distribution during periods of high demand (which usually occurs during mid-afternoon hours). This implementation can offer cost competitive power in a real time electricity pricing market. Another implementation is for backing up the local distribution network when electricity from the local network is unreliable (i.e. weak grid). In this application a variety of resources would be on standby, ready to pickup instantaneous drops in supply from the macrogrid. This application is very desirable in remote regions where local utilities cannot meet high electric reliability due to a number of reasons. In this case, microgrids can backup local supply and provide residents with a higher reliability source of electricity.

2.2.1 Microgrids for Disaster Recovery

One area of particular interest, and the basis of this thesis, are microgrids for disaster recovery operations. In this situation, the microgrid must provide power to the entire electric load for an indefinite period of time. In previous research, [10] and [11] proposed microgrids for disaster recovery, looking at both probability of micro-source failures and modeling of controls. In [10] a small system is proposed consisting of a doubly-fed induction wind generator and a small hydro-

power turbine. This paper looks at both the connection to and disconnection from the grid during a disaster event. In [11] the authors investigate a significantly more complex microgrid with multiple wind turbines, diesel generators, and battery storage array. In this paper, the reliability of a microgrid during a disaster event is evaluated. Of principle importance is the ability to maintain power supply to the customer when one or more units go offline. During a widespread outage, damage to the microgrid infrastructure must also be considered. The robustness of the microgrid from internal faults should also be considered.

2.3 Clean Energy and Fuel Independent Microgrids

There is limited research available on microgrids that do not use either a diesel generator or a microturbine as the primary generation source. During a prolonged power outage, the risk of generation units losing their fuel supply is very high. This can be partially mitigated by maintaining a large emergency fuel supply, but this has its drawbacks. Difficulty in predicting fuel supply needed presents a major risk in not having enough storage or having too much storage (which can result in fuel quality degradation over time). There is also safety concerns associated with storing vast quantities of fuel in regards to poisoning or risk of fire. A fuel independent system eliminates the risks associated with fuel consumption and storage. There have been research and pilot projects in clean energy microgrids, but they have not focused explicitly on disaster recovery [12]. At the time of writing this thesis, there is limited research on clean energy and fuel independent microgrids that have been proposed for disaster recovery.

2.4 Trends in Microgrid Research & Development

Interest in microgrids has grown substantially over the past decade. In addition to new and innovative research efforts, a large number of projects are starting to come online. Pike's Research Group in Boulder, CO performs market research on the current state of microgrid development and the expected growth in the future [13]. As indicated by Figure 2.2 below, exponential growth in the microgrid market is expected over the next 4 years.

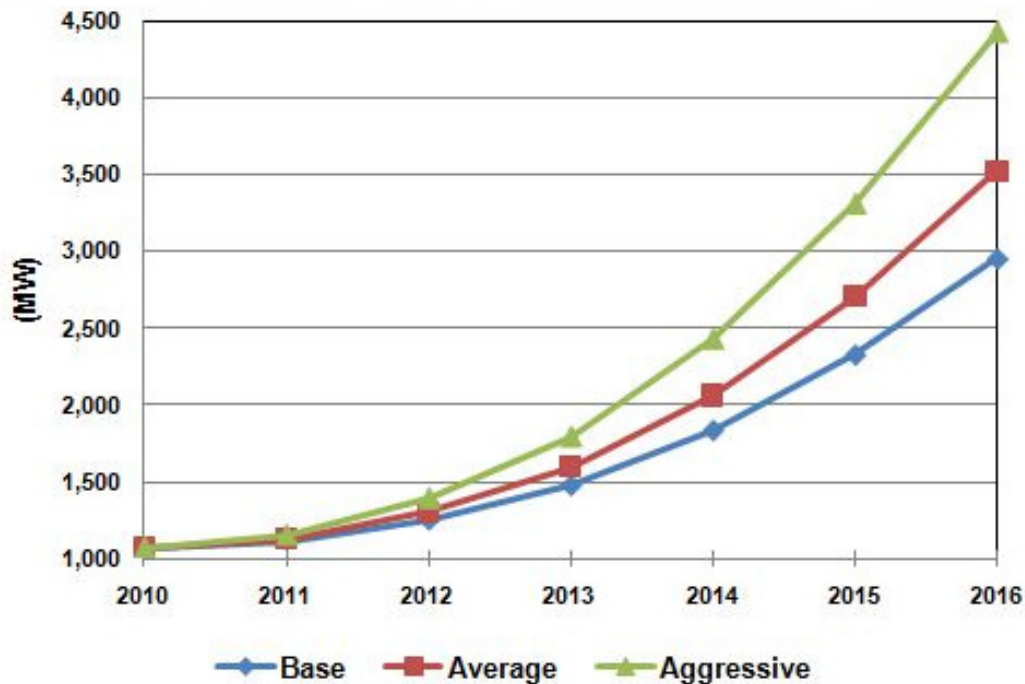


Figure 2.2: Microgrid Megawatt Capacity Growth Projections [13]

The aggressive projection has microgrids doubling in capacity every 2 years. Even the base projection has them doubling in capacity every 3 years. As they continue to grow at a rapid pace, so too will their capabilities. Increasing efficiency of small scale generation sources, better power flow through power electronics, and more advanced communication are expected to drive their increased development. This will lead to a greater expansion in the applications of microgrids and the markets that they can be introduced into. The largest market potential is in residential based systems, which is the focus of this thesis.

Chapter 3

Hurricane Occurrence and Impact

Prior to designing a microgrid that can meet this challenge, it is important to first briefly review hurricanes and their historical impact on electric power delivery. The widespread devastation caused by major hurricanes is the primary motivation for this thesis topic. Investigating the implementation of a practical microgrid that can be utilized to maintain power delivery to a residential demand during and after a major storm is very beneficial. With this motivation, the design can move forward.

3.1 Brief Overview of Atlantic Hurricanes

Hurricanes (also known as typhoon and cyclones) are major storms that form over warm tropical waters. They are characterized by strong winds and heavy rain in a self-sustaining spiraling storm system. They are formed when the heat from vaporization of the warm tropical waters creates a heat cycle, caused by the cooling of the water molecules as they rise in the air [14]. This result in cooler moisture being forced down and warm water vapor rising back up. When this cycle becomes sustainable, strong winds form causing a rotational spiral [14]. As the storm begins to move, it will strengthen as it continues pass over the warmer waters that provide additional energy for the system. Figure 3.1 shows the anatomy of a self sustaining hurricane.

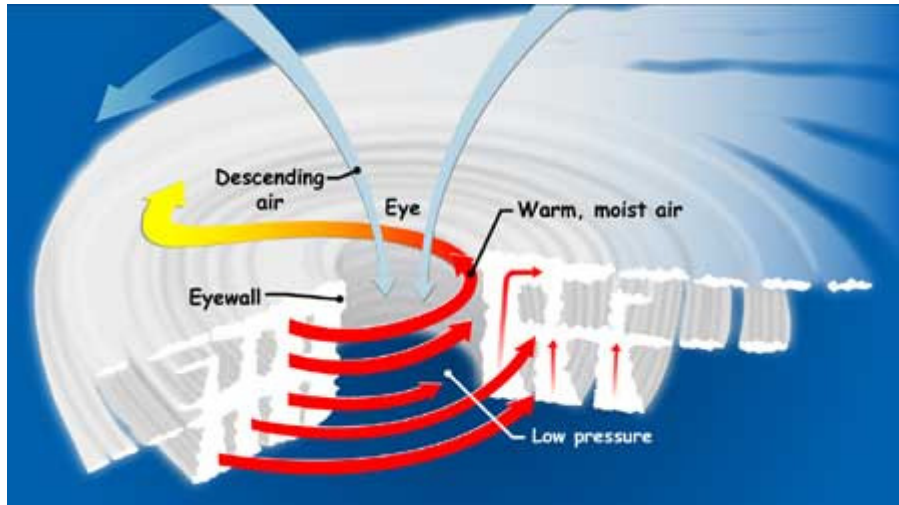


Figure 3.1: Hurricane Cyclone Formation [14]

When winds sustained up to 38 MPH classify the storm as a tropical depression, between 38 and 74 MPH is a classified as a tropical storm, and winds 75 MPH and higher are classified as a hurricane [14]. The National Hurricane Center categorizes hurricanes on a scale of 1 to 5, based off of sustained wind speed. Major hurricanes are those being category 3 or higher. In the Northern Atlantic Ocean, hurricanes typically formed near the Cape Verde islands off the coast of Western Africa. They can also form in the southern Gulf of Mexico [14]. These storms cause the most significant damage to people and property when they make landfall. Figure 3.2 is a map of the largest hurricanes that hit the United States in 2005 and 2008, which are the most devastating in recent history [2].



Figure 3.2: Major Landfall Hurricanes in 2005 and 2008 [2]

3.2 Hurricane Impact to Electricity Delivery

The high winds and heavy rain from hurricanes often results in widespread power outages. The major brunt of the damage is to overhead distribution lines that are taken out of service during the storm due to trees, line pole failures, and debris that comes in contact with lines. Damage can also occur to power plants, transmission lines, and substations. The duration of a power outage can range from several hours to several weeks.

3.2.1 Case Studies: Katrina, Wilma, Ike

To further motivate research into microgrids for disaster recovery, a review of 3 major hurricanes that previously occurred was performed. Hurricanes Katrina, Wilma, and Ike are review in this section. These storms were particularly devastating to local infrastructure. In

particular, the level of power outages that occurred from each of these storms was very widespread. They were also selected given their relatively recent history. Hurricane records go back to the 1850's, but only the past few years of storms have been selected to assess the impact on power outages for contemporary power systems.

3.2.1.1 Hurricane Katrina

Hurricane Katrina was a major hurricane that hit large portions of Florida and the Gulf Coast states in August, 2005. The storm peaked at category 5 rating while at sea before eventually making landfall as a strong category 3 [2]. Hurricane Katrina was one of the most widespread devastating storms to ever hit the continental United States, both in terms of physical damage and loss of life. It remains the costliest storm in U.S. history and one of the deadliest with over 1,200 people killed either directly or indirectly [2]. Rebuilding efforts in the areas of New Orleans hardest hit by the storm are still ongoing. Hurricane Katrina was a unique storm in that it made landfall twice, once in southeast Florida and then a week later in Louisiana. Both landfalls resulted in widespread disruptions in power service. When Katrina hit Florida, over 1 million customers lost power for several days [2]. After the second landfall in Louisiana, over 2.7 million customers were without power in four states [2]. Two weeks after the first landfall, electric service had been restored to all affected residents in Florida, Mississippi, and Alabama. However, given the widespread damage in Louisiana, over 40 percent of the customers were without power [2]. Significant sections of the New Orleans area were without power 2 months after the storm, as shown in Figure 3.3 below.

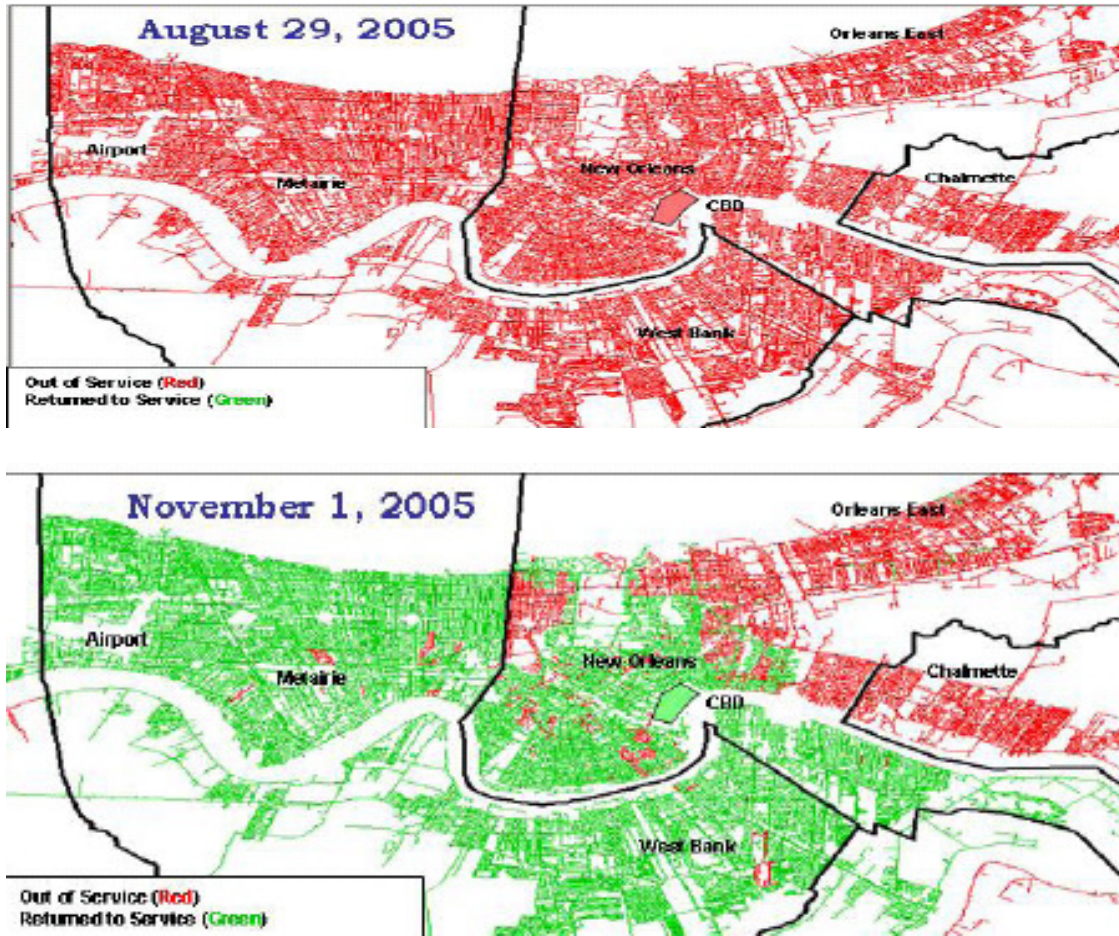


Figure 3.3: New Orleans and Surrounding Vicinity Power Outage Map [2]

(red = offline, green = online)

3.2.1.2 Hurricane Wilma

Hurricane Wilma was a major hurricane that struck southeast Florida in October, 2005. Wilma was a strong category 5 storm at sea that weakened to a category 3 when it made landfall. Over 3.5 million customers were initially without power from the storm, including airports, hospitals, and major ports [2]. Two weeks after the storm, power had been restored to all but 100,000 customers [2]. In all, it took over 3 weeks to restore power to all areas. Making matters more difficult, fuel shortages plagued the area. Many residents that depended on emergency gas generators for electricity during this outage were soon found to be without at gas [2].

3.2.1.3 Hurricane Ike

Hurricane Ike made landfall on the eastern Texas gulf on September 13, 2008 as a strong category 2 storm. The storm was particularly noted for high wind gusts which reached category 4 strength at times. Over 2.1 million customers were without power in the greater-Houston area, which bore the brunt of the storm [2]. Furthermore, the remnants of Ike remained a powerful storm system as it worked its way through the interior of the United States, knocking out power to an additional 1.8 million customers in Arkansas, Louisiana, Missouri, Kentucky, Indiana, Ohio, and New York [2]. Much of the Houston metro remained without power for 10 days after the storm, due to the widespread devastation. Two weeks after the storm, power had not been restored to over 600,000 customers, as shown in Figure 3.4 below. It would take over 6 weeks until power was restored to all customers impacted by the storm.

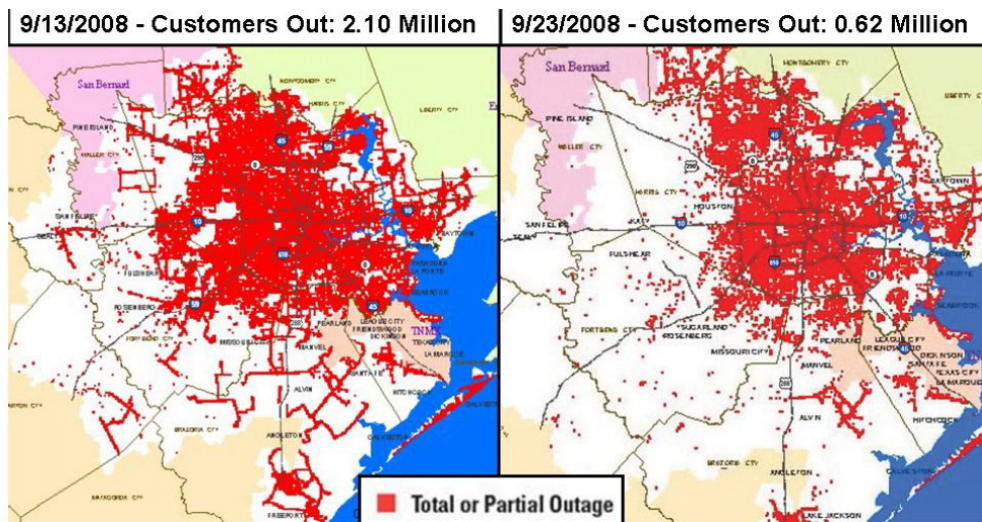


Figure 3.4: Power Outage Map in the Houston Metro [2]

3.2.2 Summary of Case Studies

The previous studies showed the widespread impact a major hurricane can have on electric power service. In all of the case studies, power was not fully restored until weeks afterwards.

While the majority of power outages are resolved within the first few days of the storm, a small minority of customers in rural areas and/or areas hard hit by the storm can be without power for an extended period. As shown in Figure 3.5 below, all of the major hurricanes that struck the U.S. in 2005 and 2009 resulted in widespread damage.

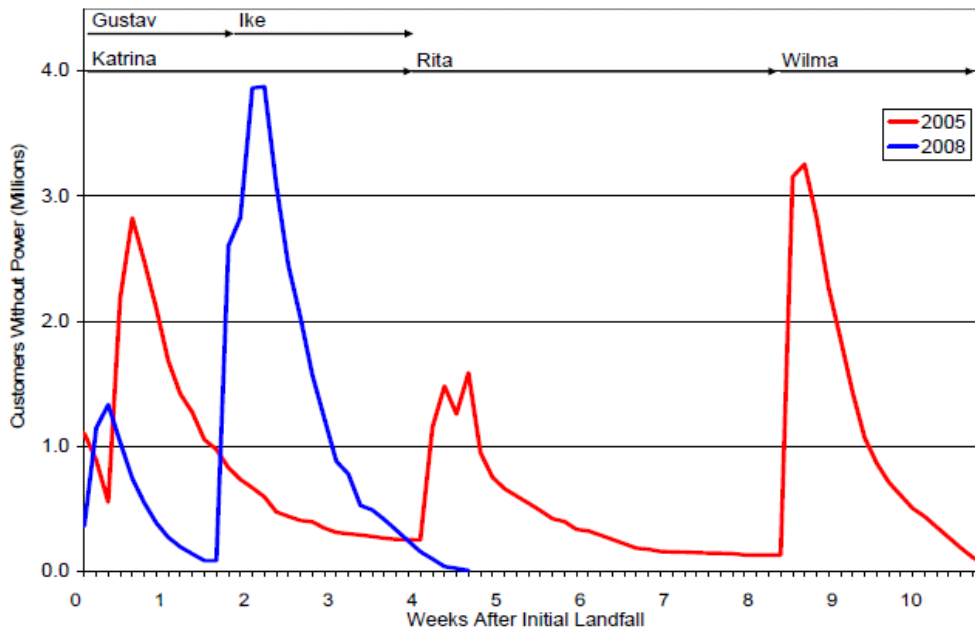


Figure 3.5: Number of customers without power vs. number of weeks since landfall [2]

The significant damage these storms bring to overhead lines and substations can result in prolonged outages to a large number of customers. Table 3.1 below shows the impact the various major storms in 2005 and 2008 had on the non-generation electricity infrastructure.

Table 3.1: Electrical Infrastructure Impact from Major Hurricanes [2]

Infrastructure Impacted	2005			2008	
	Katrina	Rita	Wilma	Gustav	Ike
Utility Poles Destroyed	72,447	14,817	~14,000	11,478	10,300
Transformers Damaged	8,281	3,580	NA	4,349	2,900
Transmission Structures Damaged	1,515	3,550	NA	241	238
Substations Off-line	300	508	241	368	383

Chapter 4

Modeling Overview

In this chapter, the individual sub-models for the microgrid are detailed. This includes the environmental model, wind turbine, photovoltaic array, battery array, and residential loads.

These transient models are connected together to cover the dynamics of the environment, loads, and sources. The individual models form the building blocks of the full model. The interconnections of these resources into the complete microgrid are detailed in the next chapter.

4.1 Environmental Characteristics Model

An accurate model of the environment in the region where the microgrid is installed is critical for sizing the generation needs and predicted energy output. For this design, the reference site is the South Florida region of the United States. The model will focus on typical weather patterns during the month of September (i.e. the peak of hurricane season). This region is a humid tropical climate with average temperatures in September between 76 to 88 degrees Fahrenheit [15]. Rainfall in September averages over 9 inches, with afternoon storms typical [15]. The environmental model for the microgrid will assume the average conditions for wind speed and solar irradiance during this time of year.

4.1.1 Wind Resource Environmental Model

Several published environmental studies have been performed to assess the wind resources in Florida. The consensus is that the overall wind resource in the state is inconsistent for large scale

onshore commercial wind power development. Figure 4.1 show the average wind speed across the state.

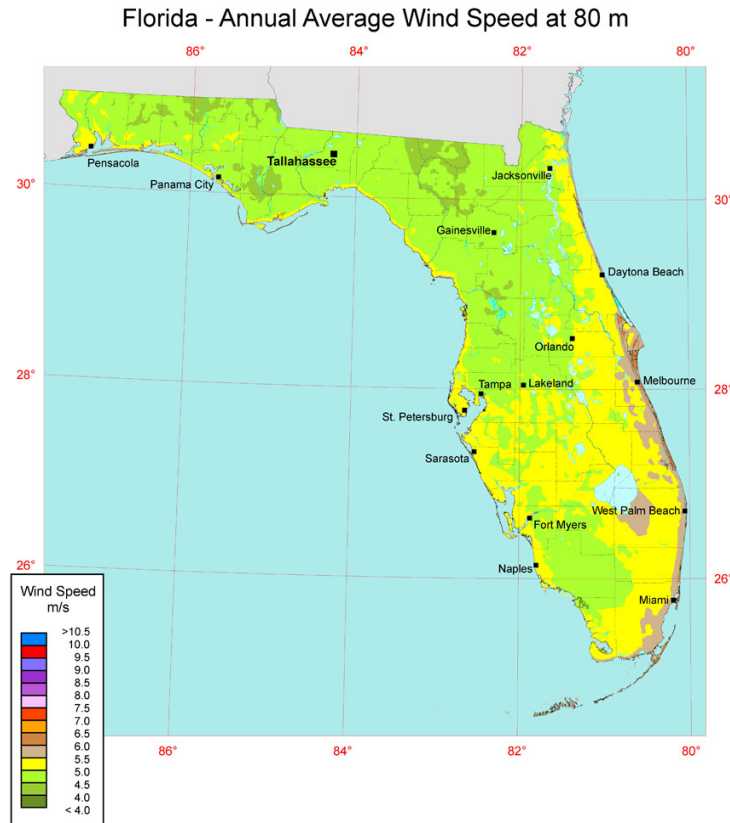


Figure 4.1: Annual Average Wind Resource for the State of Florida [16]

Coastal parts of the state have significantly better wind resources than the interior, but due to the high population density near the coast, the development of commercial wind sites is unlikely [17]. Although Florida is a low resource for large scale wind development, the resource that is available is sufficient for small scale wind turbines in a distributed generation scheme. The wind system will have a relatively low capacity factor and will experience extended periods of low to no power output. With that in mind, the wind turbine can be sized with enough rated power to still accommodate a significant part of the customer electricity demand. For the wind environmental model for this system, an accounting of the average hourly wind resource, at the

expected height of the rotor is required. Figure 4.2 shows the hourly average wind speed for a typical site in South Florida, collected over a 4 month period [18].

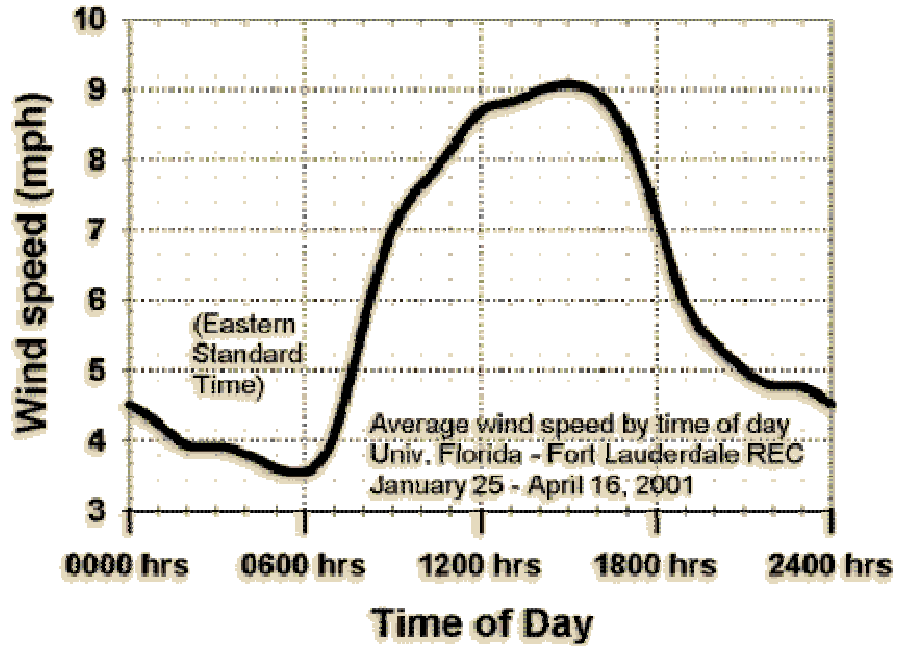


Figure 4.2: Average South Florida Wind Speed Sample near Sea-Level [18]

Using this data, the basis of the wind resource model can be developed. Higher frequency perturbations such as wind gusts will not be included in the standard wind model, but will be addressed in the dynamic scenarios in Chapter 7. The last step for this model is to adjust the wind speed for the appropriate height of the wind turbine will operate at. Following the wind profile power law, the wind speed in the previous figure can be evaluated at the expected height of the wind turbine. The wind profile law is referenced from [19] and given as

$$V_x = V_r \cdot \left(\frac{z_x}{z_r} \right)^\alpha, \quad (4.1)$$

where

V_x = Wind speed at new height,

V_r = Wind speed at rated height,

z_x = New height,

z_r = Rated height,

α = Scaling exponent, assumed to be approximately 1/7 for most wind resources.

For residential permitting considerations, it is typically required that residential structures do not exceed 30 feet in height to comply with local ordinances [20]. Taking this limit as the maximum height, and using the data from Figure 4, the revised hourly wind model for South Florida at a height of 30 ft is given in Figure 4.3.

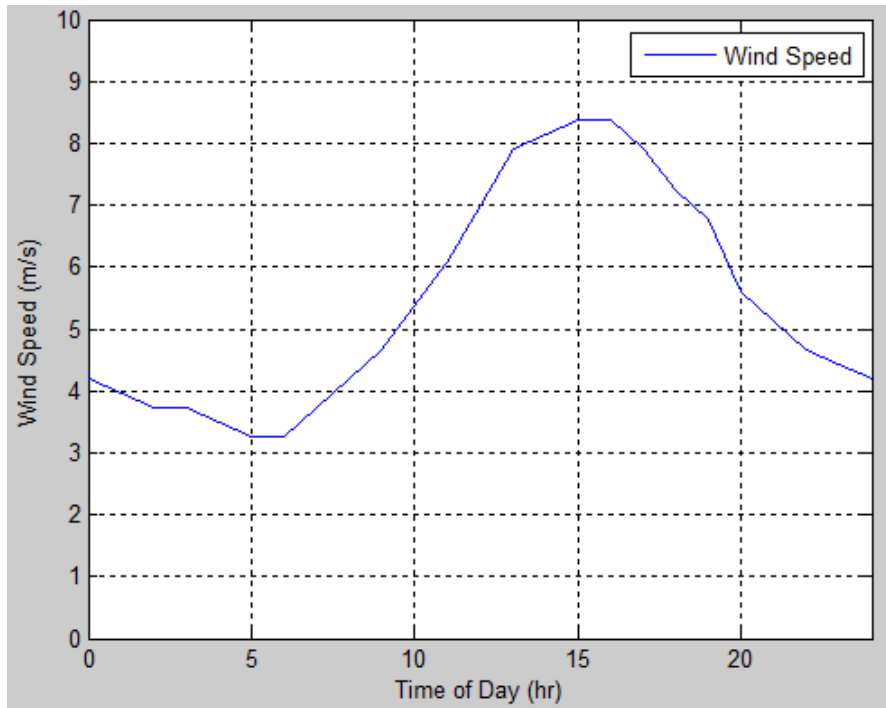


Figure 4.3: Average South Florida Wind Speed Sample at 30 feet Height

4.1.2 Solar Resource Environmental Model

There have been numerous studies performed on the solar resource in the state of Florida. In contrast to the wind resource, the solar resource in Florida is significant and is economical for residential, commercial, and utility scale solar production. South Florida has the largest solar

resource on the east coast of the United States. The solar resource for the country is given in Figure 4.4.

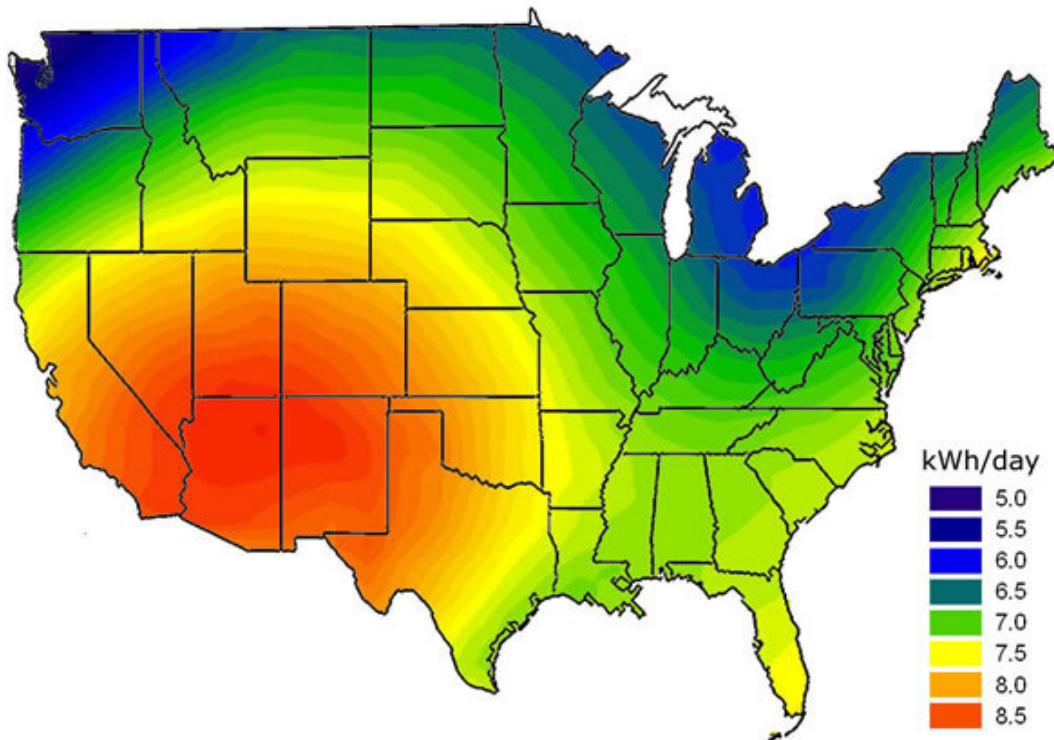


Figure 4.4: Average Solar Energy Resource for the Continental United States [21]

Given the availability of this resource as compared to wind, the dominant energy resource for the microgrid will be solar power. The primary utilization of the solar resource will be for electricity generation. A secondary utilization is water heating, which results in a reduction of electricity demand (discussed further in 4.5). To develop the transient weather model, hourly solar data is needed. This data is available through the National Solar Radiation Data Base (NSRDB) data provided by NREL [22]. Using the NSRDB empirical information, data from 1,454 meteorological stations nationwide are available for reference for hourly site data from 1991-2005. Using this data, the solar environmental model is constructed. Using the previously established condition that September environmental data for West Palm Beach airport is

referenced. The solar irradiation data for the total radiation with respect to the surface is used. The hourly data from [22] is plotted as the average solar resource environmental model shown in Figure 4.5.

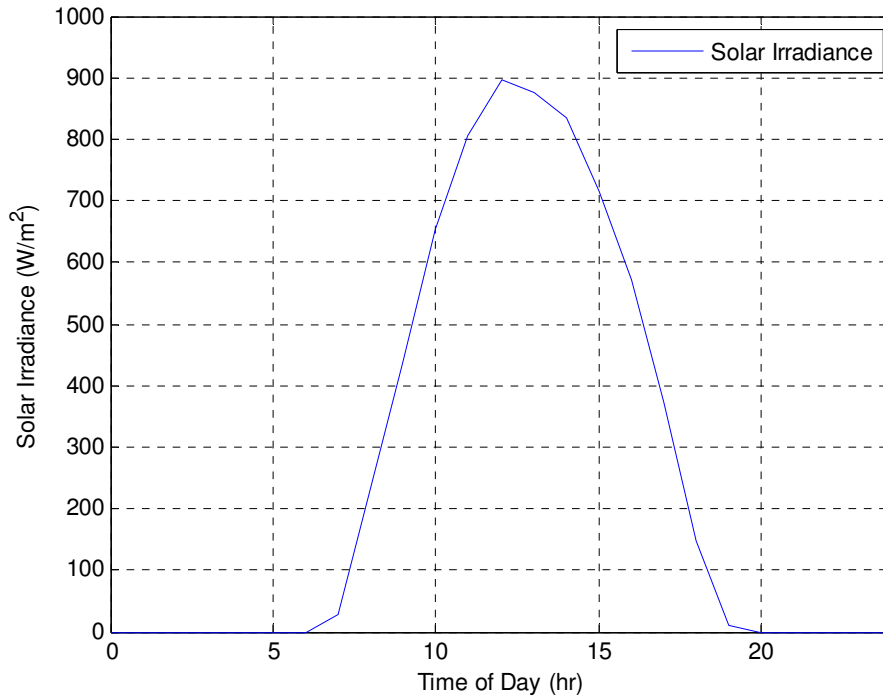


Figure 4.5: Average Hourly Solar Irradiation for September in South Florida

This model serves as the basis of the photovoltaic design in Section 4.3. Short duration transients such as cloud cover are not taken into account with the baseline solar resource model, but they will be looked at in the transient scenarios in Chapter 6. One final consideration for photovoltaic utilization is the changes in temperature. For the solar data selected (i.e. South Florida September average), the daily average temperature is expected to vary from 77 to 89° F throughout the day. Taking this into account, for short term transient events that are less than 1 hour in duration, the temperature will be treated as a constant.

4.2 Battery Storage Model

The next step in modeling the microgrid is to develop the set of sub-models for the various sources, including battery storage. There are several battery chemistry technologies that are viable for microgrid energy storage. These include, but are not limited to, lead acid, nickel cadmium, nickel metal-hydrate, and lithium-ion. The benefits of the various types are dependent on implementation specific constraints. Typically, lead-acid batteries are used in implementation where charge cycling is the primary requirement, as is the case with renewable storage. Lead acid battery array's typically offer a lower price and longer life than the alternatives. As a result, lead acid batteries are utilized for this microgrid model.

The battery storage model implemented in this microgrid system is referenced from [23]. It is based of the charge & discharge characteristics of the terminal voltage of a battery throughout the charge cycle. The classical battery model of a controlled voltage source and impedance in series is utilized for this model. More advance models of batteries using time varying components, variable resistances, and other elements have been proposed in various papers [24]-[25], but are not implemented in this model. The need to limit runtime and minimize system-level model made it compelling to use the classical, but still largely accurate, transient model rather than the advanced proposed models. To apply practical constraints on sizing and specifying the parameters of the battery array, the Sun Extender® battery modules datasheets were referenced [26].

4.2.1 Battery Voltage Source Model

The behavior that the battery transient model must follow is shown in Figure 4.6. As the level of charge, typically measured as amp-hour (Ah), in the battery changes the terminal voltage will

vary according to the voltage profile. In [23], the classical model is proposed to evaluate the performance of plug-in electric hybrid vehicles. This same battery cell characteristic applies to renewable storage batteries, like the ones used in a microgrid.

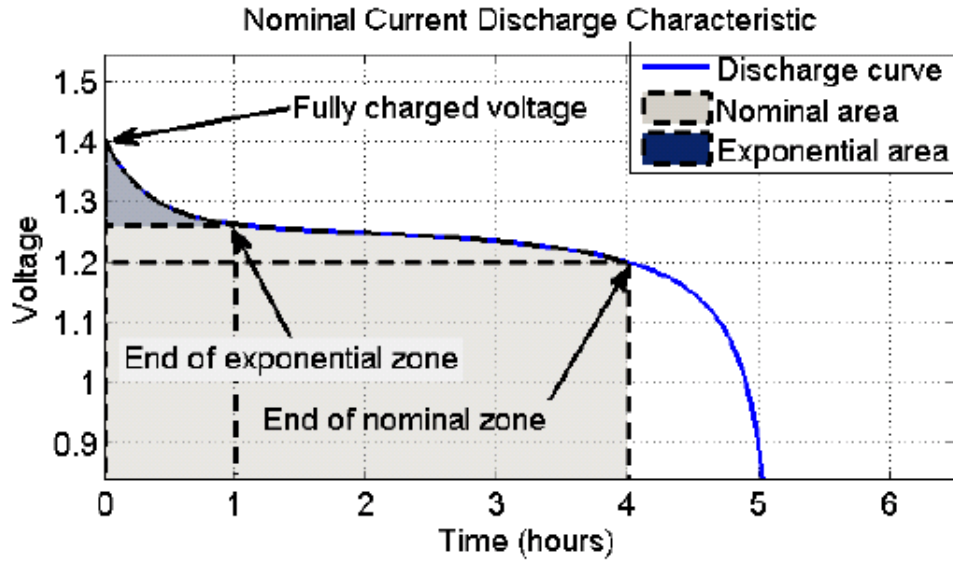


Figure 4.6: Typical Battery Discharge Curve of a 1.2 V Lead Acid Cell [23]

The fundamental equation for the internal voltage of a battery cell is referenced from [23] and given by

$$E = E_0 - K \frac{Q}{Q - it} + A \exp(-B \cdot it), \quad (4.2)$$

where

E = Battery cell internal voltage (V),

E_0 = Constant cell voltage (V),

K = Polarization voltage (V),

Q = Battery rated capacity (Ah),

it = Current Ah discharge rate (Ah),

A = Exponential voltage range (V),

B = Exponential capacity ($A h^{-1}$).

The value of Q is a known quantity that is located in the vendor datasheet for the battery cell.

The other unknown quantities can be evaluated by referencing the discharge curve for the given battery cell. Evaluating 3 points on the discharge curve, the fully charged voltage, the end of the exponential region, and the end of the nominal region, the battery model can be fully defined.

Knowing that the fully charged voltage occurs when current discharge rate is zero, the following relationships are defined as

$$E = E_0 - K \frac{Q}{Q-0} + A \exp(-B \cdot 0) = E_0 - K + A, \quad (4.3)$$

$$E_0 = E_{full} + K - A. \quad (4.4)$$

Since the A parameter is defined as the exponential region voltage, this value can be found by simply subtracting the full voltage from the exponential voltage:

$$A = E_{full} - E_{exp} \quad (4.5)$$

Finally, knowing that $E = E_{nom}$, $Q = Q_{nom}$, in the nominal range, K and B can be evaluated.

Applying those constraints and solving for K yields

$$E_{nom} = (E_{full} + K - A) - K \frac{Q}{Q - Q_{nom}} + A \cdot \exp(-B \cdot Q_{nom}), \quad (4.6)$$

$$K = [E_{full} - E_{nom} + A\{\exp(-B \cdot Q_{nom}) - 1\}] \cdot \left(\frac{Q}{Q - Q_{nom}} \right). \quad (4.7)$$

The same expression can be derived for the exponential region, yielding

$$K = [E_{full} - E_{exp} + A\{\exp(-B \cdot Q_{exp}) - 1\}] \cdot \left(\frac{Q}{Q - Q_{exp}} \right). \quad (4.8)$$

Finally, the two values of K can be set equal to each other, and an explicit solution for B can be found. With all of these quantities known, the equivalent transient model of the battery cell is complete and is represented in Figure 4.7.

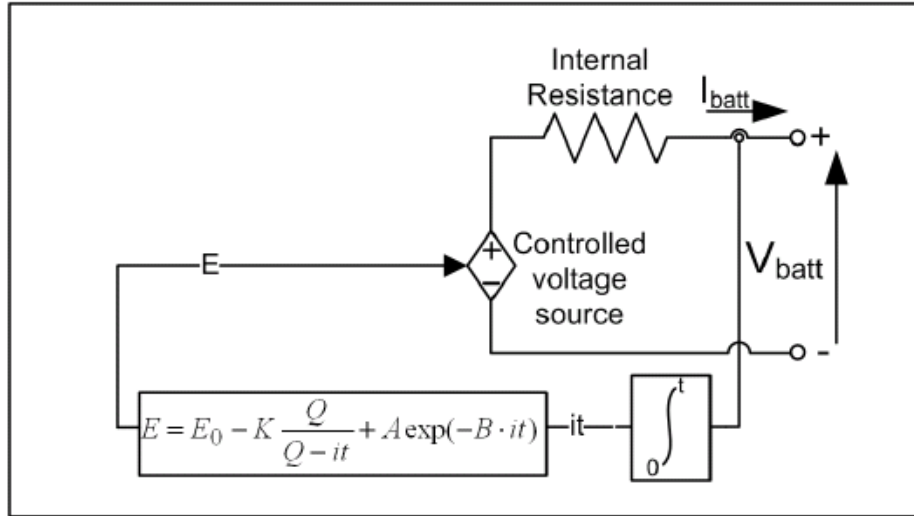


Figure 4.7: Equivalent circuit of a battery cell [23]

The last parameter in the model is the internal resistance of the battery. While this parameter is dependent on a number of factors such as cell temperature and rated charge/discharge rates, the cell resistance is typically given on vendor datasheets. With the cell model now defined, the cells can be scaled in series (voltage scaling) and parallel (current scaling) to meet the size requirement for the energy storage in the microgrid.

4.2.2 Battery Array Model and Implementation

The battery model for the microgrid serves 2 main purposes for the system. The primary purpose is to provide energy storage and supply load during low renewable resource availability. The secondary purpose is to provide a voltage, phase angle, and frequency reference to the microgrid when the main distribution network is offline. By implementing this secondary function into the design of the microgrid, a near seamless transition from grid-connected to islanded-mode

operation occurs. To accommodate this battery, the system must be centralized and located electrically close to the point of interconnection with the utility. Chapter 5 will discuss in detail the system-level microgrid layout. Control of the battery system charge & discharge rate is handled by the single phase inverter control. Chapter 5 provides more information on the power control system. For the sizing of the battery array, several factors need to be determined. First is the expected peak-output and duration the battery for all of the residential loads. The second factor is the level of reserve margin required to maintain reliability. Finally, the battery array output voltage must be determined such that cells are discharged at a safe rate and optimal efficiency of the battery array is maintained. The charge rate of the battery array can be calculated by determining when the maximum differential in power produced by the renewable sources and the power demanded by the loads occurs. This can be represented by

$$P_{source-max} - P_{demand} = P_{store} , \quad (4.9)$$

where

$P_{source-max}$ = Maximum power generated by the renewable resources,

P_{demand} = Demand of residential load during maximum power generation,

P_{store} = The power being generated that is directed to store in the battery array.

The charge rate of the battery can now be expressed as

$$I_{charge-max} = \frac{P_{store}}{V_{batt}} \quad (4.10)$$

Note the value of the battery voltage can be adjusted to limit the magnitude of the charging current. This is achieved by tying more individual battery modules in series to increase the terminal voltage. From the Sun Xtender datasheet guide, the maximum current discharge for a 24 hour battery system are less than 40 amps [26]. Using this constraint and referencing source and

load data curves in Section 4.5, the battery voltage is set to a nominal 125 Volts DC. The total energy storage of the battery of the can be determined from

$$E_{source} - E_{load} = E_{store} \quad (4.11)$$

Taking into account the efficiency of the battery system during charging, the effective stored energy is calculated as

$$E_{store} = (E_{source} - E_{load}) \cdot \eta_{batt} \quad (4.12)$$

A margin of 25% is applied on top of the final energy calculation. This provides contingency for atypical weather pattern and/or the loss of a generation unit. From the load data calculated in Section 4.5, the total amp-hour capacity of the battery is determined to be 750 Ah. Referencing the Sun Xtender® PVX-340T battery modules, the total array requires 10 batteries tied in series and at least 23 series strings tied in parallel [26]. This sums to a total of 230 batteries required for the central battery storage bank.

4.2.3 PSCAD Implementation and Verification

The model discussed in the 4.2.1-2 is implanted in PSCAD. Using the control block in PSCAD for constants, arithmetic, integration, and exponents the system in Figure 4.7 is implemented in PSCAD in Figures 4.8 and 4.9.

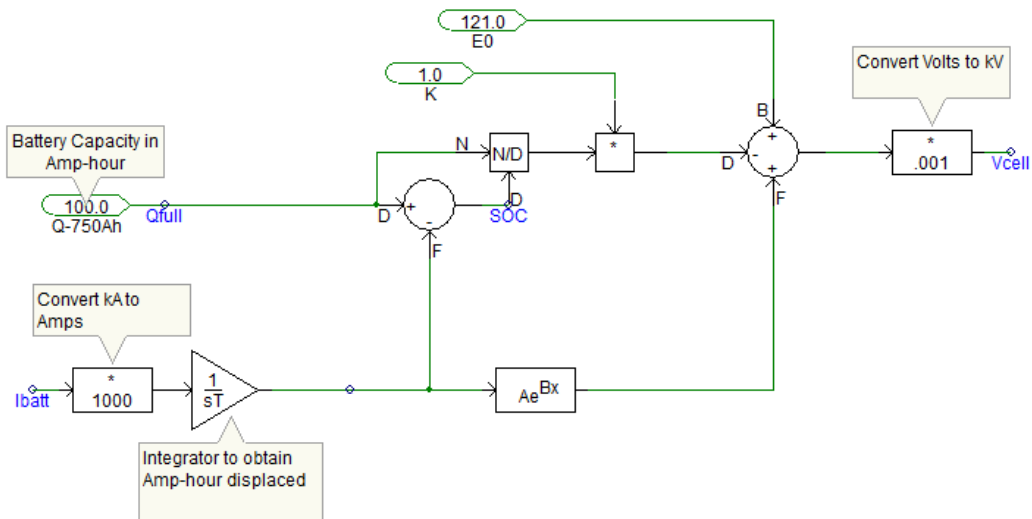


Figure 4.8: PSCAD Implementation of the Battery Model Control.

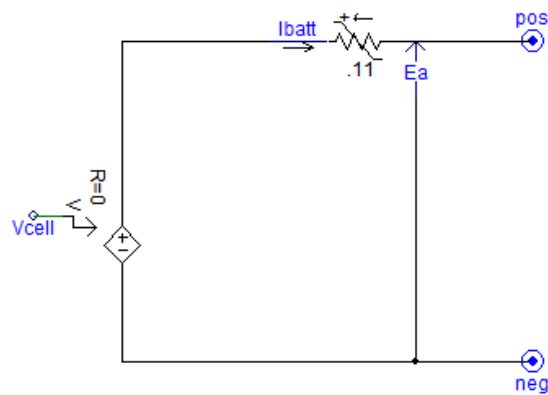


Figure 4.9: PSCAD Implementation of Battery System Equivalent Circuit.

While the inverter and controller of the battery system are covered in other sections, the performance of the battery system is shown in Figure 4.10. The response of the battery system from a change in operation from discharging to charging is depicted in Figure 4.10 with discharging power flow referenced as being positive.

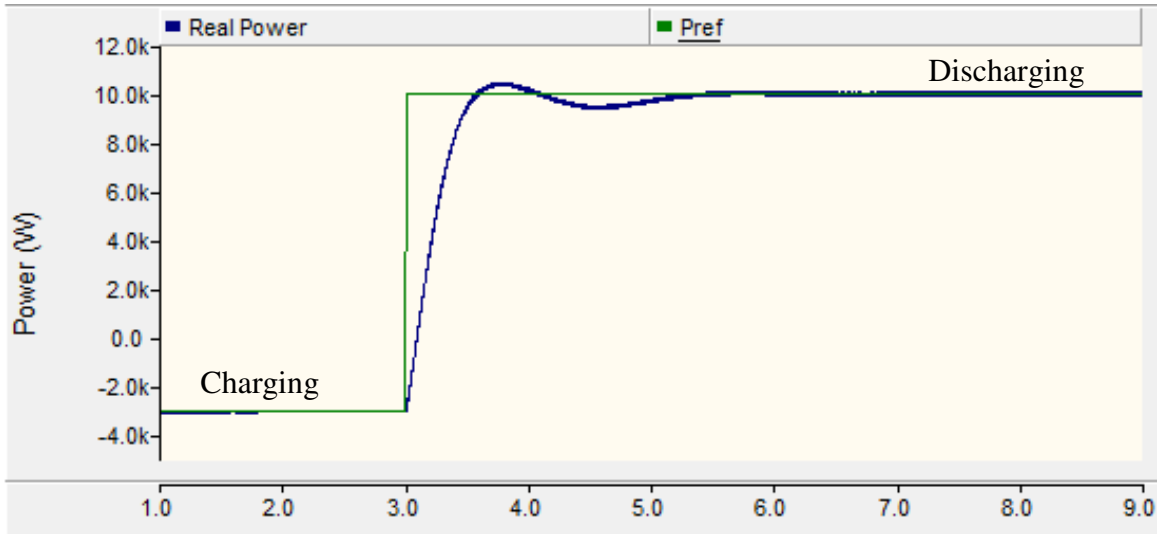


Figure 4.10: Response of Battery System from Discharging to Charging State

The system responds to the change in control input in a constant rate of change before settling to the new operating point within 2 seconds. The oscillations dissipate a few seconds later. Finally the efficiency of the battery system is given in Figure 4.11. The efficiency from terminal to delivered power, of the battery array at a maximum power output of 10 kW is nominally 94.5%. Note that high frequency oscillation in the efficiency shown in Figure 4.11 is due to inverter circuit switching.

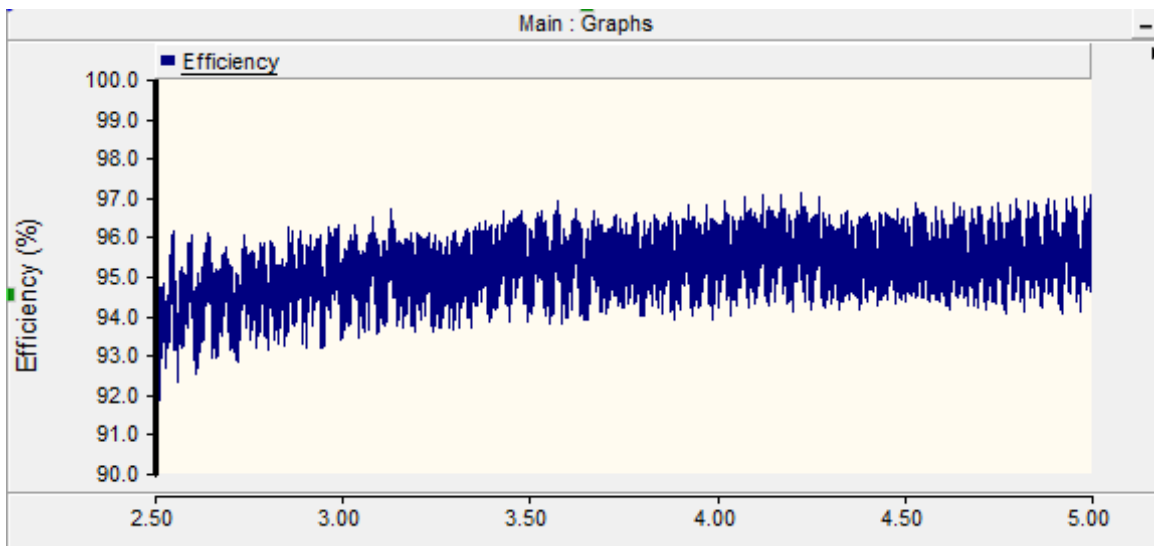


Figure 4.11: Battery System Efficiency at Nominal Discharge

4.3 Photovoltaic (PV) Model

The photovoltaic model implemented in this microgrid system is referenced from [27]. It is a classical PV model that uses a current source, series and shunt resistance, and a turn-on diode to represent the behavior of a single cell. The model will be verified against the parameters of commercially available BP Solar 200 Watt module.

4.3.1 Current Source Diode Model

Modeling of the PV array is performed by developing an equivalent circuit that represents the characteristic performance of the current–voltage (I-V) curve for a given panel. The I-V curve for the referenced panel is given in Figure 4.12.

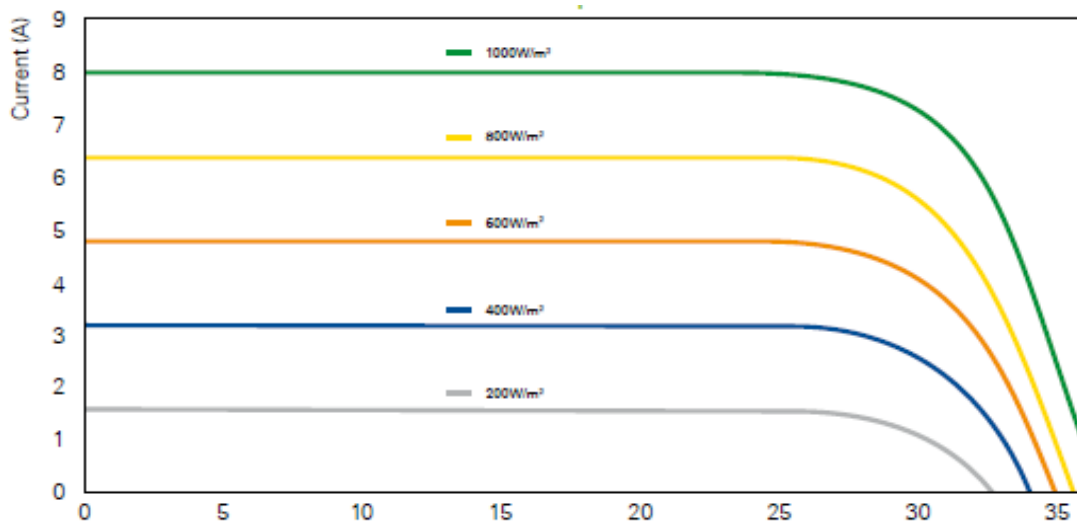


Figure 4.12: The I-V curve for a BP 220 Watt module [28]

The most common PV model used in electric transient modeling is the single diode/current source. In this model, the non-linear characteristics of the PV cell are captured in the diode turn-on voltage. More advanced models have been proposed in [29] – [30], which have multiple

diodes in series and parallel to represent the I-V curve characteristic of a PV panel. However, for this effort, the classical single diode equivalent circuit is implemented [27].

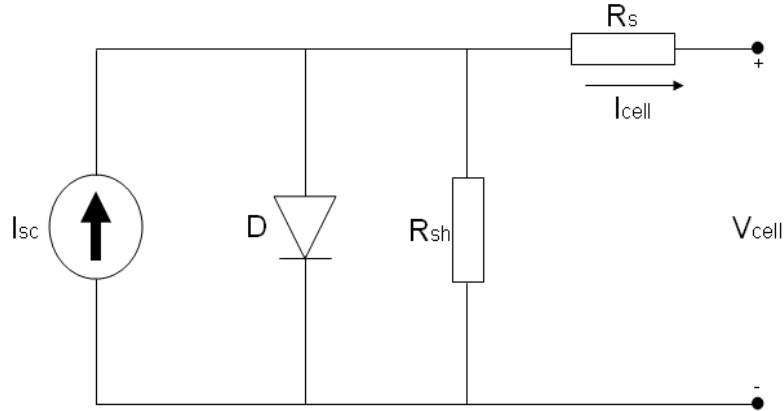


Figure 4.13: PV cell equivalent circuit model

To derive the values and/or dependencies for the equivalent circuit model, the following relationships are derived as:

$$I_{sc} = I_D + I_{SH} + I_{cell} \quad , \quad (4.13)$$

$$V_{cell} = I_{cell} \cdot R_S + I_{Rsh_s} \cdot R_{SH} \quad . \quad (4.14)$$

The current through the diode can be represented as

$$I_D = I_0 \cdot (e^{\frac{q \cdot V_D}{kT}} - 1) \quad , \quad (4.15)$$

where

I_0 = Diode saturation current (A),

q = Magnitude of electron charge (1.6×10^{-19}),

k = Boltzmann's constant (1.38×10^{-23}),

V_D = Diode turn-on voltage (V),

T = Cell temperature (K).

From 4.14, it can be seen that V_d can be represented as the sum of the cell voltage plus the drop across the series resistance. This results in the following expression

$$I_D = I_0 \cdot \left(e^{\frac{q(V_{cell} + I_{cell} \cdot R_S)}{kT}} - 1 \right). \quad (4.16)$$

Solving for cell current, the following relationship can be derived as [27]

$$I_{cell} = I_{sc} - I_D - I_{SH}, \quad (4.17)$$

$$I_{cell} = I_{sc} - I_0 \cdot \left(e^{\frac{q(V_{cell} + I_{cell} \cdot R_S)}{kT}} - 1 \right) - \frac{V_{cell} + I_{cell} \cdot R_S}{R_{SH}}. \quad (4.18)$$

Knowing the characteristics of the cell, all the parameters can be calculated that are needed for the model. The open-circuit cell voltage, not the general cell voltage, can be determined by using the previous equation, and realizing that the cell generates no current in the open circuit condition. Also, knowing that the shunt resistance is generally very large, it can be effectively ignored for equivalent circuit calculations. Therefore, the open circuit voltage can be determined as

$$I_{cell} = 0 = I_{sc} - I_0 \cdot \left(e^{\frac{q(V_{OC,cell} + 0)}{kT}} - 1 \right) \rightarrow V_{OC,cell} = V_{t,cell} \cdot \ln\left(\frac{I_{SC}}{I_0}\right), \quad (4.19)$$

where

$$V_{t,cell} = \frac{k \cdot T}{q} \quad (4.20)$$

Eq. 4.19 can now be used to solve the absolute diode current and eliminate that term from the short-circuit current expression

$$I_0 = I_{SC} \cdot e^{-\frac{V_{OC,cell}}{V_{t,cell}}}, \quad (4.21)$$

$$I_{cell} = I_{SC} - I_{SC} \cdot e^{-\frac{V_{OC,cell}}{V_{t,cell}}} \cdot e^{-\frac{(V_{cell} + I_{cell} \cdot R_S)}{V_{t,cell}}} = I_{SC} \left(1 - e^{-\frac{(V_{cell} - V_{OC,cell} + I_{cell} \cdot R_S)}{V_{t,cell}}} \right). \quad (4.22)$$

Equation 4.22 is the final expression for the cell current. Since the I_{cell} is also in the exponent, an explicit solution is not possible. Therefore, for numerical solvers in MATLAB are used to estimate the voltage & current pair. The next component to determine in the system is the series resistance. By definition, the cell resistance is given by the ratio of fill-factors times the ratio of open-circuit voltage to short-circuit current at standard test conditions (STC). This is expressed as follows [27]

$$FF_{STC} = \frac{P_{MPP,cell @ STC}}{V_{OC,cell @ STC} \cdot I_{SC,cell @ STC}}, \text{ PV cell fill factor at STC,} \quad (4.23)$$

$$FF_{0,STC} = \frac{voc_{STD} - \ln(voc_{STD} + .72)}{voc_{STD} + 1}, \text{ Fill factor with normalized STC,} \quad (4.24)$$

where

$$voc_{STD} = \frac{V_{OC,cell @ STC}}{V_{t,cell}}, \quad (4.25)$$

$$R_{S,cell} = \left(1 - \frac{FF_{STC}}{FF_{0,STC}} \right) \left(\frac{V_{OC,cell @ STC}}{I_{OC,cell @ STC}} \right). \quad (4.26)$$

The values for cell voltage, current, and maximum power can be determined directly from the manufacturer's datasheet for a given PV module. The final expressions needed for the model are the correction factors for changes in solar irradiance and cell temperature. The relationship between cell current and solar irradiance is directly proportional, whereas the relationship between cell temperature and open circuit voltage are inversely proportional. The correction factors, by definition, are given by

$$I_{SC,cell} = I_{SC,cell@STC} \left(\frac{G}{G_{STC}} \right) + \alpha(T - T_{STC}), \quad (4.27)$$

$$V_{OC,cell} = V_{OC,cell@STC} + V_{t,cell} \cdot \ln \left(\frac{G}{G_{STC}} \right) + \beta(T - T_{STC}), \quad (4.28)$$

where

α = Temperature coefficient of short-circuit current (A/° C),

β = Temperature coefficient of open-circuit voltage (A/° C),

T = Actual cell temperature (° C),

T_{STC} = Rated STC cell temperature (° C), typically 25° C,

G = Actual solar irradiance (W/m²),

G_{STC} = Rated STC solar irradiance (W/m²), typically 1000 W/m².

With the general PV model defined, the BP 200 specific parameters can be applied to the model for implementation in PSCAD.

4.3.2 Photovoltaic Sizing

Using the constraints of available rooftop square footage, panel cost, and optimal array orientation, the PV array can be sized appropriately. The electrical characteristics of the BP 3220 module are given in Table 4.1.

Table 4.1: Electrical Characteristics of the BP 3220 Panel [28]

Characteristic	Value @ STC
Footprint	18 ft ²
Maximum Power @ MPP	220 W
Voltage @ MPP	29.0 V

Current @ MPP	7.6 A
Short Circuit Current	8.4 A
Open Circuit Voltage	36.2 V

The PV array is scaled such that the PV array can supply the maximum daytime residential demand with additional margin in the event of an atypical irradiation and also to supply excess generation to the central battery array. Given these constraints, the PV array is sized for 3500 W maximum output. This requires a minimum of 16, 220 W panels to satisfy this output. However, the minimum of 16 panels is for normal operating parameters. The solar resource shown in Figure 4.5 is below the rated output of the panels. The standard rule of thumb for derating of a PV array for non-ideal solar resource is 125% DC to AC power ratio [31]. That is, 1.25 times the rated AC power output is required from the DC power rating of the array. As a result, the total number of panels required is 20 per array. The panels are tied in parallel to limit the magnitude of the voltage swing seen by the inverter. Therefore, the DC link voltage will be within 5 Volts +/- of the 29 V nominal MPP. With 20 panels in parallel, the maximum current through the DC link will be almost 120 Amps. This is relatively high given the size of the unit. While it will impact the overall efficiency of the inverter, it does allow for a relatively simple installation and configuration of the array. The total square footage of the PV array is 288 ft², which is sufficient for a standard home with ample space for spacing support structure for the panels.

4.3.3 PSCAD Implementation and Verification

The implementation of the PV array in PSCAD is realized through the control blocks and electrical elements. The PV Array equivalent circuit is shown in Figure 4.14.

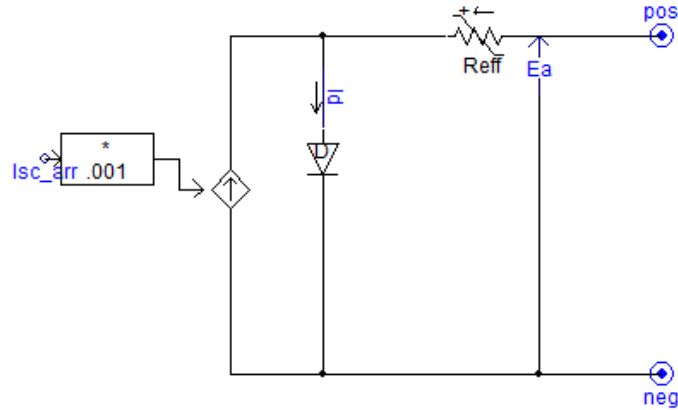


Figure 4.14: PV Array Equivalent Circuit Implemented in PSCAD

The calculation of the maximum power point in PSCAD is needed to determine the appropriate setpoint for the inverter. The calculation is based on the approximation that the MPP voltage occurs at approximately 73.3% of the open-circuit voltage [28]. Using this and filtering out the switching harmonics with a FFT block, the MPP calculation carried out as shown in Figure 4.15. It is important to note that MPP is tracked and calculated actively in modern inverter control systems; however the 73.3% approximation is sufficient for the scope of this research. The open-circuit voltage and short circuit voltage calculations are based on the equations given in 4.3.1. The PSCAD implementation of the OC-Voltage and SC-Current are given in Figure 4.16.

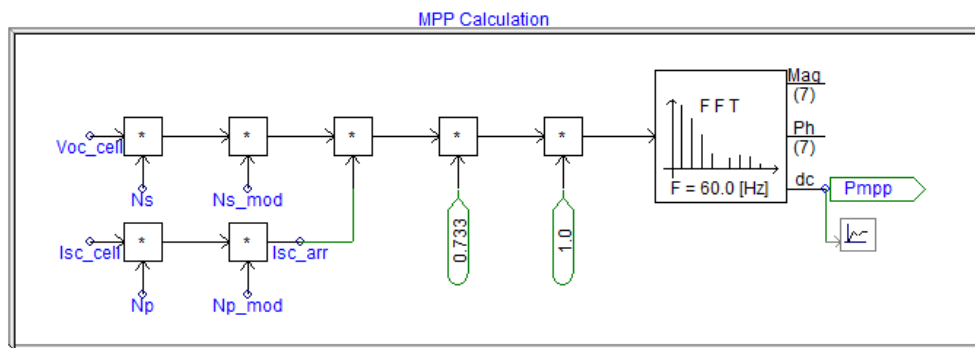


Figure 4.15: Calculation of the Maximum Power Point Implemented in PSCAD.

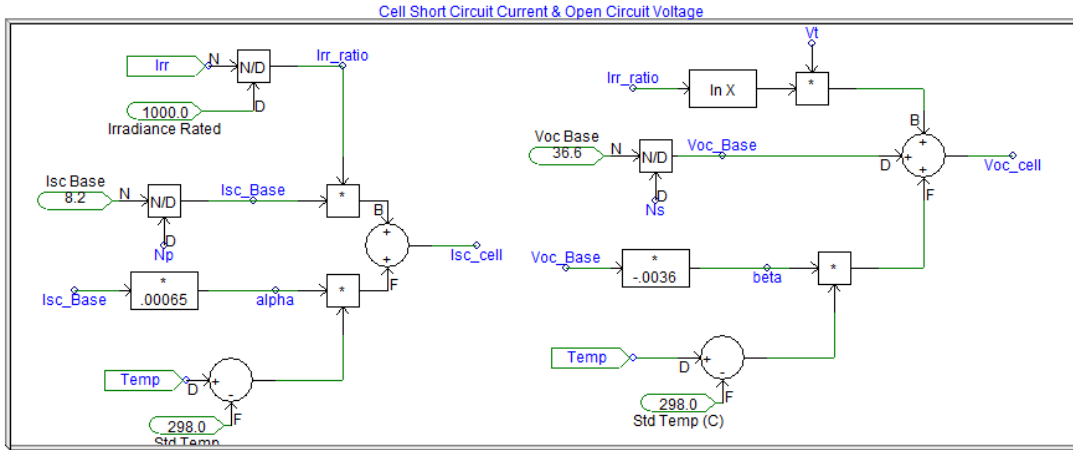


Figure 4.16: Short Circuit Current and Open Circuit Voltage Calculation in PSCAD.

The fill factor and resistance calculation are also implemented in PSCAD and are shown in Figures 4.17-18. The parameters vary as the configuration of the array changes

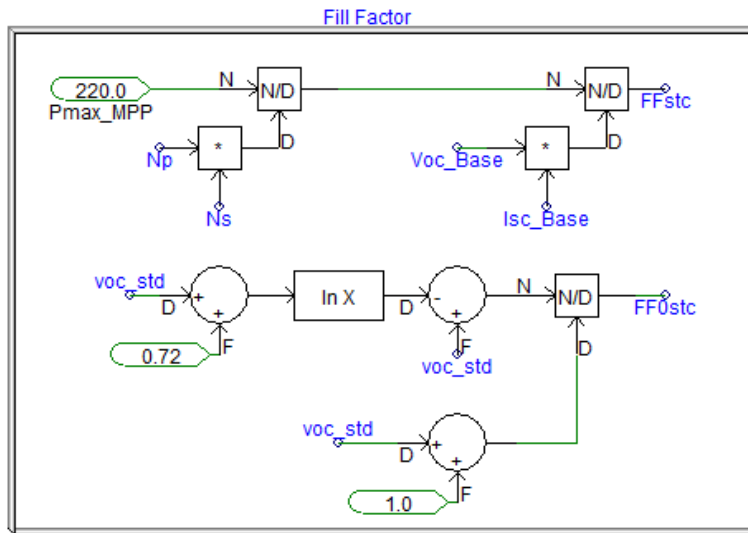


Figure 4.17: Fill Factor Calculation for the PV Array.

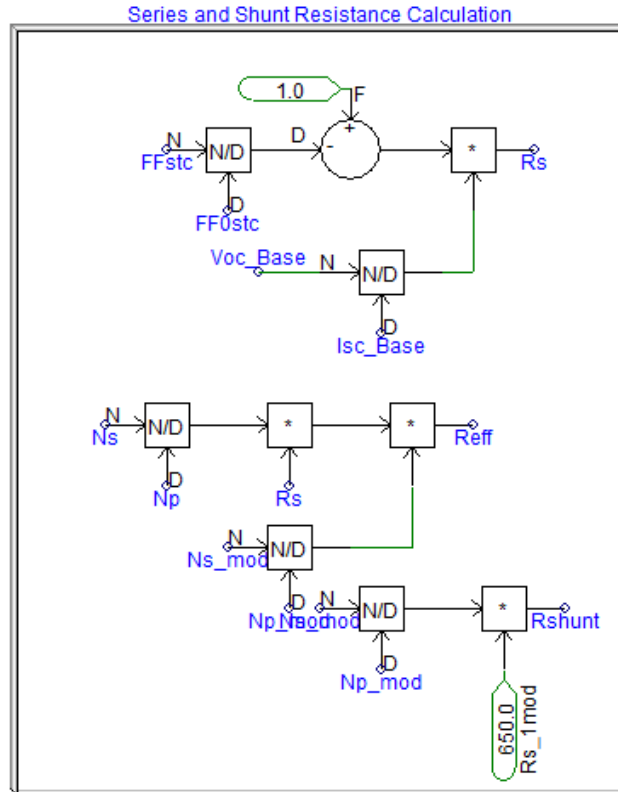


Figure 4.18: Calculation of the Series and Shunt Resistance of the PV Array.

With the full system implemented in PSCAD, the performance of the model is verified. The output of the PV array is dependent, primarily, on solar irradiance. As the solar irradiance varies, the power output will vary accordingly. Figure 4.19 shows the change in output power as irradiance varies. At time equals 5 seconds, the irradiance changes from a constant to a triangular wave with a 10 sec period as the output varied from 1000 to 600 W/m². The system responds accordingly with a slight lag due to the stored energy of the filtering. Finally, the efficiency of the PV array is verified at full power. The nominal efficiency, from the terminals of the panel to interconnection point, at maximum power is approximately 91.5%. Efficiency is higher at lower power levels due to reduced line current. This is shown in Figure 4.20.

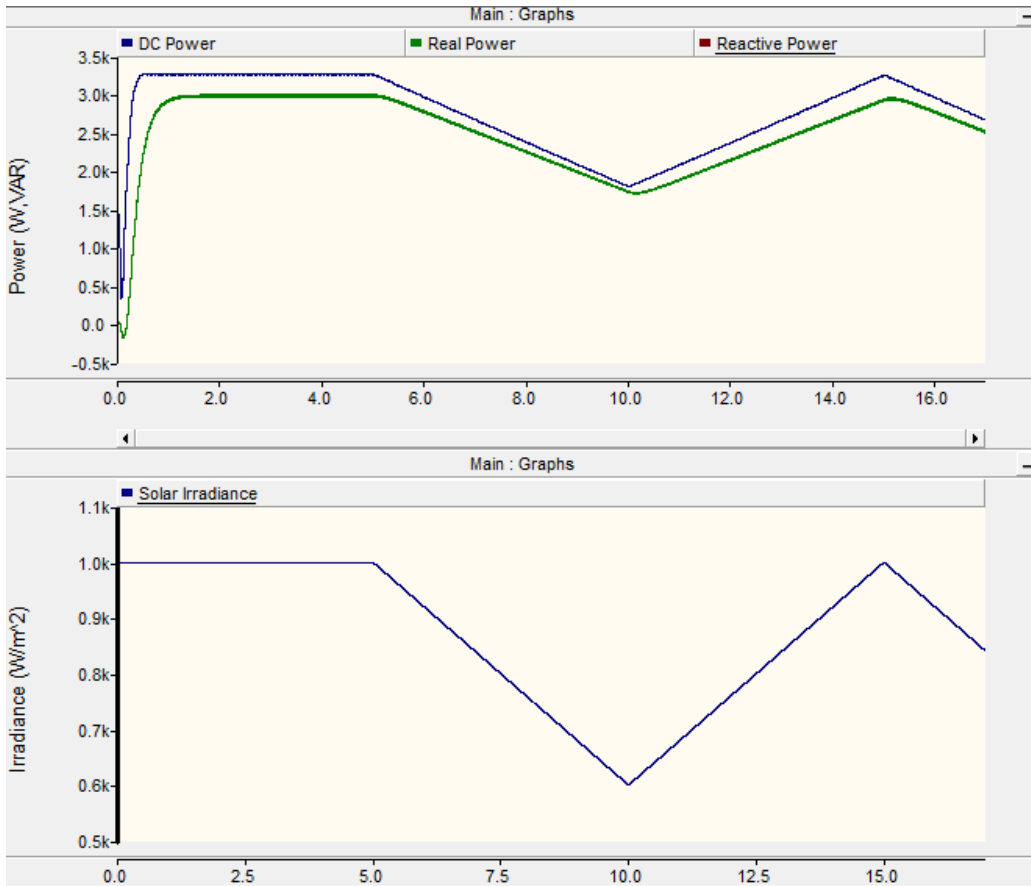


Figure 4.19: The Power Output Response to a Change in Solar Irradiance

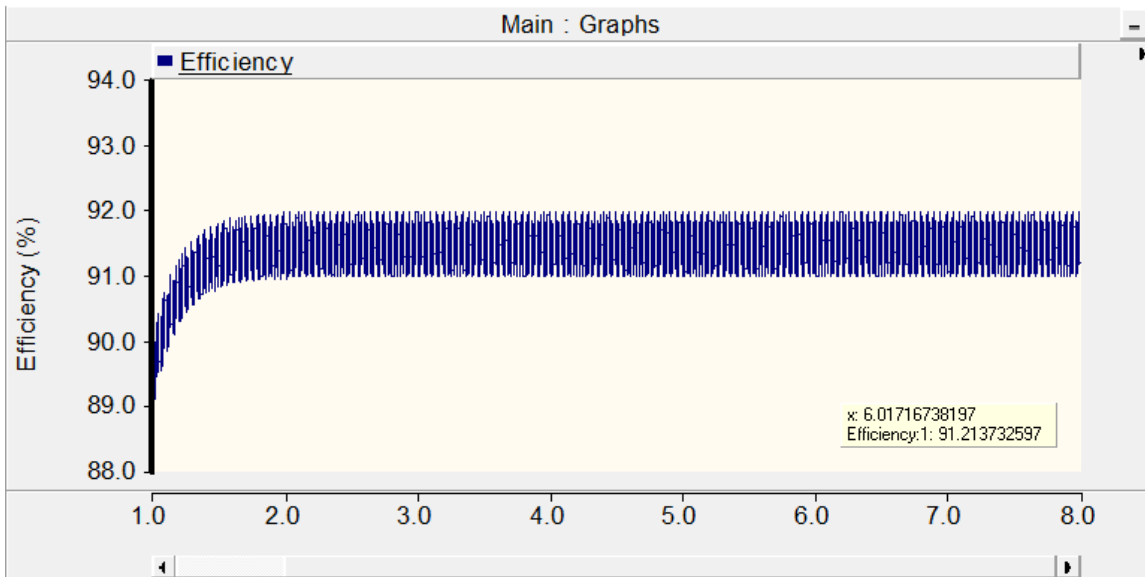


Figure 4.20: Efficiency of the PV Array System which Includes Inverter Losses

4.4 Wind Turbine Model

The wind turbine generator (WTG) model for the microgrid systems is partially referenced from [32] with several custom modeling features added. It is based on the permanent magnet machine characteristics for generators attached to a varying source. While the design of the wind turbine model is custom for this application, it does reference the Hummer Wind Power 5-kW unit to apply practical limits to the WTG [33]. This unit is also referenced because it uses an auto-adjusting yaw-drive axis, such that the turbine is always pointing in the direction of the wind. In a low energy resource area, like Florida, this feature is important because it allows for maximum energy harvesting in all wind directions, and also allows for a simpler model. Compared to the battery and photovoltaic model where there is a single model entity, the wind turbine model contains several discrete sub elements. The first is the wind turbine model which uses the input of wind speed to drive the power level output. The second is the permanent magnet generator which uses speed characteristics of the wind to vary the input torque to the generator and produce a 3-phase sinusoidal output. The final segment is the 3-phase rectifier and filter which rectifies to DC the output of the generator. Since these results in a significantly more complex model than the solar and battery system, a block diagram is given in Figure 4.21.

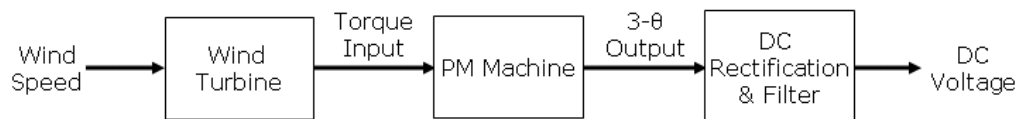


Figure 4.21: Block Diagram of the Wind Turbine Transient Model

4.4.1 Wind Turbine Transient Model

The first step in developing the transient model is to determine the equations that drive the transient model. The following sections cover the design of the individual sub-elements that make up the turbine model.

4.4.1.1 Wind Turbine Approximate Model

Wind power uses the kinetic energy from the flow of air mass to generate electricity. The relationship between the mass flow and the power produced is given by

$$E = .5 \cdot m \cdot v^2 . \quad (4.29)$$

This is the fundamental equation for kinetic energy. The energy of the mass of air through an area is given as the following:

$$E = .5 \cdot m \cdot v^2 = .5 \cdot (Avtp) \cdot v^2 = .5 \cdot Atp \cdot v^3 , \quad (4.30)$$

where

A = The area the flow of wind passes through,

p = The density of air (approximately $1.2 \text{ kg}/\text{m}^3$),

t = total time energy is produced.

Solving for power gives the fundamental wind power equation, which is expressed as

$$P = \frac{E}{t} = .5 \cdot p \cdot A \cdot v^3 . \quad (4.31)$$

The amount of energy extracted from the wind by the turbine depends on another important factor, namely the tip-speed ratio (TSR). The TSR is defined as the ratio between the speed of the turbine blade tip, time rotor radius, divided by the wind speed [34]. Finally we have

$$TSR = \frac{\Omega R}{v} , \quad (4.32)$$

where

Ω = The rotational speed of the tip,

R = The rotor radius,

v = The wind speed.

From the previous equation it can be seen that this parameter varies as the wind speed varies. In turbines with variable pitch, the tip speed ratio can be made relatively constant by adjusting the blade geometry to maintain a constant speed on the tip. For fixed pitch application, which is used in this implementation, the TSR will vary, while being at its maximum at rated power output of the turbine. The last parameter that needs to be considered for the model is the coefficient of power, C_p . The C_p is actually a ratio of extracted energy over total energy available. In a well-designed turbine, the C_p ratio will be over 40% at its rated power output. It is also a function of TSR. As the TSR varies, the C_p ratio will vary. The detailed relationship of these two quantities is beyond the scope of this thesis, but using the fundamental relationship between the two, the power Eq 4.31 can be further refined to take into account C_p as

$$P = .5 \cdot \rho \cdot A \cdot v^3 \cdot C_p(TSR), \quad (4.33)$$

where

C_p : Function of TSR.

For the implementation of the wind turbine in this model, it is important to realize that the full machine dynamics of the turbine can be approximated for the electrical transient model. This is important because it reduces the model complexity and decrease simulation runtime. Taking this into account, the model of the turbine is therefore simplified into a lookup table. The lookup table is based off the output of the Hummer Wind 5 kW turbine. Using the relationship between power and wind speed shown in Fig. 4.22, the turbine model can be expressed as transfer

function of wind speed to mechanical power. Through a lookup table, this model can be directly built into PSCAD (see section 4.4.2).

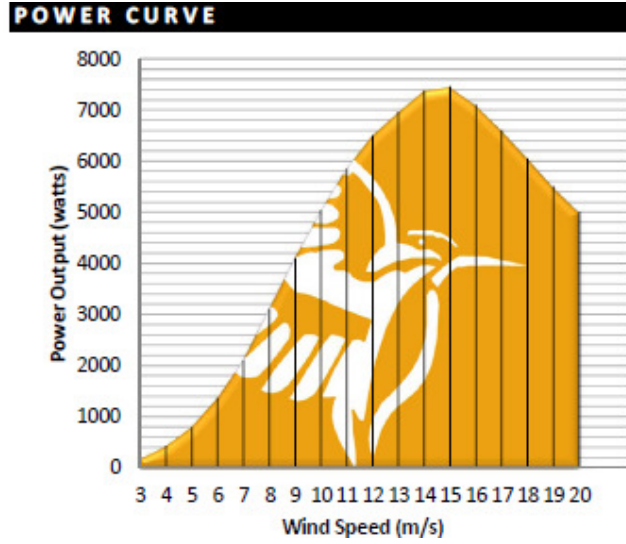


Figure 4.22: The Power Curve of the Hummer Power Unit [33]

4.4.1.2 Permanent Magnet Machine Model

The generator for the wind turbine is a permanent magnet (PM) generator. The latter is coupled to the wind turbine, typically through a gearbox, to transfer energy from the turbine to the generator. Its output varies as shaft torque and speed vary. This results in the generator outputting a variable frequency and voltage magnitude. For this research, the existing machine models in PSCAD are leveraged to develop the overall WTG model. The existing PSCAD machine transient model is based on the park transformation of electric machines. The equations that drive the model are given by

$$v_q = r_s \cdot i_q + \frac{d\lambda_q}{dt} + \lambda_d \frac{d\theta_r}{dt}, \quad (4.34)$$

$$v_d = r_s \cdot i_d + \frac{d\lambda_d}{dt} + \lambda_q \frac{d\theta_r}{dt}, \quad (4.35)$$

$$v_0 = r_s \cdot i_0 + \frac{d\lambda_0}{dt} = 0, \quad (4.36)$$

$$0 = r'_{kd} \cdot i_{kd} + \frac{d\lambda'_{kd}}{dt}, \quad (4.37)$$

$$0 = r'_{kq} \cdot i_{kq} + \frac{d\lambda'_{kq}}{dt}, \quad (4.38)$$

where:

$$\lambda_q = L_q \cdot i_q + L_{mq} \cdot i_{kq}, \quad (4.39)$$

$$\lambda_d = L_d \cdot i_d + L_{md} \cdot i_{kd} + \lambda'_m, \quad (4.40)$$

$$\lambda_0 = L_{ls} \cdot i_0 = 0, \quad (4.41)$$

$$\lambda'_{kq} = L_{mq} \cdot i_q + L'_{kq} \cdot i'_{kq}, \quad (4.42)$$

$$\lambda'_{kd} = L_{md} \cdot i_d + L'_{kd} \cdot i'_{kd} + \lambda'_m. \quad (4.43)$$

Section 4.4.2 shows the PSCAD implementation of the PM machine model, consolidated into a single block representation.

4.4.1.3 Three Phase Rectifier Model

From the permanent magnet generator, a rectifier is inserted into the circuit to rectify the output to DC. There are several rectification types that can be implemented for this application. Active rectification, where switching transistors are used instead of diodes to maintain a constant DC voltage through variations in the front-end AC voltage, are widely used now in a number of wind power electronics systems. However, given the relative small operating envelope that the PM generator operates in and the need to a simple model for runtime optimization, a classical diode rectification scheme is used. In the diode rectification model, the negative half-cycles are inverted to the positive side and results in a crude DC output. As shown in Figure 4.23, the

rectifier outputs a rippled DC output that requires further filtering. The output voltage for a full wave rectifier is the square-root of 3 times greater than the peak current as shown in

$$V_{DC} = V_{AVE} = \frac{3\sqrt{3} \cdot V_{peak}}{\pi} \cos(\alpha) \approx \sqrt{3} \cdot V_{peak} \cos(\alpha), \quad (4.44)$$

where

V_{DC} = The fully rectified DC voltage,

V_{AVE} = The average voltage of the rectified waveform,

V_{peak} = The peak voltage of one AC line-line input waveform,

α = Firing angle for the rectifier ($\alpha = 0$ for diode rectification).

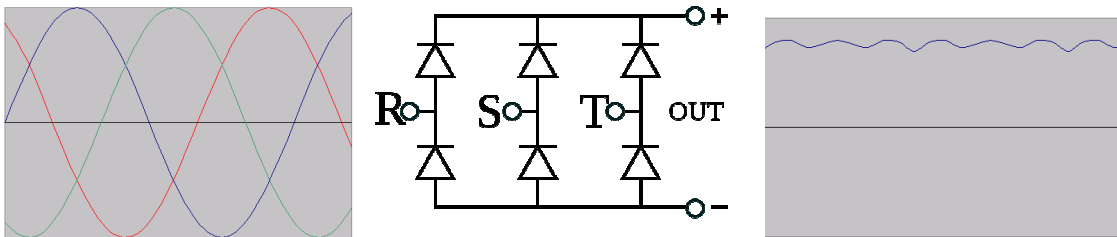


Figure 4.23: The Effect of a 3-Phase Full Wave Rectifier

Finally, the filter capacitors for the rectifier can be determined from

$$V_{ripple} = \frac{V_{peak}}{R_{load} \cdot C \cdot f}. \quad (4.45)$$

For this application, the DC link serves no purpose other than to feed the inverter. As a result, the inverter can accept a wide range of voltage inputs. It has the ability to boost low voltage input to maintain the fixed output voltage on the interconnection side. As a result, a voltage swing of up to +/- 5 Volts or a ripple voltage of 10 Volts is permissible. Like with the PV array, while a large voltage swing can be managed by building it into the inverter controller design, limiting the

swing to less than 10 volts reduces simulation sampling time and simplifies the controller. Using this constraint and referencing the Hummer Wind datasheet for nominal power output, the filter capacitor can be calculated as

$$C = \frac{V_{peak}}{R_{load} \cdot V_{ripple} \cdot f} = \frac{V_{peak}}{\left(\frac{P_{nom}}{V_{RMS}^2}\right) \cdot V_{ripple} \cdot f}, \quad (4.46)$$

$$C = \frac{48}{\left(\frac{5000}{(48/\sqrt{2})^2}\right) \cdot 10 \cdot 360} = .003072F = 3.072mF .$$

Note that the frequency of the full wave bridge is 6 times the fundamental frequency since all the peaks are inverted to the positive waveform. The frequency is therefore 360 Hz. The capacitance is rounded to the nearest decimal place. Therefore, 3 mF is an acceptable filter capacitor for the rectifier.

4.4.2 PSCAD Implementation & Verification

The three independent sub-elements in Section 4.4.1 are consolidated into the full wind turbine model that is implemented in PSCAD. The first segment is the wind turbine approximation model shown in Fig. 4.24. This model inputs the wind speed and outputs the per unit rotational speed of the turbine shaft based on a lookup table. The mechanical power generated is used to determine the setpoint for the inverter controller. The PM machine model is an existing model within PSCAD and one of the few consolidated models leveraged for this research as shown in Fig. 4.25. The PM machine model inputs a rotational speed from the turbine and outputs a 3-phase sinusoidal voltage. It also outputs the loaded electrical torque of the system for feedback to

the turbine, but it is not used in the application since the inverter load is set to match the turbine rated power.

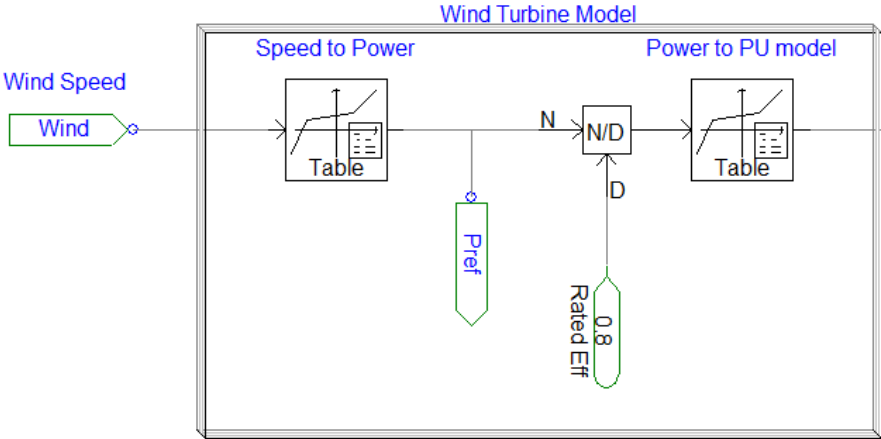


Figure 4.24: Wind Turbine Approximation Model

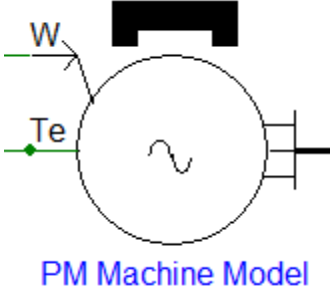


Figure 4.25: Existing PSCAD PM machine model.

Finally, the full wave diode bridge and filter capacitor, with equivalent ESR, are shown in Figure 4.26.

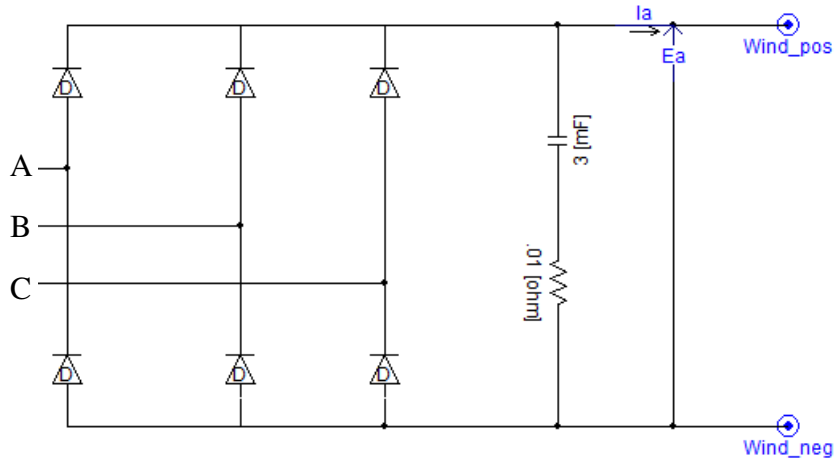


Figure 4.26: 3-Phase Rectifier Bridge for Wind Turbine Model

The model performance is verified by looking at the steady-state and transient response of the turbine model to changes in wind speed. Electrical transient events are covered in Section 4.6. The response of the real power output and reactive power load of the wind turbine is shown in Figure 4.27. From that figure, it can be seen that the power output follows the change in wind, but with a sharper slope since the power generated is the cube of the wind speed.

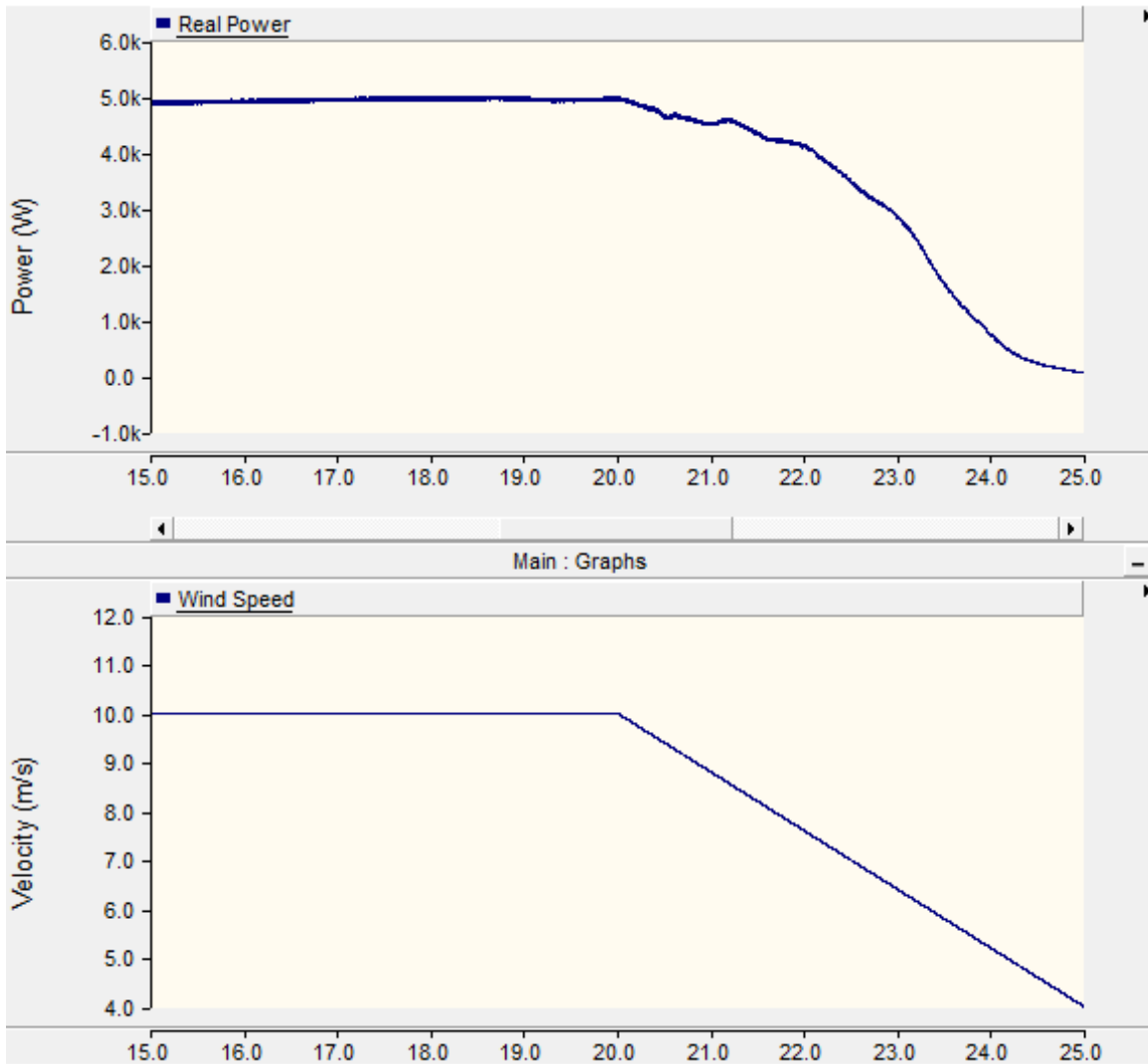


Figure 4.27: Wind Turbine Response to a Change in Wind Speed

Finally, the efficiency of the wind turbine is verified at nominal power. The nominal efficiency, from mechanical shaft power to electrical point of interconnection, at maximum power is approximately 79%. While the efficiency is relatively low, it is accurate of the specification of the Hummerwind 5 kW unit. Higher efficiency can be achieved with large turbines, but this is not part of the scope of this research. This is shown in Figure 4.28.

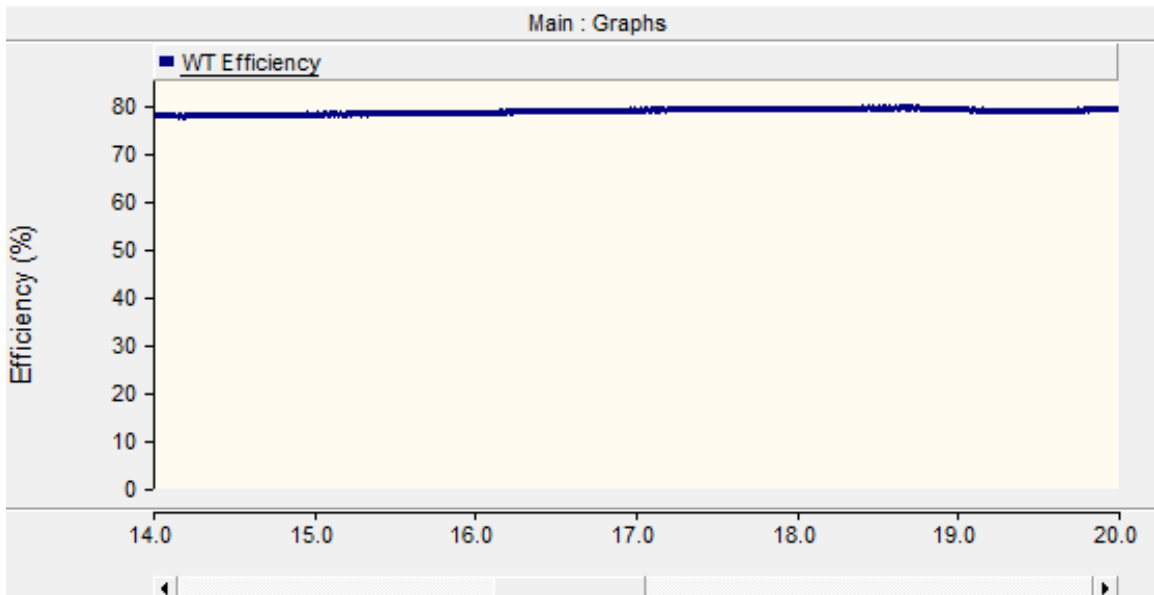


Figure 4.28: Efficiency of the Wind turbine System which Includes Mechanical, Generator, Rectifier, and Inverter Losses

4.5 Residential Load Model

For a long term islanded microgrid, management of the load is needed for power reliability. A typical household load with heavy load duty cycles with inefficient appliances makes the implementation of a long duration, fully renewable, microgrid impractical. To support this implementation, a high efficiency residential load is required. The residential load model has several key features such as high efficiency HVAC, refrigeration, solar water heating, high efficiency windows, and nighttime auto-switches for consumer electronic loads. Another important feature of the residential load is the ability of external load switching from the master power management controller (PMC). This is required for emergency events when the battery array is at a significant state of discharge and the renewable sources are unavailable to pick-up the load. Under this scenario, the PMC will remotely switch-off various loads to conserve the available energy in the battery system until the emergency condition has subsided. This demand

management helps protect the microgrid from a complete system wide loss of power. To determine the savings from a high efficiency home, the NREL-UCF report [35] on “smart homes” in Florida is consulted. In this report, a control home and a high efficiency home are referenced to determine the level of financial savings achieved from a high efficiency home with rooftop solar PV panels installed. The comparison of the control home and the high efficiency home are shown in Figure 4.29.

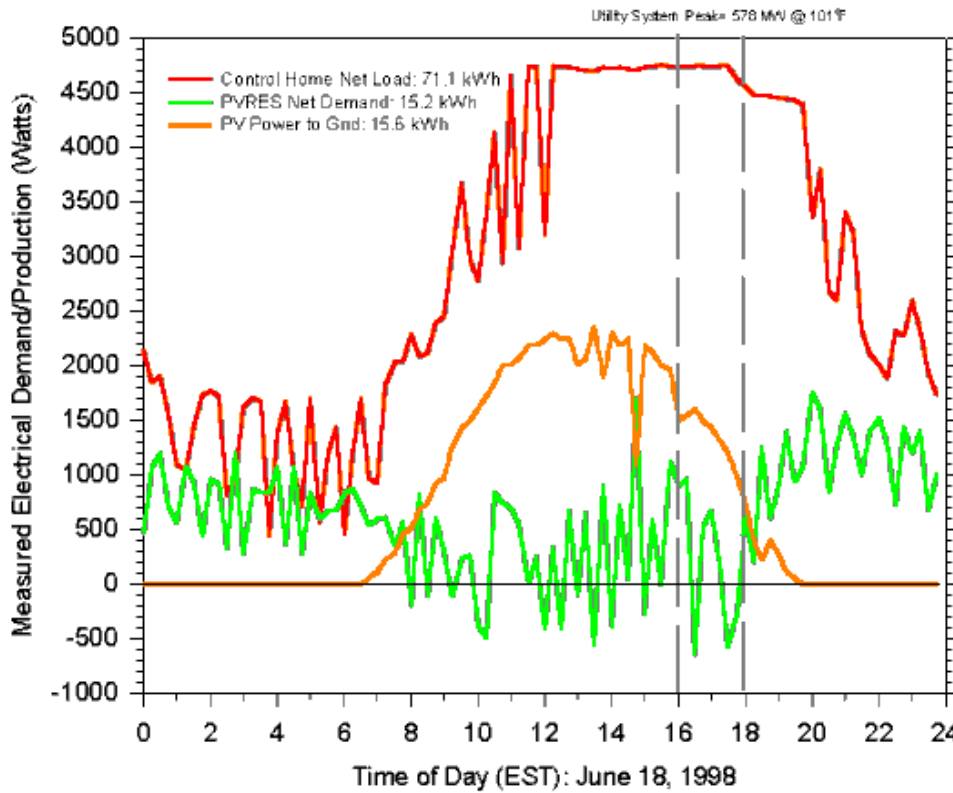


Figure 4.29: Hourly Energy Consumption Profile of a Standard Home and Home with PV and High Efficiency Appliances [35]

According to the report, the high efficiency consumes 55% less energy throughout the day than the standard home. This savings is applied across the yellow demand curve depicted in Figure

4.29. This results in the demand load profile in Figure 4.30. For a single home, the nameplate generation from sections 4.3 and 4.4 give 8.6 kW of generation and 2.3 kW peak demand from the residence. The surplus of generation is made up for by the inconsistent wind resource in Florida, the need to store energy in the central battery array, and 50% margin for loss of up to 2 renewable sources in the microgrid. As a result, for a single residence, the average hourly wind, solar, and demand are plotted together in Figure 4.31. The total energy generated versus energy consumed is shown in Figure 4.32.

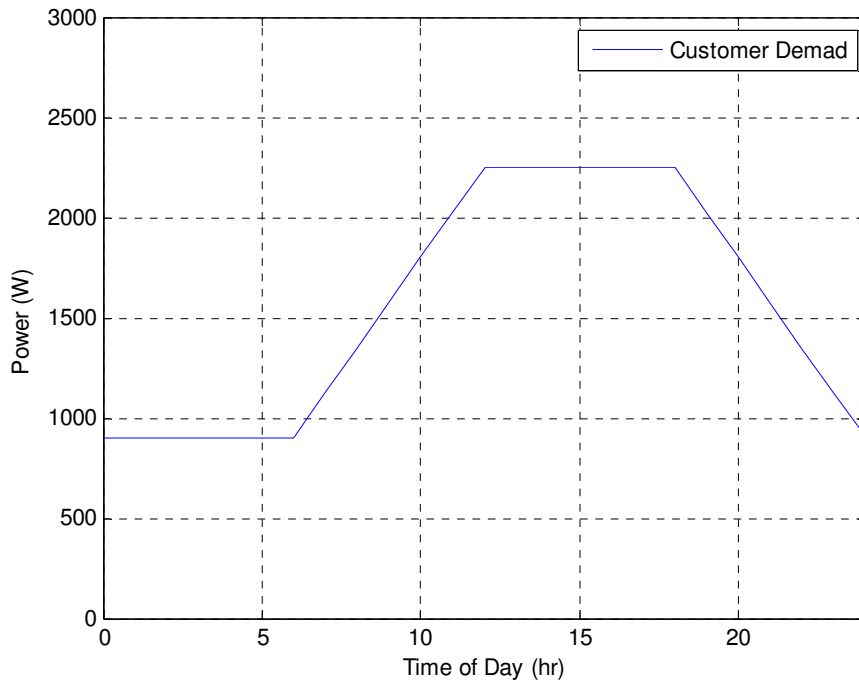


Figure 4.30: Hourly Demand Curve for High Efficiency Microgrid Home

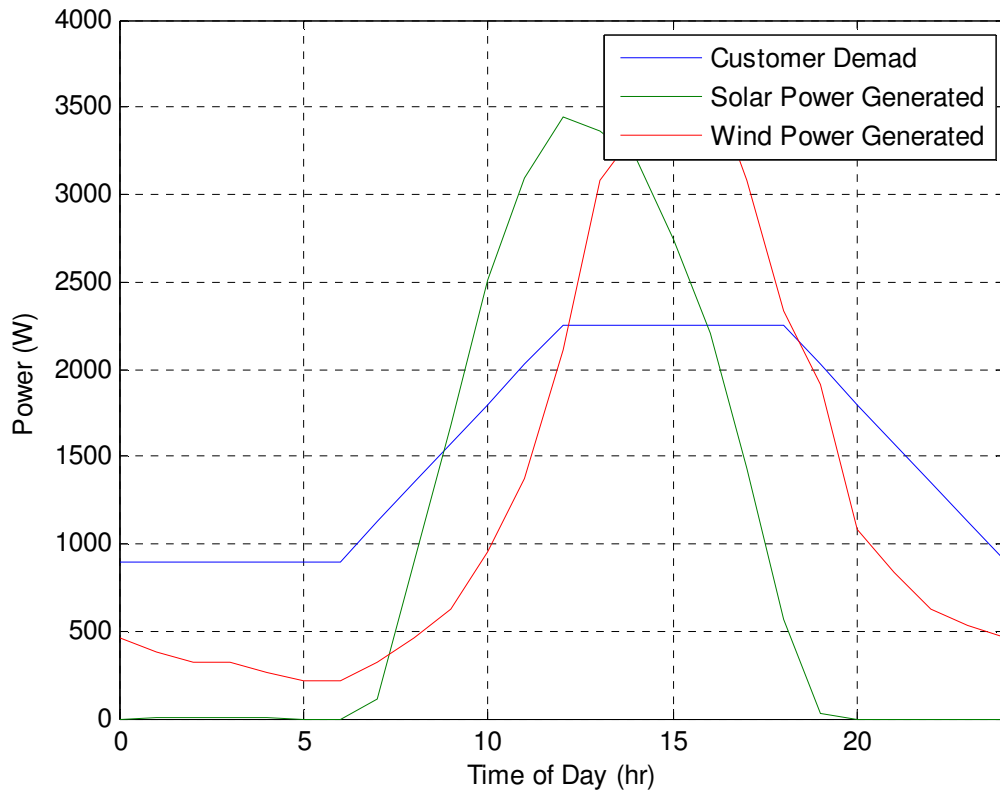


Figure 4.31: Single Residence Average Hourly Generation and Demand Profile

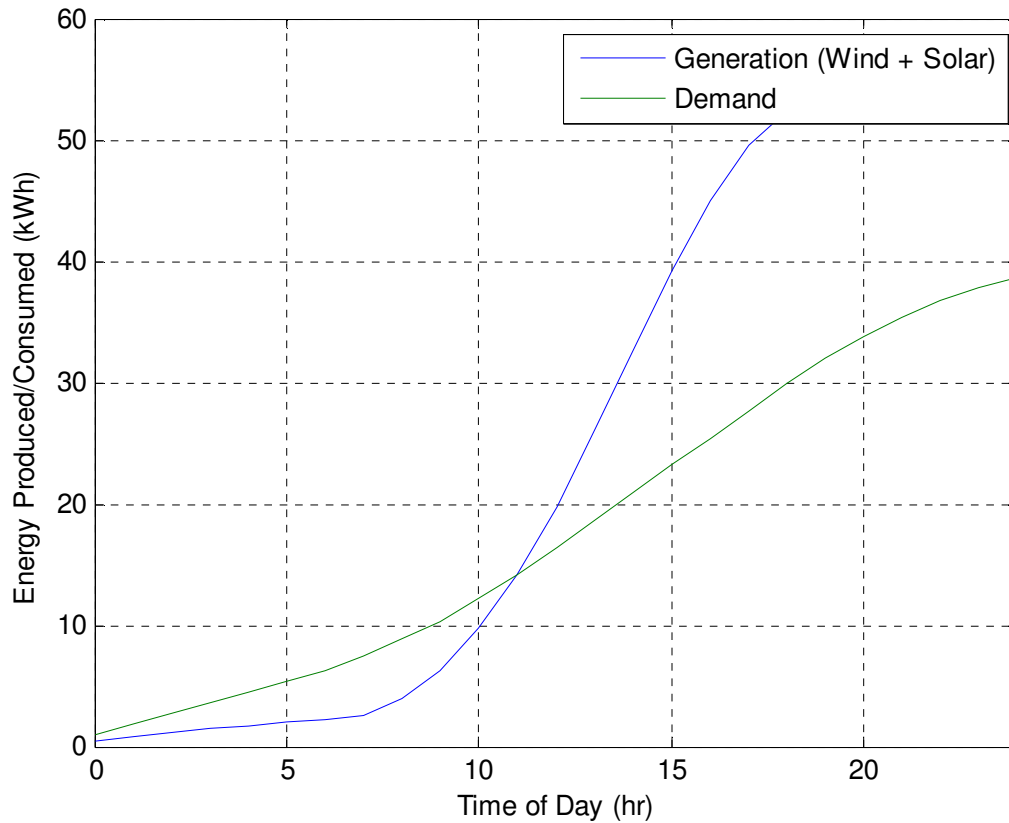


Figure 4.32: Total Average Energy Generated and Consumed in a Single Residence

In Figure 4.32, it can be seen that during the early nighttime hours, generation is less than demand and energy must be pulled from the central battery array. After approximately 10 am the generation and load become equal and afterwards generation becomes greater in demand. The excess energy is either stored in the battery array, or one or more generation units will be turned off to meet demand. This forms the basis of the residential demand model. Note that this is the typical case, and margin is provided to correct for sustained periods of abnormal operation.

Chapter 5

Microgrid Control System

This chapter provides an overview of the layered control system for the microgrid. The controller utilizes top level control through the power management controller (PMC) that regulates system-wide power flow and local control through PQ power regulation with droop control. The PMC implemented balances supply and load with available resource and battery capacity. The PMC presented in this thesis is an introductory step in the design of this style of microgrid control. Droop control for island mode operation is also covered in this section.

5.1 Concept of Operation

The microgrid is designed to operate in two principle modes of operation: grid-connected and island mode. Since this particular application is for disaster recovery, the emphasis is on sustainable island mode operation. The control system is tiered such that local droop control are contained with the generating units and higher level dispatching is centralized. Figure 5.1 shows the control pyramid for the microgrid.

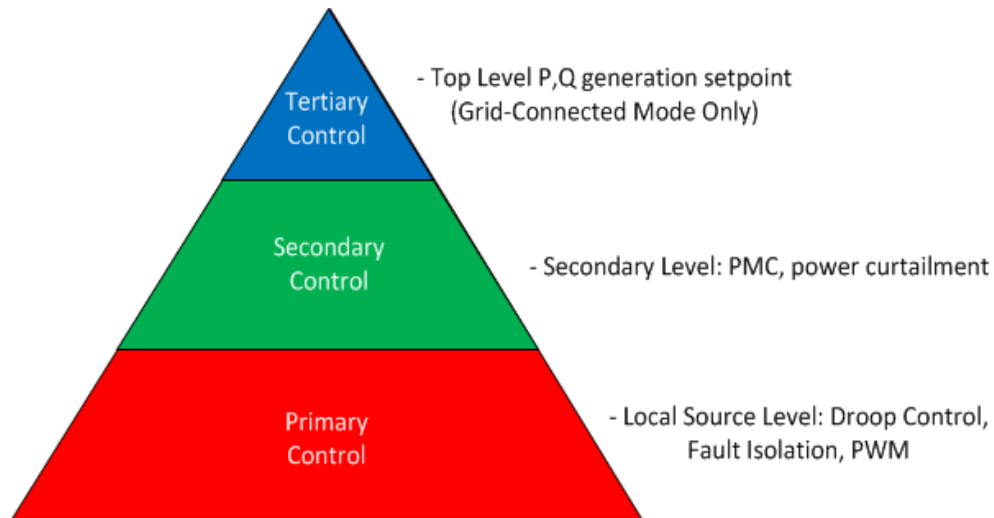


Figure 5.1: Top-Level Controller Hierarchy

For both modes of operation, the inverters for the renewable sources set their power flow based off a reference voltage and phase angle. In the case of grid-connected mode, this is the distribution voltage at the common bus. In the case of islanded mode, the reference is the output of the battery inverter module. Because of this, it is the principle operation of the battery to emulate the behavior of the distribution network during island mode. Therefore the battery system shall maintain a relatively constant voltage as the units are brought online and be able to deliver power or absorb power depending on the level of power being generated. These two modes of operation are illustrated in Figure 5.2.

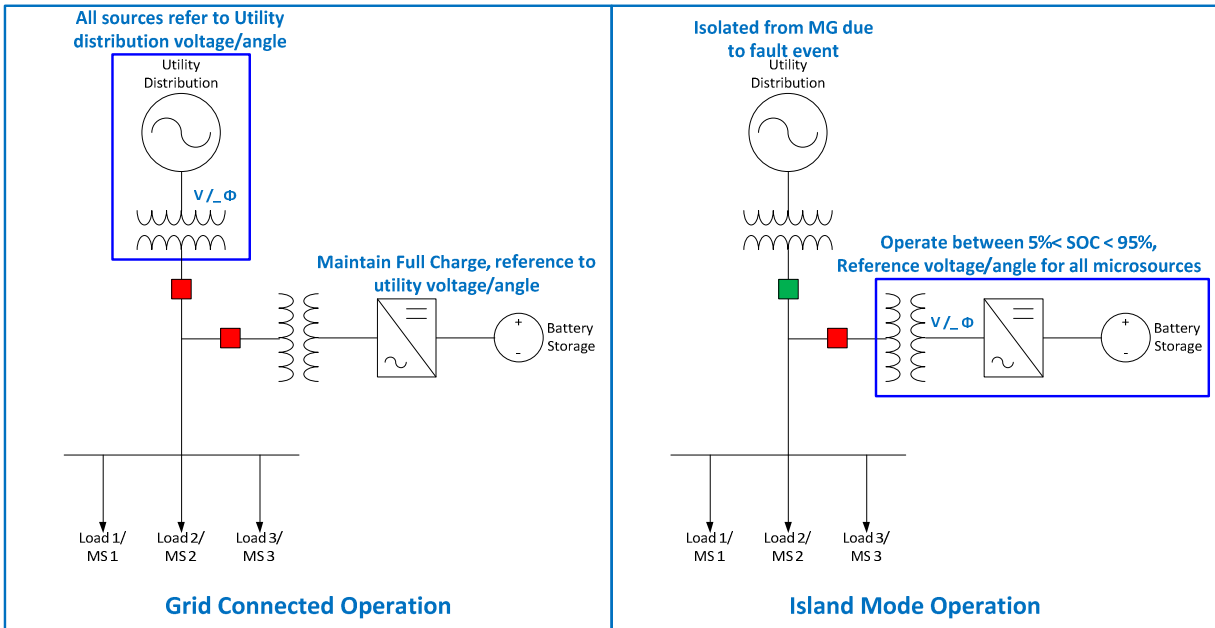


Figure 5.2: Microgrid Operation and Reference Points

For both modes of operation, the battery will be able to quickly respond to transient events through inverter control. Figure 5.3 shows the battery inverter notional power control waveform. The PQ control algorithm for the inverter allows for the output to be varied according to these 3 parameters.

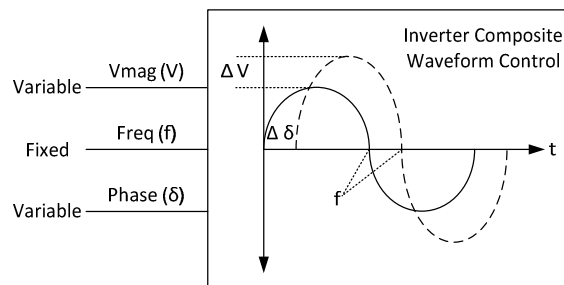


Figure 5.3: Battery Inverter Control Concept of Operation

5.2 Inverter Model

The fundamental hardware element of the microgrid control is the inverter. The latter handles real power and reactive power flow to and from the sources connected to it. The inverter model implemented for this research is the H-Bridge single-phase inverter. This inverter design is advantageous over other single-phase inverter designs, primarily because it allows for variable sinusoidal voltage output with only half of the peak-peak voltage applied on the DC link. This results in switching at much lower voltages. Figure 5.4 is referenced from [36] and shows a typical configuration for an H-Bridge inverter from DC source to grid connection. The inverter model and controller design for this research provides for a low level of fidelity and design details. In chapter 8, recommendations are made to improve the controller design and include bandwidth limitation, hardware constraints, and higher order filter design. However, the proposed inverter model for this research is sufficient for analytical studies.

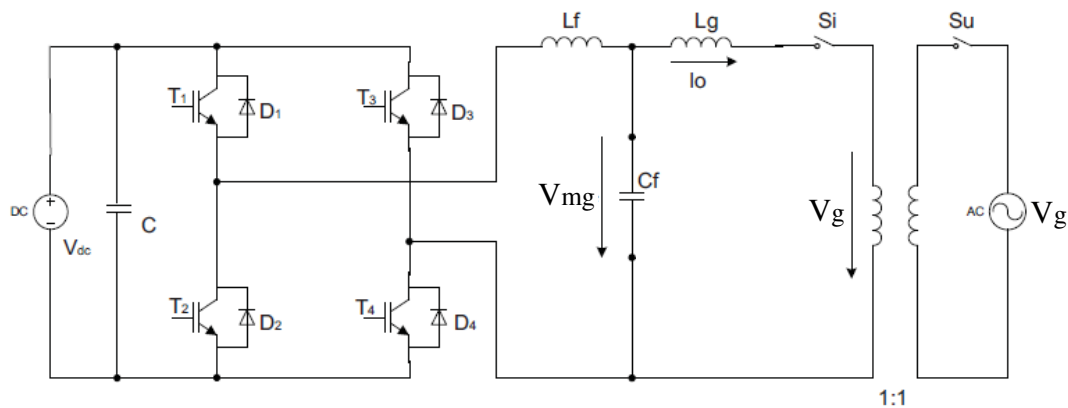


Figure 5.4: H-Bridge Inverter with Filtering and Grid Connection

5.2.1 Inverter Design

The inverter hardware design consists of the power electronics bridge, filter, and isolation transformer. The bridge consists of 4 transistors, with fly-back diodes, switching at 10 kHz. This

switching frequency was selected to reduce the size of the filtering. While ideally the switching frequency should be set as high as possible to reduce filtering, it must be traded with physical limitations of the circuit and latency of the switching controller. For the simulation, the switching time should be limited such that the simulation runtime does not become excessively long. The nominal output voltage for the bridge is 48 volts nominal for the renewable sources. This voltage is selected to match the nominal voltage of the renewable sources and limits the size of the flyback diodes for switching transients. For the battery array, 125-V nominal is selected due to its requirement of being able to charge and discharge into the entire microgrid. The only changes between the hardware of the 48-V and the 125-V bridge are the filtering devices and the isolation transformer sizing.

The inverter bridge is designed to be universal between the 3 sources (i.e. PV array, WT, and battery array). Therefore, its maximum power rating will be based on the maximum power flow through the battery array. The maximum load of the battery system is 7.5 kVA nominal.

Allowing for 33% additional margin for short term transients, the maximum size of the inverter is 10 kVA. For the 48-V bridge design, this results in a maximum current flow of 208 A and 80 A for the 125 V bridge.

The switching devices used for this inverter are insulated gate-bipolar transistor (IGBT). The IGBT is a versatile power electronics device that is well suited for power switching applications. In Figure 5.5, it can be seen that IGBT meets the requirements for the inverter bridge defined in this section (i.e. 48V/125V, 10 kVA, and 10 kHz switching).

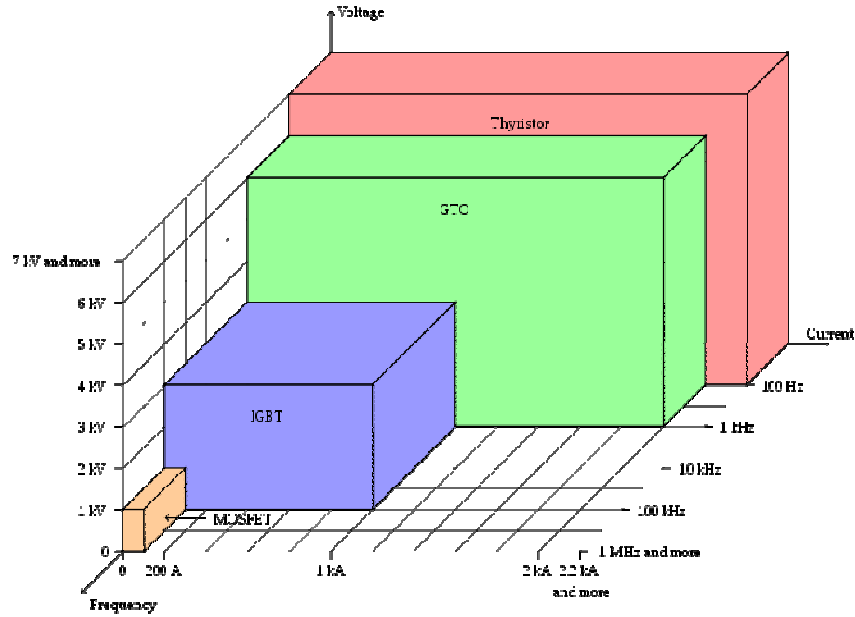


Figure 5.5: Power semiconductor capability chart [37].

Finally, an isolation transformer is required, as shown in Figure 5.3. Since the H-Bridge by design is ungrounded, a ground reference must be provided on the secondary side for interfacing the inverter to the existing residential distribution. Another reason for the isolation transformer is to step up the bridge voltage to the residential distribution level voltage level. In the U.S., residential homes are serviced by a medium voltage feeder that steps down, through a transformer, to 120/240 V inside the residence. The microsources will interconnect on the 240 V side on of the residential feeder. As a result, the transformer has turns ratio of 48 V / 240 V for the PV & WT sources and 125 V / 240 V for the battery storage array. With the hardware elements fully discussed, the summary of the inverter design is given in Table 5.1.

Table 5.1: Inverter Hardware Specification

	PV Array and WT	Battery
Voltage	48 V	125 V
Power Rating	10 kVA	10 kVA

Current	208 A	80 A
Switching Frequency	10 kHz	10 kHz
Power Semiconductor	IGBT	IGBT
Isolation Transformer	48 V / 240 V	125 V / 240V

The last element of the hardware design, which also feeds the controller design, is the LC filter.

It is discussed next.

5.2.2 LC Filter Design

A well designed filter is important for reducing harmonics generated by the bridge. It allows margin for reactive power control, and maintains stability through transient events. For this application, a traditional LC filter is selected. The LC filter provides blocking of high-order harmonics through a low-pass filter. The filter is tuned such that the 10-kHz switching and all associated odd number harmonics are filtered out while maintaining the fundamental sinusoid.

The resonance frequency of the filter is given by

$$f_{res} = \frac{1}{2\pi\sqrt{LC}}. \quad (5.1)$$

The resonance frequency ideally defines the spot where the frequency components below frequencies are passed through and components above are blocked. In a real filter, the resonance frequency represents the point where blocking begins and signal attenuation continues until the higher frequency harmonics are at a negligible power level. The gain of the filter is important as well for understanding the impact of the filter on system output. As shown in [38] the filter gain is expressed as

$$G(s) = \frac{v_2(s)}{v_1(s)} = \frac{1}{1 + \frac{s}{Q\omega_0} + \left(\frac{s}{\omega_0}\right)^2}, \quad (5.2)$$

where

$\omega_0 = 2\pi f_0$ the resonance frequency of the filter,

$Q = R\sqrt{\frac{C}{L}}$ the quality factor of the filter.

The Q factor is used as part fo the design criteria. A Q factor larger than 0.5 results in an underdamped system where a change in input will result in a sinusoidal and exponential decay to the new settling value. However, for very large values of Q, the greater the amplitude and the longer the settling time. As a result, the filter is designed such that the Q value is optimized. For determining the value of L and C, the following constraint for a well designed LC filter for AC inverters is applied [39]:

$$10\omega_0 \leq \omega_{res} \leq \frac{\omega_{sw}}{2}, \quad (5.3)$$

$$C = \frac{\alpha \cdot P}{\omega_0 \cdot V_{rated}^2}, \quad (5.4)$$

where

ω_0 = Rated AC frequency of inverter (377 rad/sec),

ω_{sw} = Switching frequency of the inverter bridge (62,381 rad/sec),

α = Reactive power factor (<5% for WT & PV array, 15% nominal for battery).

The filter capacitance for the battery array was determined for the battery array and WT & PV inverter filters was determined and shown in Table 5.2. The value of the inductance is found using the equation given in Eq 5.1. Through iteration to find the appropriate resonant frequency,

that satisfies the constraint in Eq 5.3, the values for inductance are given in Table 5.2. The full design of the filter design is given below. The value of Q is sufficient for both applications and the filter resonant frequency satisfies all constraints.

Table 5.2: LC Filter Specification

	Battery Array	WT & PV Array
ω_{res}	750 rad/sec	2,250 rad/sec
L	150 μ H	50 μ H
C	300 μ F	100 μ F
V	125 V	48 V
P	10 kW	5 kW
Q factor	2.21	0.65

5.2.3 Inverter PQ Controller

The controller for the inverter is based on the PQ control theory for power flow-calculation [36]. It provides the fundamental relationship between real power and phase angle, as well reactive power and voltage differential. The relationship for power flow through an arbitrary point on an electrical network can be stated as

$$P = \frac{V_{mg} \cdot V_g}{X} \sin(\delta), \quad (5.5)$$

$$Q = \frac{V_{mg}^2 - V_{mg} \cdot V_g \cdot \cos(\delta)}{X}, \quad (5.6)$$

where

V_{mg} = The AC voltage of the microgrid source,

V_g = The AC voltage of the point of interconnection,

δ = The phase angle difference between the two voltages,

X = The impedance of the equivalent inductance between the two voltages (usually a transformer).

From Eqs. 5.5-5.6, the values of V_g and X are fixed by the network and are not practically adjustable. However, the values of V_{mg} and δ are directly controllable by adjusting the PWM sequence feeding into the IGBT bridge. The relationship between varying these two parameters can be seen by taking the partial derivatives of the previous equations. For varying V_{mg} and δ , the effect on real and reactive power are determined by deriving their partial derivatives with respect to these variables, yielding

$$\frac{\partial P}{\partial V_{mg}} = \frac{V_g}{X} \sin(\delta), \quad (5.7)$$

$$\frac{\partial P}{\partial \delta} = \frac{V_{mg} \cdot V_g}{X} \cos(\delta). \quad (5.8)$$

It can be seen from Eq 5.7 that varying the voltage has no impact on the power output, for small deviations, due to the term being eliminated by the partial derivative. However in Eq. 5.8, it can be seen that varying the phase angle has an impact on the changing power output. Similarly, we derive the partial derivative of the reactive power with respect to V_{mg} and δ to get

$$\frac{\partial Q}{\partial V_{mg}} = \frac{2 \cdot V_{mg} - V_g \cdot \cos(\delta)}{X}, \quad (5.9)$$

$$\frac{\partial Q}{\partial \delta} = \frac{V_{mg} \cdot V_g \cdot \sin(\delta)}{X}. \quad (5.10)$$

It initially appears that both the phase angle and voltage have an impact on the reactive power, but constraints still need to be applied. It is important to note that the value of the angle δ is

generally quite small (typically smaller than $< 10^\circ$). Therefore, the sinusoidal function in Eq. 5.10 is typically very small for changing Q . As a result, the reactive power changes little for changing voltage angle. By the same constraint the cosine function is very close to 1, and therefore the right-side of Eq. 5.9 is a constant, and the Q value is directly proportional to the change in V_{mg} . In summary, the control relationship between real power P is related to varying δ and reactive power Q is related to varying V_{mg} . This is shown in Figures 5.6-5.7. The feedback loop is based on transfer function relationship in implicitly stated in Eq. 5.8 and 5.9, respectively. The PI controller is tuned experimentally in MATLAB to find the maximum points for stability. Given the difference in voltage magnitude and filter size, the gains are slightly different for the battery array as they are for the PV array and WT model.

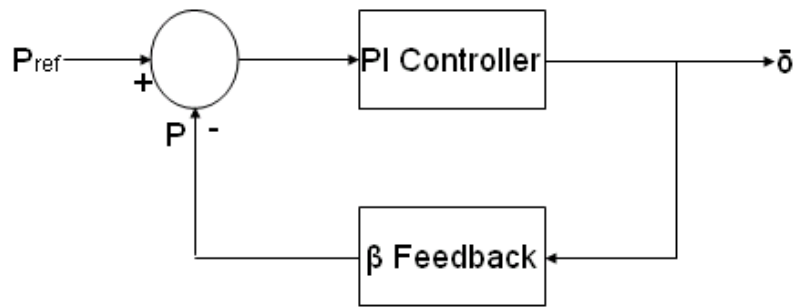


Figure 5.6: General Control Loop for Real Power Control

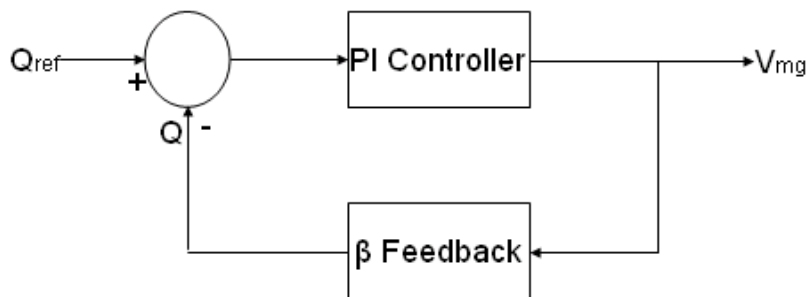


Figure 5.7: General Control Loop for Reactive Power Control

Finally, the parameters for V_{mg} and δ need to be converted into a PWM train. This is performed by using a carrier wave to sample and digitize the composite sinusoidal output of the controller. A comparator is implemented to perform this task and mark the output high or low depending on which signal is higher at a discrete point in time, the composite sinusoid or the carrier wave. This output is shown in Figure 5.8. Finally, the truth table for the IGBTs is given in Table 5.3. It shows the operating states of the inverter and its associated output.

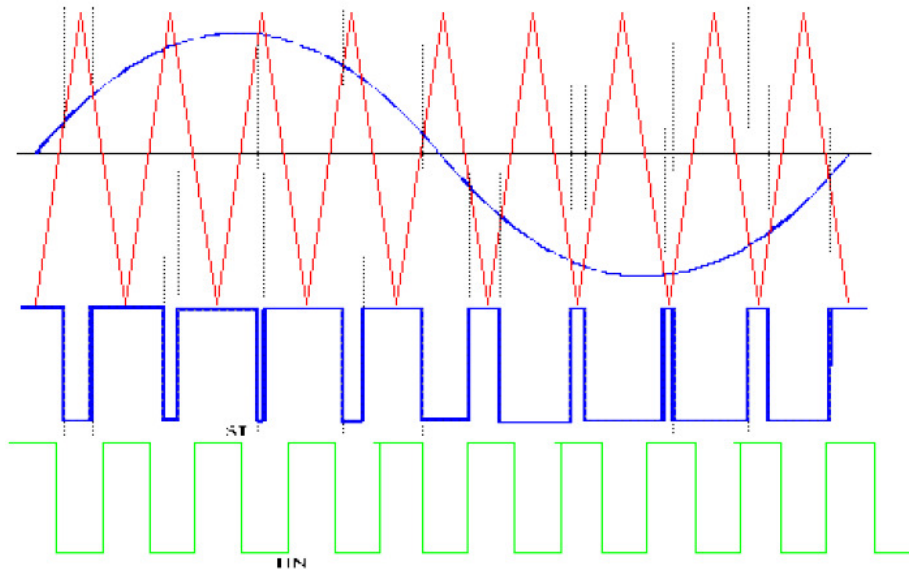


Figure 5.8: PWM Train Generated from Carrier Signal [40]

Table 5.3: Truth Table for the H-Bridge Inverter

Q1	Q2	Q3	Q4	Output
1	0	0	1	Positive Half Cycle
1	0	1	0	Zero Output
0	1	1	0	Negative Half Cycle
0	1	0	1	Zero Output

5.2.4 PSCAD Implementation

With the inverter controller design complete, the full system can be modeled in PSCAD. In the latter, the inverter hardware and control models are implemented using existing electrical and control blocks. The comparator control circuit is shown in Figure 5.9. It is implemented as a controlled sine wave generation with variable angle and magnitude input. The carrier signal generator operates at a fixed 10 kHz. The full PSCAD implementation of the inverter bridge electrical circuit is shown in Figure 5.10. The system in PSCAD also includes fly-back diodes to prevent shorting of the DC input.

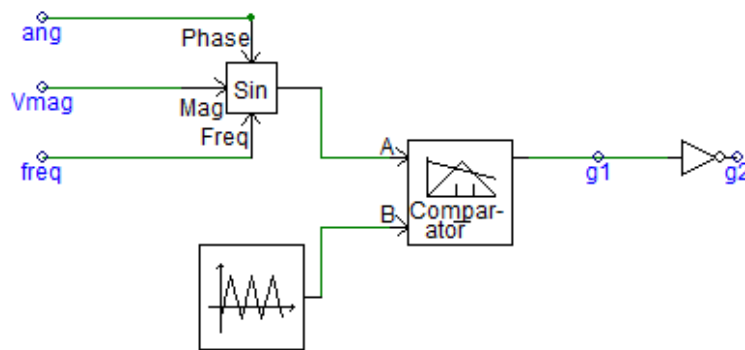


Figure 5.9: PWM Generator for PQ Controller

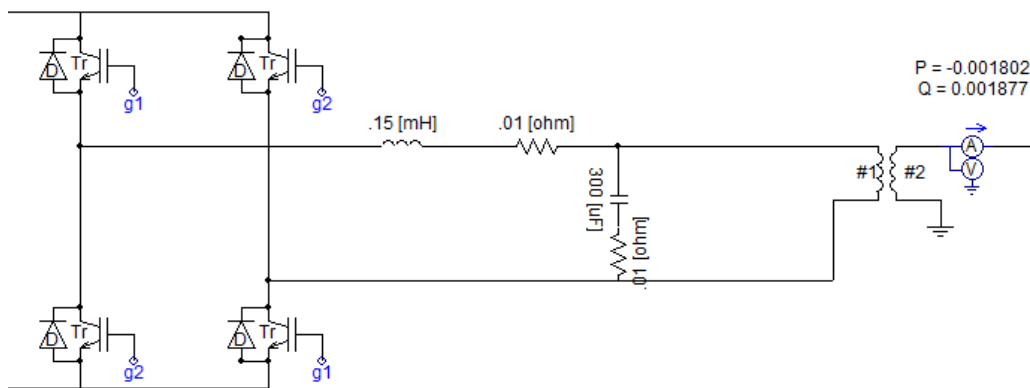


Figure 5.10: H-Bridge, LC Filter, and Isolation Transformer for the Inverter Circuit

The PI controllers for the PQ feedback loops are shown in Figure 5.11-5.12. The PSCAD implementation for the P control includes an additional step for limiting the power setpoint to a realistic value for the source, as well as a conversion of units from MW to W for power. Verification of the output of the inverter is shown in Figure 5.13. Two-phase shifted sinusoids can be seen.

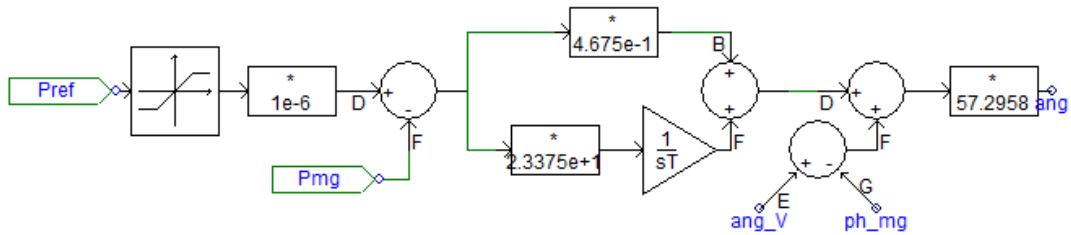


Figure 5.11: Control Loop for Real Power/Angle Control

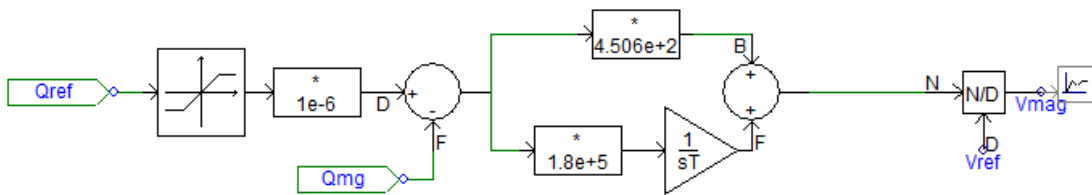


Figure 5.12: Control Loop for Reactive Power/Voltage Control

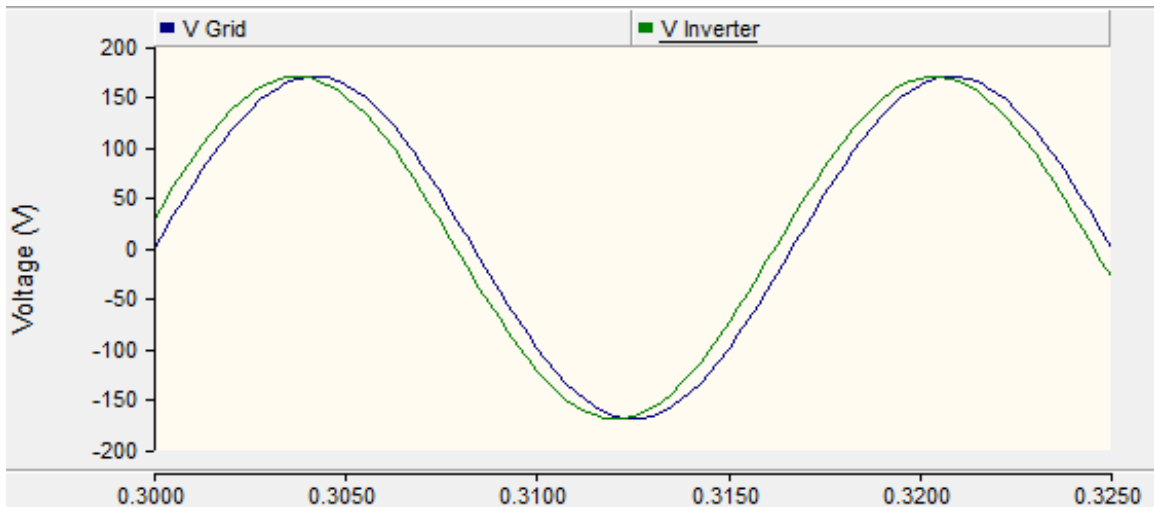


Figure 5.13: Verification of Voltage Output from the Inverter against Grid Voltage

Finally the voltage and current THD for the inverter in steady state operation are shown in Figure 5.14-5.15. From IEEE 1547, the THD is required to be less than $<5\%$ for TDD which is satisfied by both current and voltage quantities.

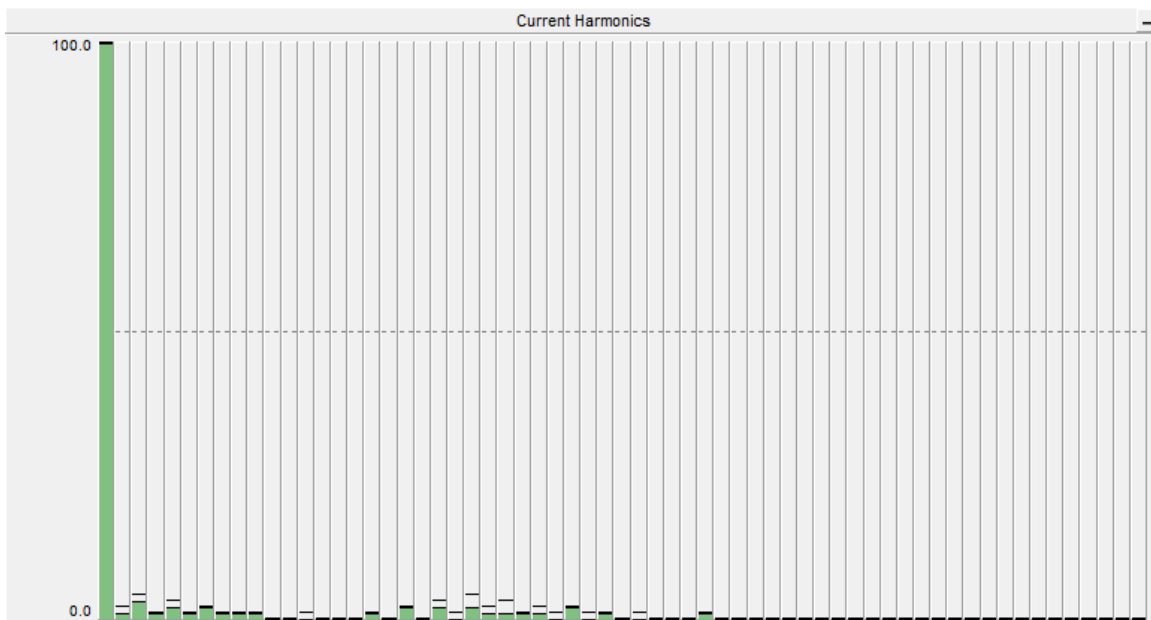


Figure 5.14: Current Harmonic Spectrum for Inverter at Full Load

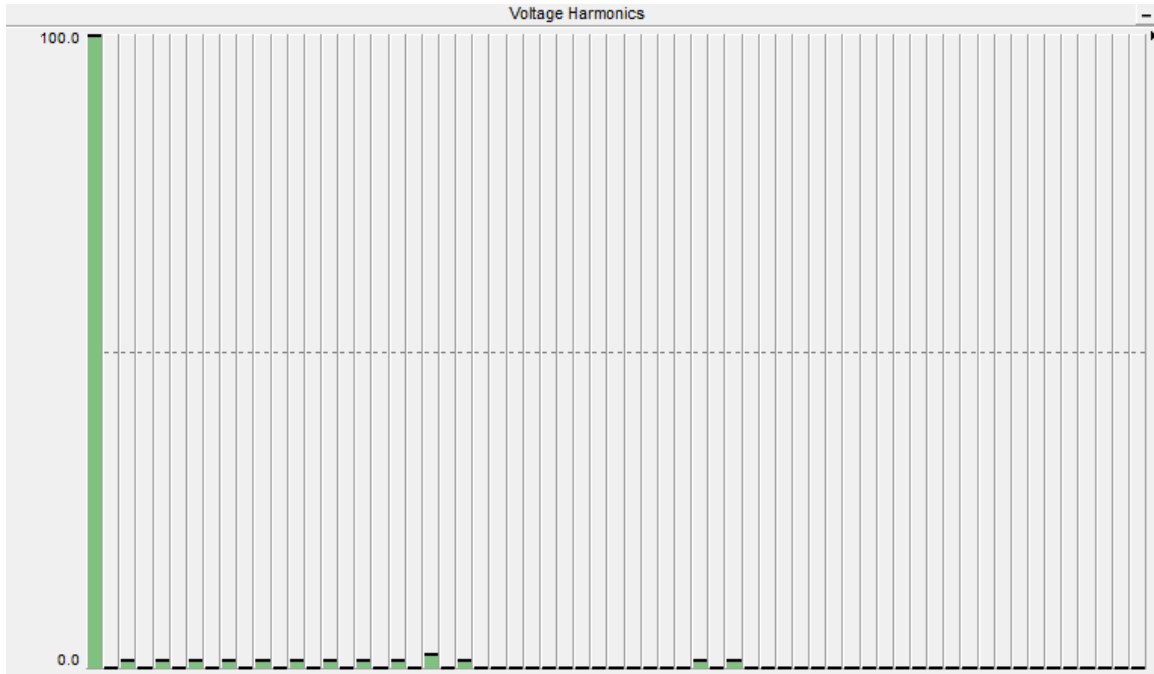


Figure 5.15: Voltage Harmonic Spectrum for Inverter at Full Load

5.3 Power Management Controller

During the grid-connected mode of operation, any excess generation or significant droop events will be handled by the distribution power system that the microgrid is connected to. For island mode operation, this is not the case and a local supervisory power control is required. For this reason, the power management controller (PMC) is developed. The PMC serves 2 functions. The first is balancing supply and load over the long term through curtailing generation units for excessive generation. The second is to curtail demand during an emergency event with low renewable production and low battery SOC. The top level control diagram for the PMC is shown in Figure 5.16. The input parameters are on the left-hand side and the output control is on the right. During island mode operation, short-term transients are handled by regulating the battery array and not the PMC. The PMC is designed to provide long time scale stability to the system by balancing source, generation, and battery SOC. The full breadths of capabilities for the PMC load balancing controller are shown in Table 5.4.

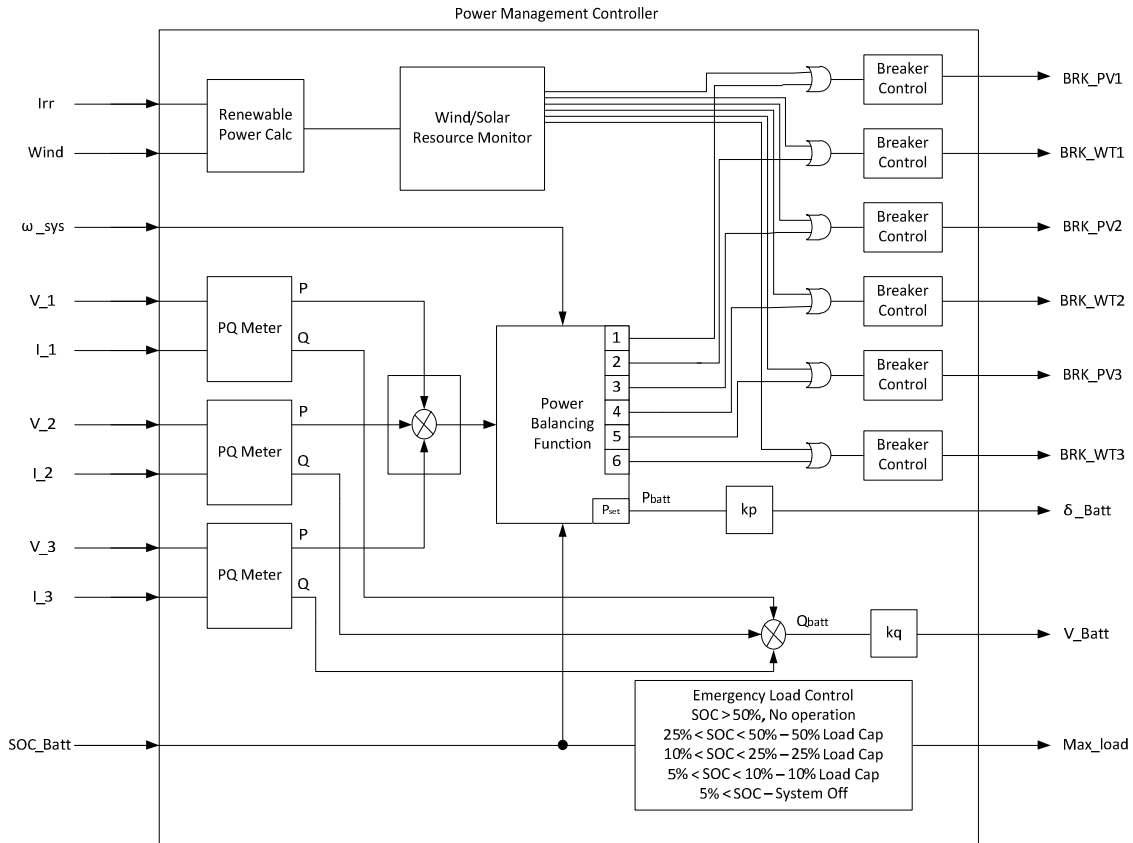


Figure 5.16: PMC Top-Level Control Diagram

Table 5.4: PMC Load Balancing Truth Table

Source	Demand	Battery SOC	PMC Action
High	High	High (SOC > 95%)	No Action if $P_{source} \approx P_{demand}$, Else switch off generation and discharge battery
High	High	Low (.5 < SOC < .95)	Charge battery
High	Low	High	Switch off source until $P_{source} < P_{demand}$, Discharge battery
High	Low	Low	Charge battery

Low	High	High	Discharge battery
Low	High	Low	Discharge battery, once SOC < 50%, start load curtailment
Low	Low	High	Discharge battery, once SOC < 50%, start load curtailment
Low	Low	Low	Discharge battery, once SOC < 50%, start load curtailment

5.3.1 Island Mode Power Flow Balancing

During island mode operation, long-term dispatch of generations is critical and is limited by the SOC of the battery array. Short of transient events, this control function is needed to compensate for changes in environmental resources, battery charge state, and current demand. The system action is based on three inputs, namely resource availability, power demand, and battery SOC. The implementation of the truth table shown in Table 5.4 is accomplished by using a sequential switching algorithm. If generation is too high and the battery is fully charged, WT1 will be switched off first. After a short-time delay, the power measurement will be performed again. If generation is still too high, WT2 will be shut off. This will continue for WT3 before switching off of the PV arrays begins. The wind turbines are switched off first because they are most likely to running at some point throughout the day, whereas the PV modules have a fixed prescribed period for generation (i.e. daylight hours). This cascading switching off of units will continue until generation drop below demand and the battery begins to discharge. Once the battery SOC drops below 95%, units will begin to be switched online in reverse order. This transition is captured in Figure 5.17.

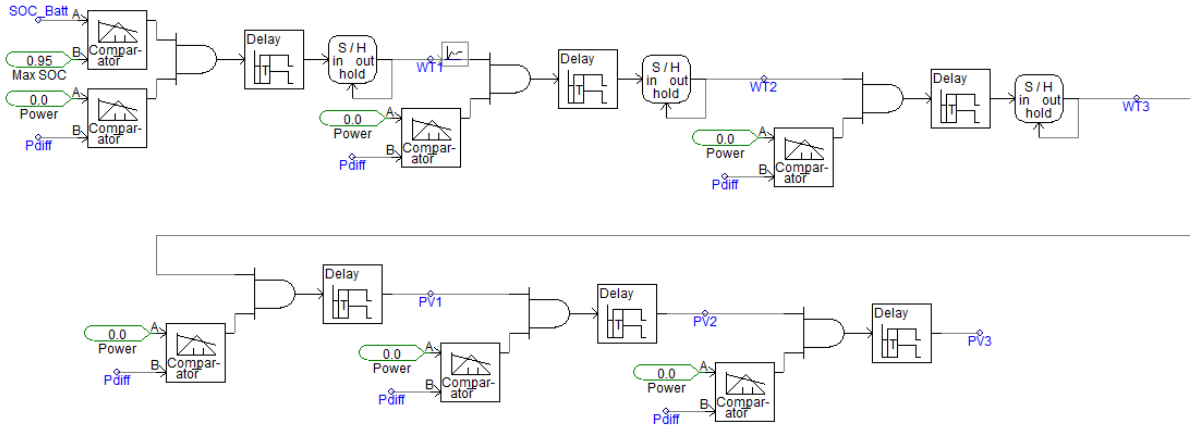


Figure 5.17: Power Balancing Function Implementation in PSCAD

5.3.2 Environmental Resource Monitor

The environmental resource monitor shuts off generation sources when the environmental parameters go out of their boundary for delivering useful power. For PV array, it is when the irradiance is too low to provide enough regulation voltage to drive the inverter. By definition, this limit is for direct irradiance, less than 100 W/m². For the WTG, it is when the wind speed is either too low to generate the minimum voltage necessary for the inverter or the wind speed is too high or pushes the mechanical limits of the WTG assembly. By definition, this limit is wind speed above 20 m/s and speeds below 3 m/s. The only action for the PMC to take is to disconnect the unit or reconnect depending on the state of the environmental condition.

For implementation in PSCAD, the monitors are modeled as comparators with a reference value. The reference value is the minimum thresholds that the PV and WTG can operate at. An output value of HIGH or 1 refers to the breaker operation to disconnect all of the sources impacted by the low resource condition. This implementation can be seen in Figure 5.18.

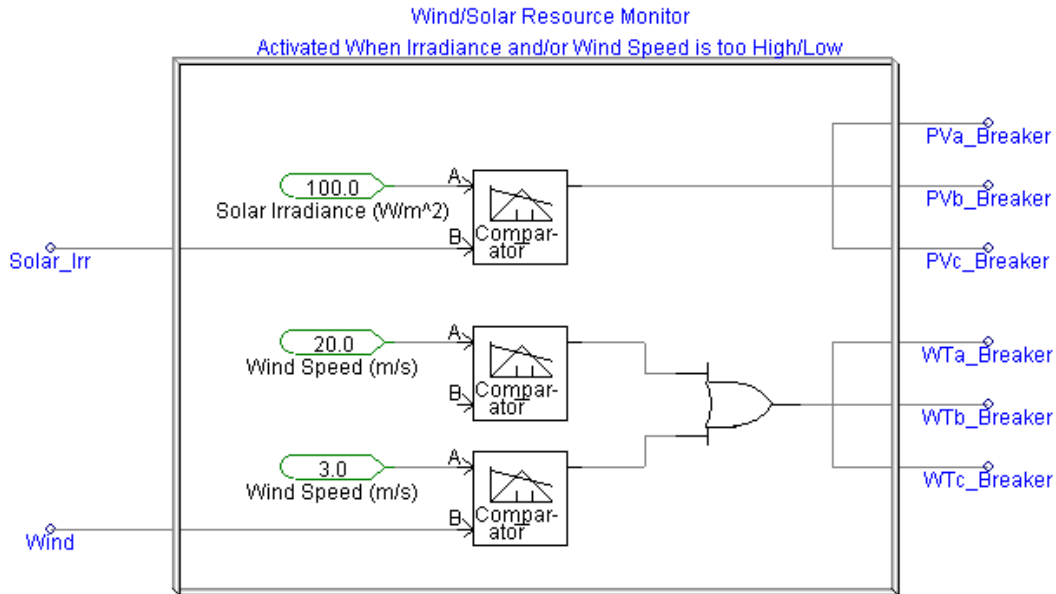


Figure 5.18: Wind/Solar Resource Monitor Implementation in PSCAD

5.3.3 Emergency Load Control

For situations where the battery SOC is low and there are little to no generation available by the renewable sources, curtailment of demand is required. This capability is added to the PMC despite the fact that for most normal operational scenarios, curtailment does not occur. Power curtailment in this microgrid is directly proportional to the SOC of the battery array. When the battery array is low, power demand will be clamped low. The opposite situation occurs in high SOC conditions. For the purpose of this thesis study, the mechanism of curtailment is not expanded beyond a fixed load value. In practical applications, curtailment would occur by remotely disconnecting large loads from the residences. Typically, remotely operated relays switch off loads such as HVAC units, refrigeration, or electric hot water heater systems during a period of weak supply. Expanding the complexity of the load model is beyond the scope of this research effort. In this model, the load is discretely reduced as the battery SOC passes certain setpoints. The load will be curtailed as the SOC drops below 50%, 25%, 10%, and 5% with the

last value being where the load is completely shut off. Implementation in PSCAD involves a measurement of the current battery SOC and comparators. As the SOC drops below the threshold value, the comparator will activate a HIGH or value 1 to command the assigned breaker to open. This can be seen in Figure 5.19.

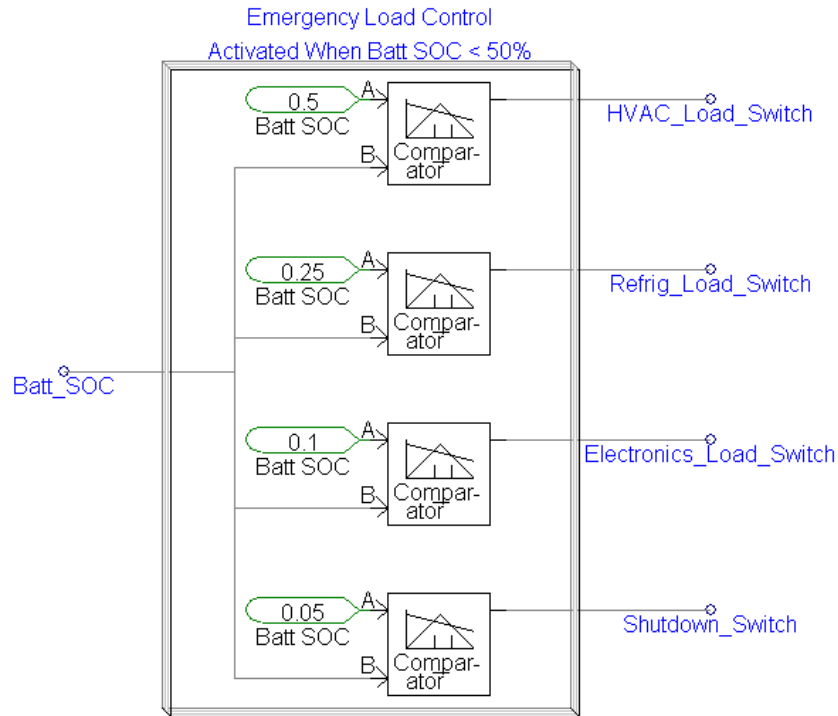


Figure 5.19: PMC Emergency Load Control Implementation in PSCAD

5.4 Island-Mode Droop Control

Maintaining stable power flow dynamics in the microgrid during islanding mode is handled by droop control. The droop controller is lower level control of the PMC that manages short duration transients in the microgrid. The droop controller will respond to transient changes on the network and compensate accordingly. The inverter for the central battery module will perform all droop control activities. The classical curves for P vs. ω and Q vs. V droop are shown in Figure 5.20.

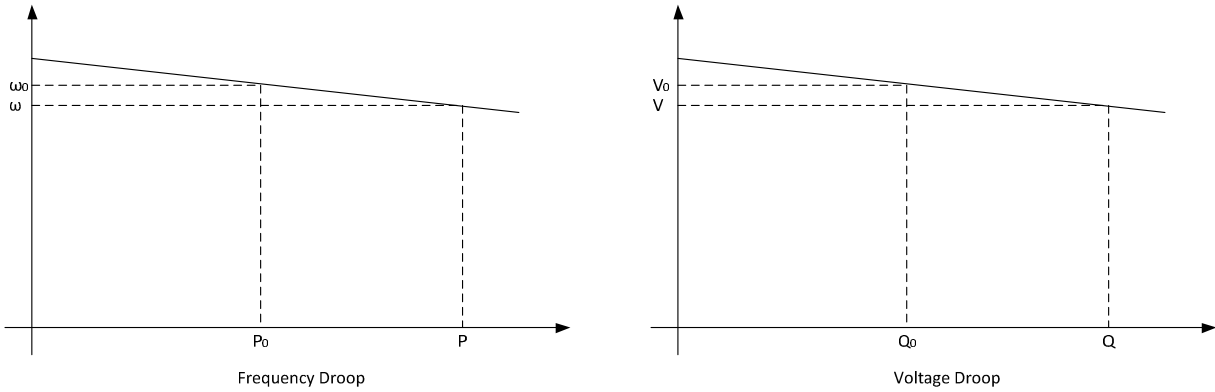


Figure 5.20: Droop Characteristics for Frequency and Voltage

One constraint to this classical implementation is the relatively short distances between generation units and the low inertia of the network, which can result in instability during frequency droop control. This can be mitigated using phase-angle droop control over frequency control. Given that generation for this microgrid is entirely inverter-based and that inverters can change their phase angle output instantaneously, phase-droop control can be implemented. Phase-droop control has been proposed in [41] as ways of providing greater stability in weak networks that have little system inertia. Given that the implemented microgrid has no direct rotating mass for generation, phase control can offer the benefit of greater stability. In this implementation, the frequency is fixed at 60 Hz, with a feedback loop to prevent long term error in frequency output. The voltage and phase-droop control are handled primarily by the battery array. As changes in supply and load occur throughout the microgrid, the battery array compensates to maintain normal operation. Consequently, the two different modes of operation, require two different control loops. For grid-connected mode, the control loop is set to an arbitrary value for P and Q to output V and δ . For island mode operation, P and Q output are not specified, while the voltage and phase angle magnitudes are maintained constant. For island mode, the control loop is a direct feedback for voltage and phase angle. As a result gain, values

for the PI controllers change with the modes of operation as well. To this end, two control loops are developed for both voltage and phase control. One is for grid connected mode operation and the other is for island mode operation. For both cases, the inverter frequency will remain fixed at 60 Hz. The controllers are shown in Figs. 5.21 and 5.22.

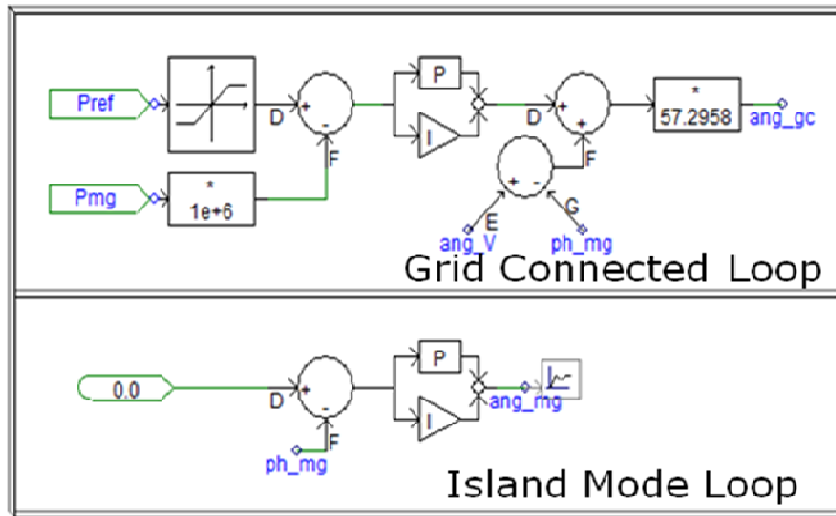


Figure 5.21: Droop Controller Implementation for Phase Control on the Battery Inverter

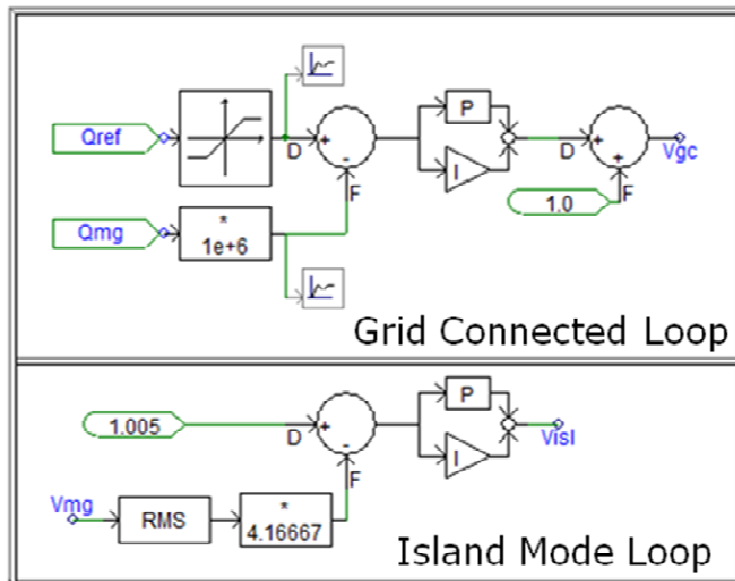


Figure 5.22: Droop Controller Implementation for Voltage Control on the Battery Inverter

The voltage and phase response during island mode are shown in Figures 5.23 and 5.24. The response droop for the voltage is less than 10% overshoot and well within the operational limits.

The droop control for the angle drops over 20% before recovery, but stabilizes in a relatively short period. Stability is maintained during the transient events. With the droop control modeled, the full model can be integrated.

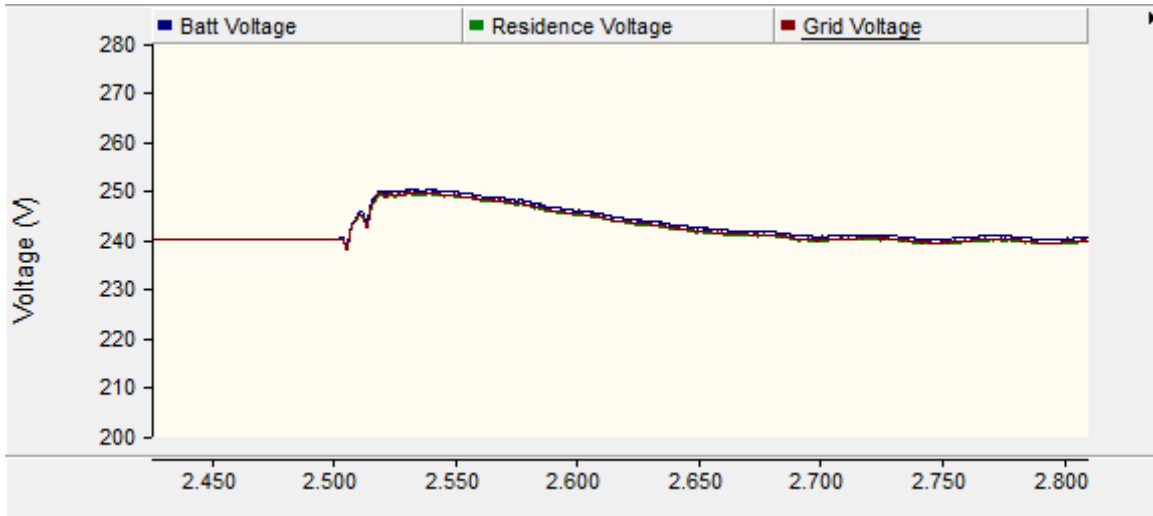


Figure 5.23: Voltage Transient Response with Droop Control

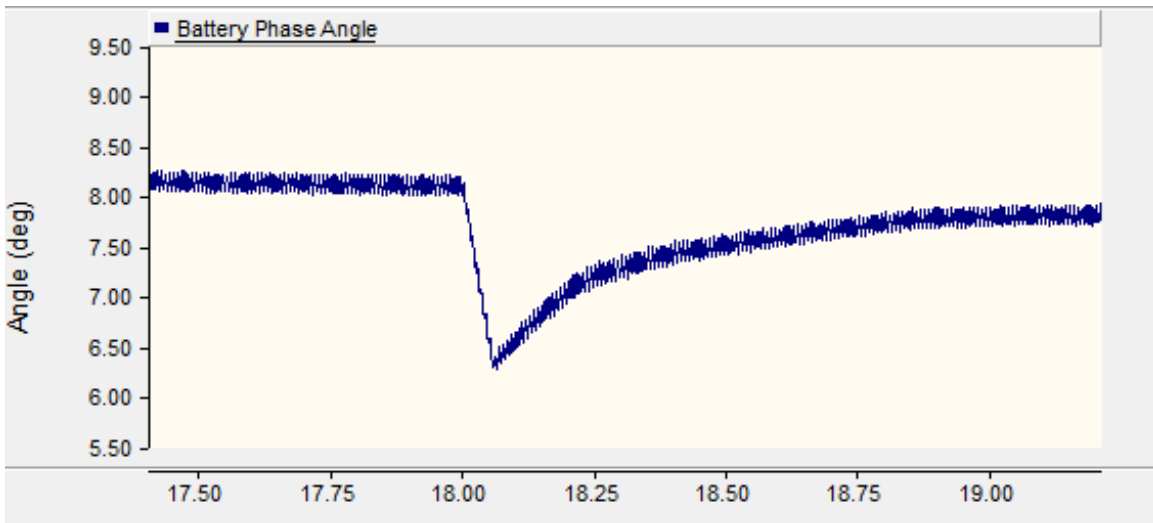


Figure 5.24: Phase Transient Response with Droop Control

Chapter 6

Integrated Microgrid Model and Steady-State

Verification Results

This chapter reviews the integration of the hardware models developed in Chapter 4, along with the control models in Chapter 5, into a complete microgrid top-level model. This complete model will provide the ability to run numerous transient scenarios with respect to the microgrid performance and response. While the microgrid presented here is limited to 3 residences, it is scalable to a much larger number of residences. The constraint of 3 residences is to limit simulation runtime while still showing the performance of the microgrid.

6.1 Microgrid Implementation in PSCAD

The full implementation in PSCAD requires that the submodels developed in Chapter 4 are consolidated into a single top-level model. The consolidation requires simplification of distribution transformers and breakers to improve simulation time and reduce model complexity. The consolidations of the transformers are discussed in 6.1.1 and the full PSCAD model presented in 6.1.2.

6.1.1 Transformer and Line-Loss Consolidation

To improve simulation runtime and reduce the complexity of non-vital system elements, the transformers shown in Figure 1.3 are reduced to their equivalent impedances. This is further simplified by neglecting the transformer resistive losses as well as core losses and focuses on the

inductive impedance of the series connection. By doing this, system-wide voltage will be referenced to the residential 240 V. It is assumed that a 7% impedance transformer is used. This results in approximately 200 μH equivalent inductance. It is also assumed that the distribution line segments are no longer than 100 yards for any distance between residences and the central battery array bus tie-in point. For simplicity, all line segments are assumed to be 100 yards in length. The underground distribution cables are assumed to be 1/0 AWG conductor size and approximated to be 30 $\text{m}\Omega$ for each 100 yard segment [42].

6.1.2 PSCAD Microgrid Model

The full model is consolidated into Figure 6.1. The test configuration is of a notional microgrid network. It is an example of a common, but certainly not the only, single-phase distribution scheme.

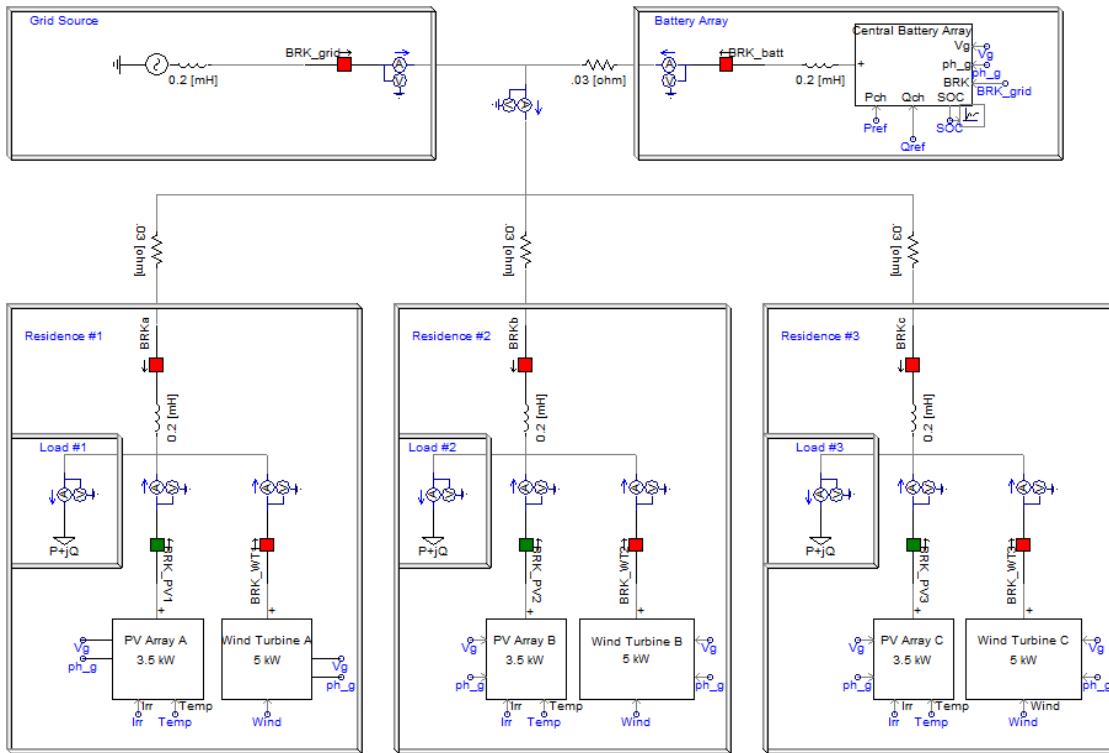


Figure 6.1: Microgrid Implemented in PSCAD

6.2 Microgrid Steady-State Performance

Prior to the transient analysis performed in Chapter 7, the model is first verified that it can operate in steady-state mode. Steady-state operation is examined for two states, namely grid-connected and island-mode operation. The scenarios described next will serve to verify the steady state stability of the model.

6.2.1 Grid-Connected Steady-State Operation

The first scenario to be validated is that the system reaches a steady-state value for power, voltage, and frequency in grid-connected mode. Here, the grid connection will be maintained and all sources will be at their full power output. Table 6.1 provides the complete generation configuration for this scenario. During this scenario, all of the breakers in Figure 6.1 are closed (red). The simulation results are shown in Figure 6.2-6.4. From the results it can be seen that power, voltage, and frequency results are constant for all sources.

Table 6.1: Grid-Connected Mode Steady State Operation Unit Status

	Grid	Battery	PV Arrays	WT Generators	Load
Unit Status	Online	Discharging (10 kW)	3 kW (1000 W/m)	4 kW (10 m/s)	6 kW 1 kVAR

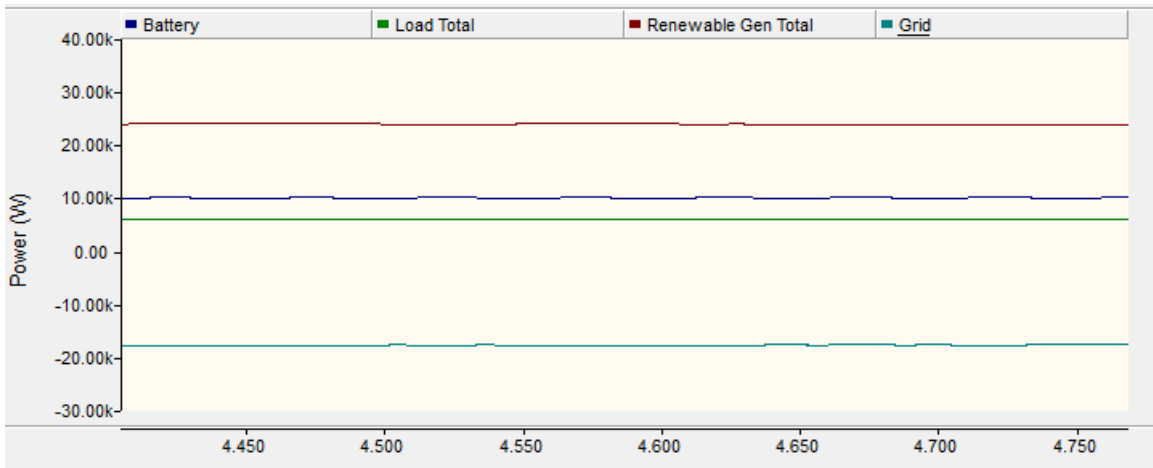


Figure 6.2: Grid Connected Steady State Power

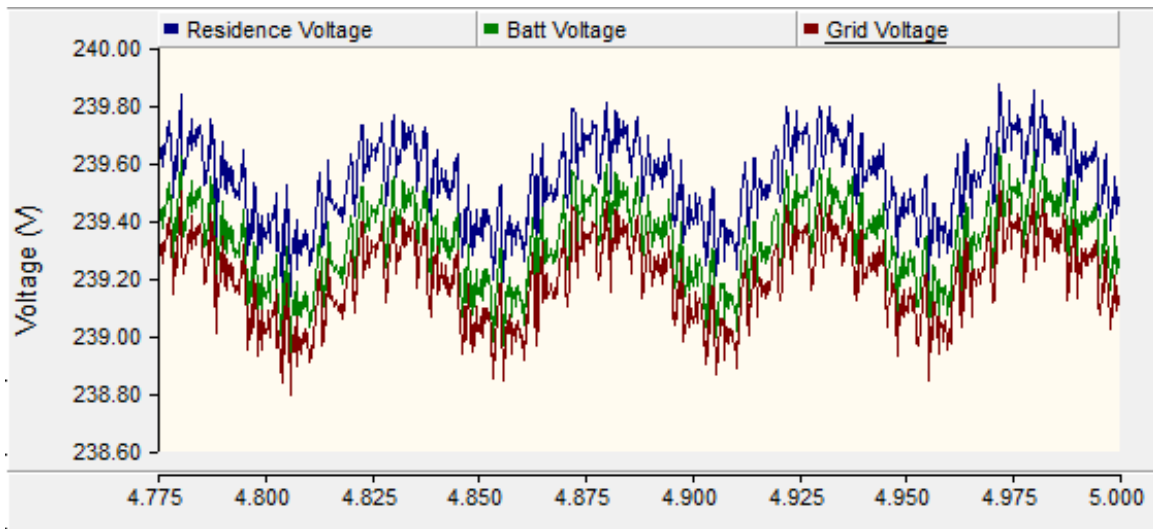


Figure 6.3: Grid Connected Steady State Voltage

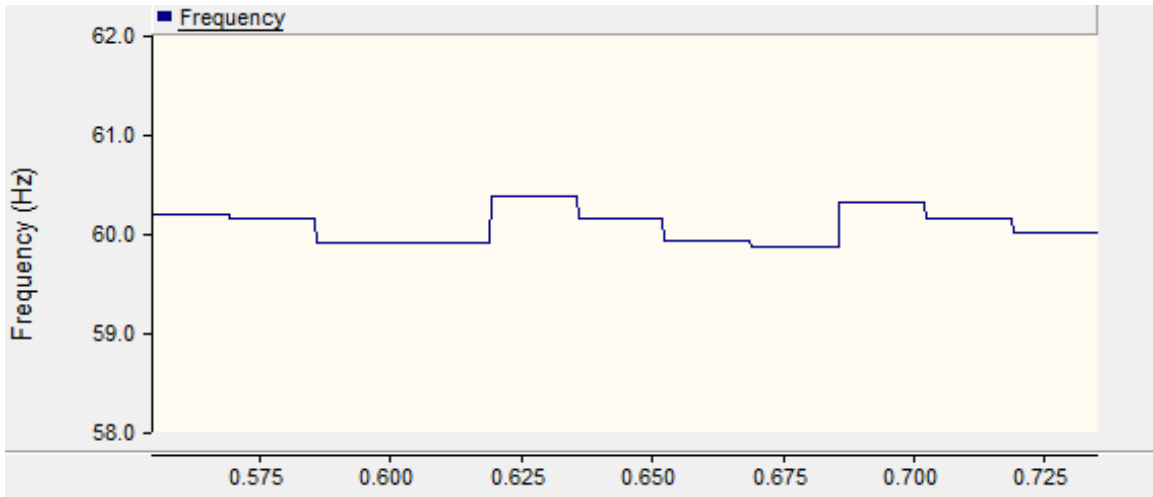


Figure 6.4: Grid Connected Steady State Frequency

6.2.2 Island-Mode Steady-State Operation

The second scenario to be validated is that the system reaches a steady-state value for power, voltage, and frequency in island-mode operation. For this first scenario, the grid connection will be disconnected and all sources will be at their full power output. The transition from a grid connected mode will not be presented here as it is covered in Chapter 7. Table 6.2 provides the complete generation configuration for this scenario. During this scenario, all of the breakers in Figure 6.1 are closed (red), except for the BRK_grid which is open (green). The simulation results of this scenario are shown in Figure 6.5-6.7. From the results it can be seen that Power, Voltage, and Frequency results are constant for all sources.

Table 6.2: Island Mode Steady State Operation Unit Status

	Grid	Battery	PV Arrays	WT Generators	Load
Unit Status	Offline	Charging (-17.5 kW)	3.5 kW (1000 W/m)	4 kW (10 m/s)	6 kW 1 kVAR

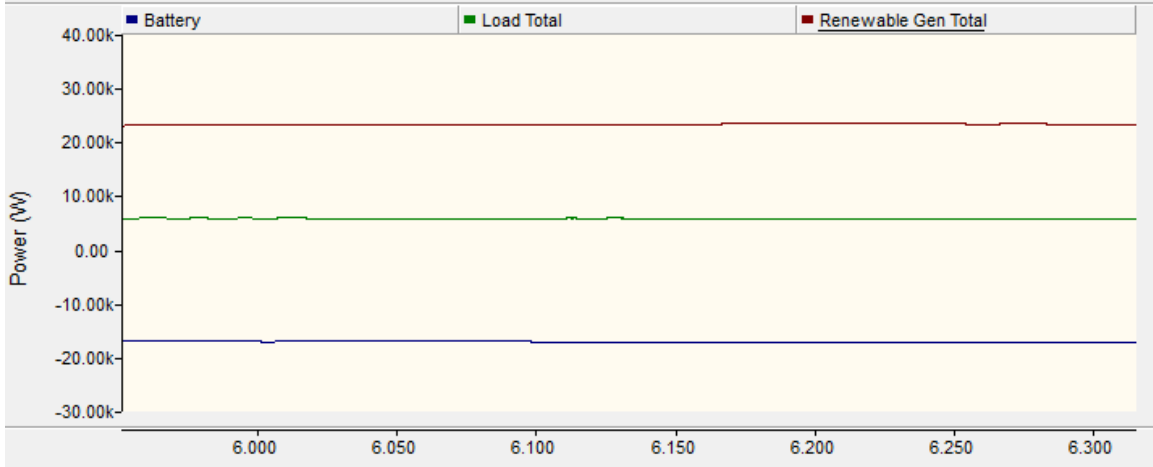


Figure 6.5: Island Mode Steady State Power

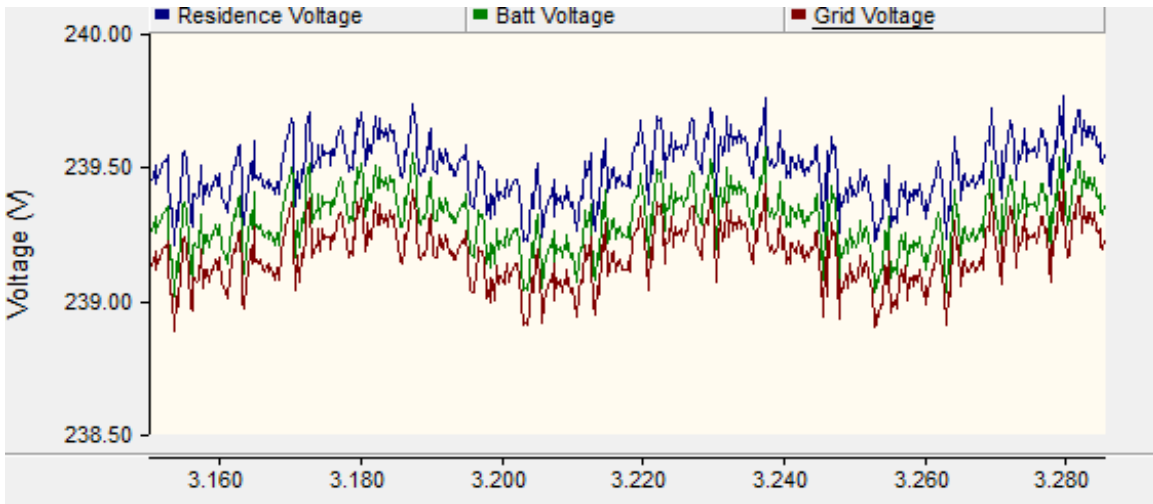


Figure 6.6: Island Mode Steady State Voltage

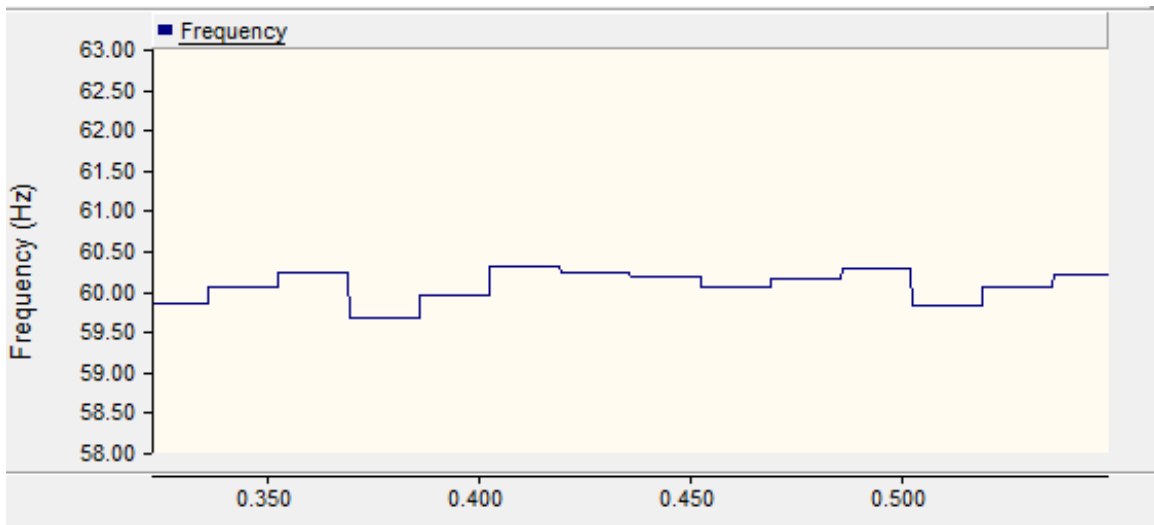


Figure 6.7: Island Mode Steady State Frequency

Chapter 7

Transient-Simulation Scenarios and Results

With the microgrid now completely developed, transient analysis can be performed for multiple-operational scenarios. The simulation results presented here cover short-term and long-term transient responses to very common electrical network events. A total of 8 transient events are presented.

The measurement points for the simulations are shown in Figure 7.1. Note that the residence voltages are only measured at one point. Based on earlier assumptions, it is assumed that each generation and load will behave the same in parallel for each residence, implying that multiple measurements are not necessary. The medium voltage measurements will be referred to the secondary side of the load transformers and will be measured at 240 V nominal.

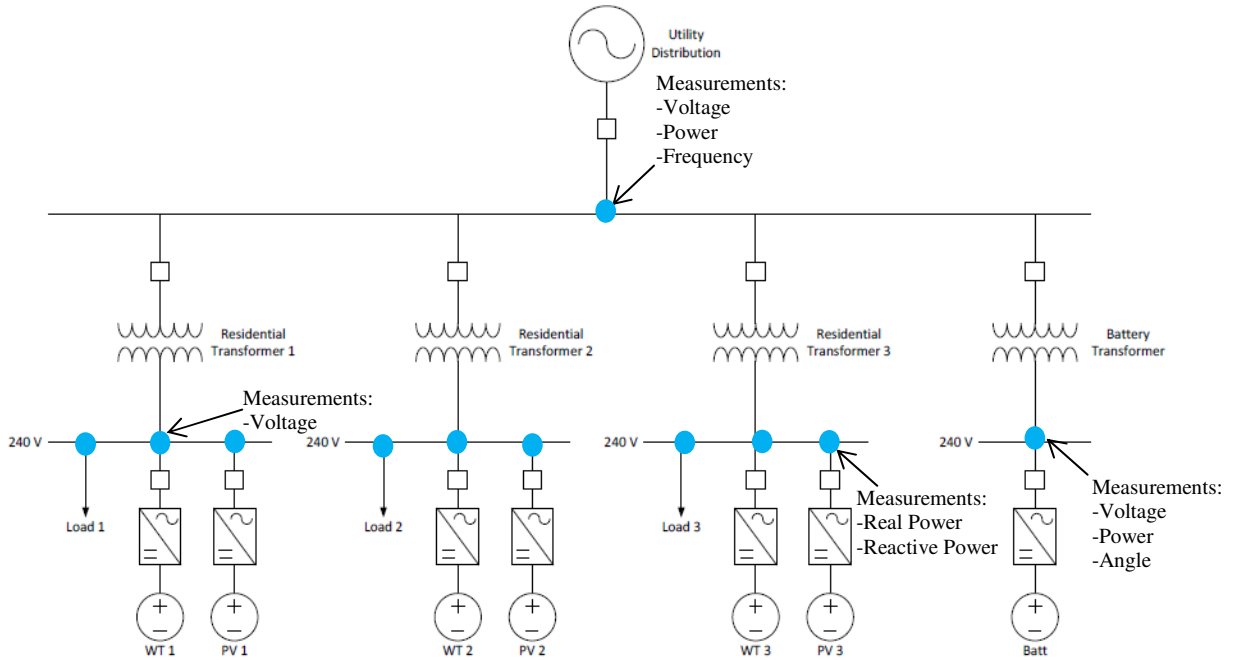


Figure 7.1: One-line Diagram of the Microgrid with Measurement Points

7.1 Scenario 1: Loss of Grid, Transition to Island-Mode Operation

The first scenario to be investigated is the response of the microgrid to the loss of the distribution source during a hurricane event. The assumptions for this scenario are that the local breaker will trip prior to a significant surge on the line is observed. Also, since this is during the early phases of a hurricane event, the PV output is assumed to be zero due to high cloud cover and the wind turbines are producing at a nominal wind speed. As the system trips offline, the battery will take on the majority of the load during this event and stabilize this system. The full system configuration for this event is given in Table 7.1. For this scenario, time is set to 15 seconds, the grid side breaker is opened and the battery begins to go online and increase its phase angle until it can supply the load at the prescribed voltage and frequency. The power output, bus voltages, battery-residence phase angle, and frequency are monitored. The results are shown in Figs. 7.2-

7.5. From the previous figures, it can be seen that the microgrid stabilizes in a short period of time. The power transient lasts for less than 150 ms for the load. As the battery is brought online, the system voltage rises rapidly to bring the battery to a full discharge state, but settled back to a nominal 240 Volts once the battery and the 3 WTG's balanced the load properly. In this scenario, the output from the WTG's drooped significantly as the changeover from grid to battery reference angle occurred, however, once the battery had reach peak output, the WTG's began to supply more power to the load. It also important to note that the system frequency overshoot was significant during the switchover. However since all of the sources are asynchronously connected, the system stabilized quickly due to phase angle droop control.

Table 7.1: System Configuration for Scenario 1

	Grid	Battery	PV Arrays	WT Generators	Load
Before Event	Online	Trickle Discharge	Offline	Online 4 kW Power (6 m/s Wind)	9 kW 3 kVAR
After Event	Offline	Discharge	No Change	No Change	No Change

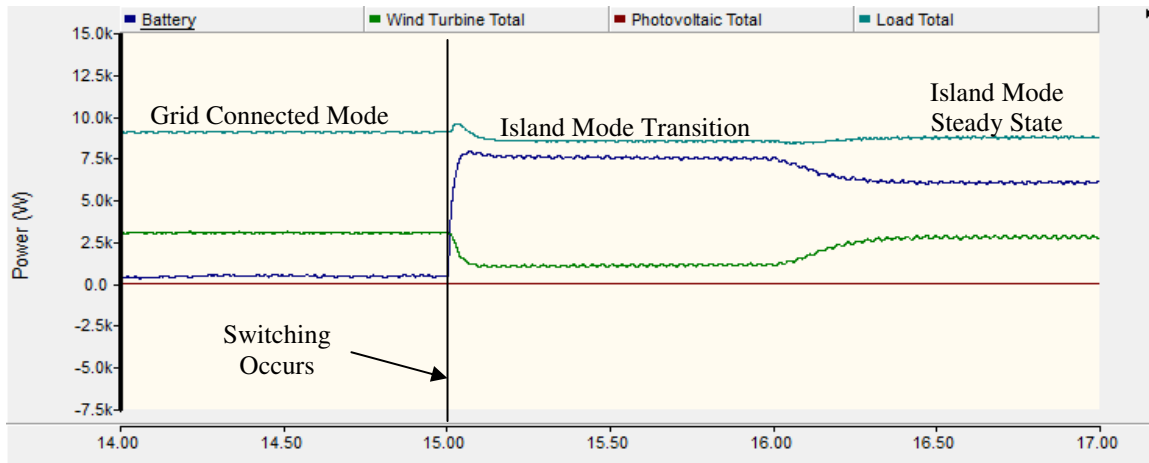


Figure 7.2: Power Load Demand and Supply from PV, Batt, and WTG

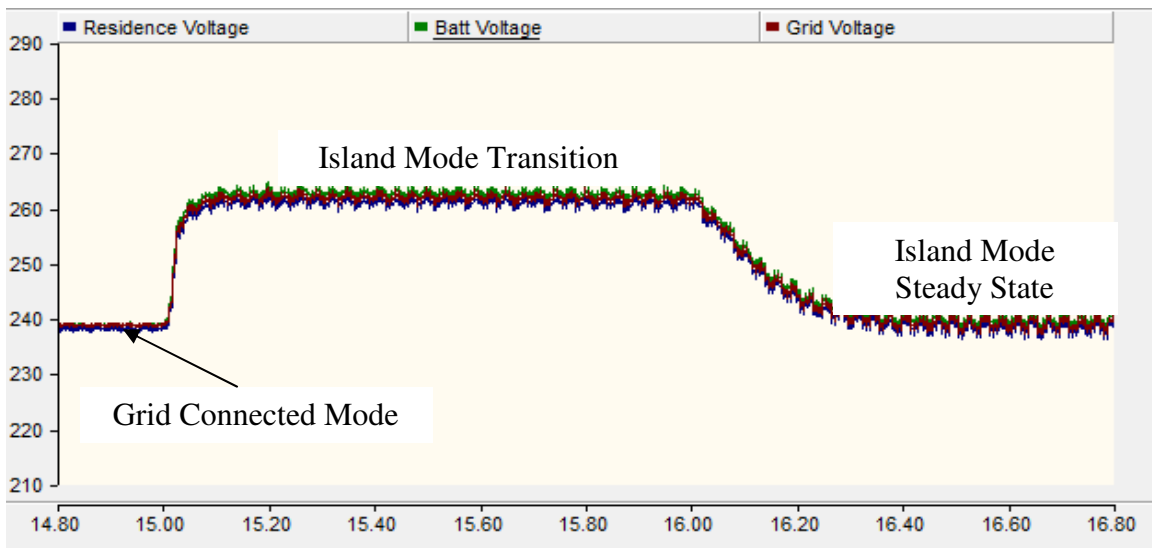


Figure 7.3: System Voltages for the Common Bus, Residence Bus, and Battery Bus

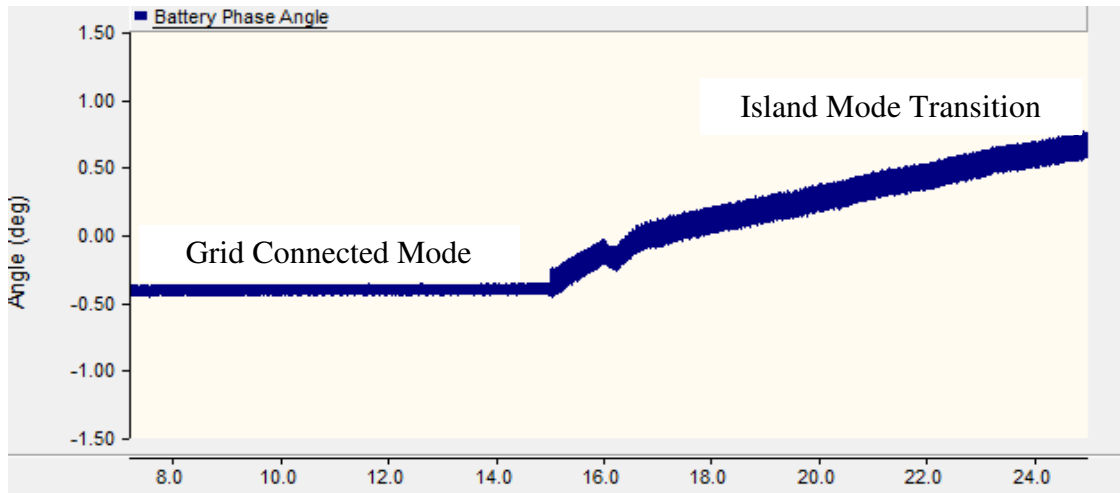


Figure 7.4: Battery Phase Angle Change (w.r.t. to Residence Bus)

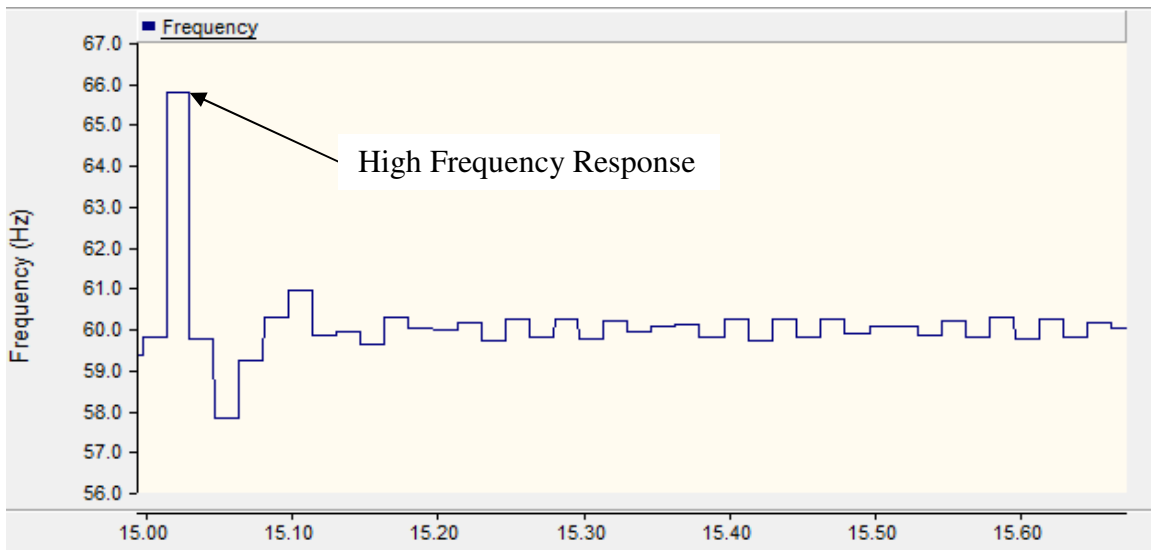


Figure 7.5: System Frequency Response during Transition

7.2 Scenario 2: Island Mode - Interconnecting PV Microsources

The second scenario to be investigated is the switching on the PV array during island mode operation. The assumptions are that battery array is 100% supporting all of the load centers. This is a very likely scenario for after a hurricane once the wind speed is reduced and the sun has come back out. Therefore, the WTG does not produce any power in this case. Here, the PV array

needs to be switched online to relieve the battery array of supplying the entire load. The full system configuration for this event is given in Table 7.2.

Table 7.2: System Configuration for Scenario 2

	Grid	Battery	PV Arrays	WT Generators	Load
Before Event	Offline	Discharging	Offline	Offline	6 kW 3 kVAR
After Event	Offline	Charging	Online (1000 W/m²)	Offline	No Change

During the simulation, when the elapsed time equals 10 seconds, the PV arrays will switch online and battery goes from a discharging mode of operation to a charging mode. It is assumed that the battery has been operating for a long time and load curtailment is activated until the battery has fully recharged. The results of the simulation are given in Figs. 7.6-7.10. It can be seen from the simulation results that the introduction of the PV array to the microgrid allowed for a very gracefully transition from battery discharge to charging mode with the load power being maintained. The frequency drooped significantly as a result of the transition, but the low value mark is still within the range of most modern electronic hardware tolerances [43].

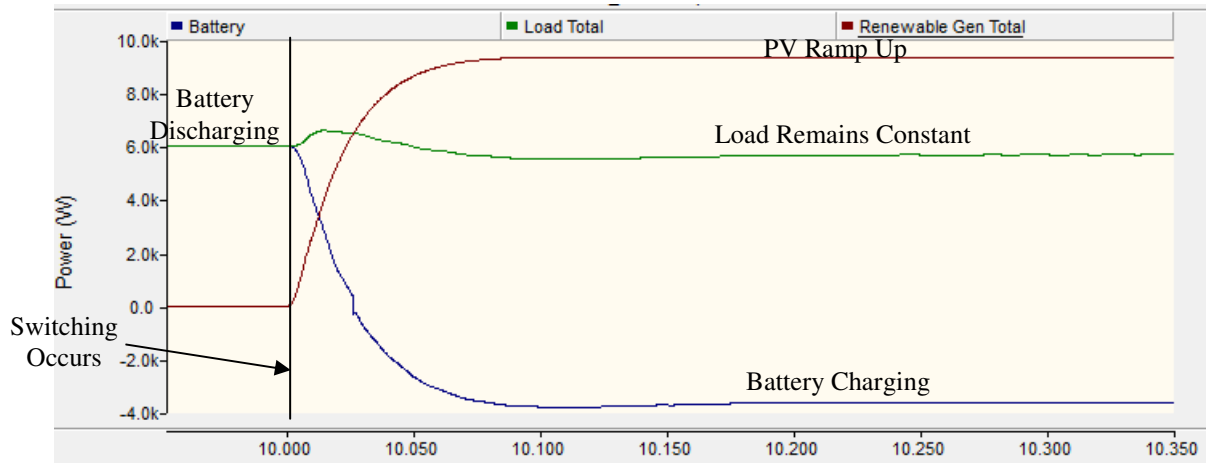


Figure 7.6: Change in Power Output during Transition

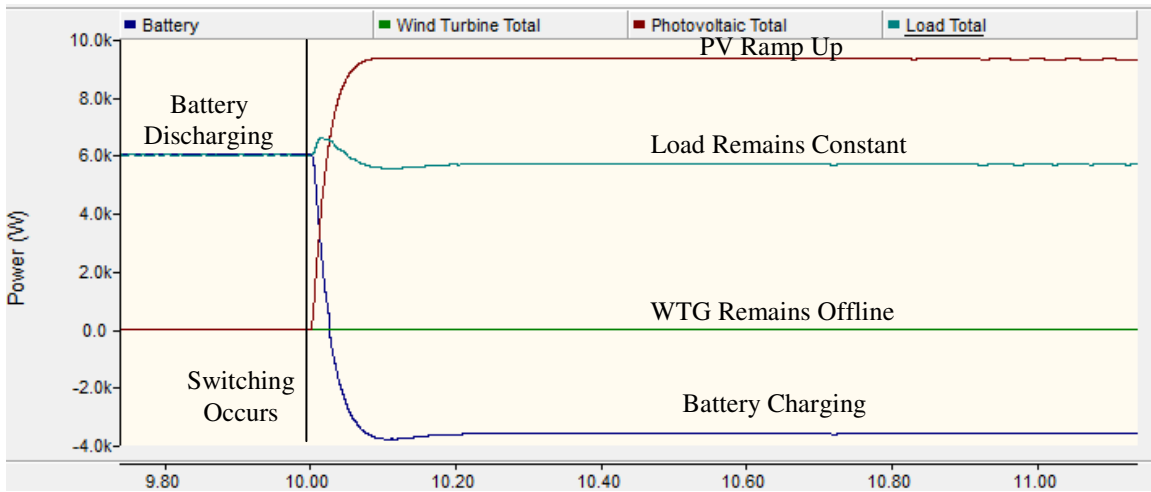


Figure 7.7: Change in PV and Battery Output during Transition

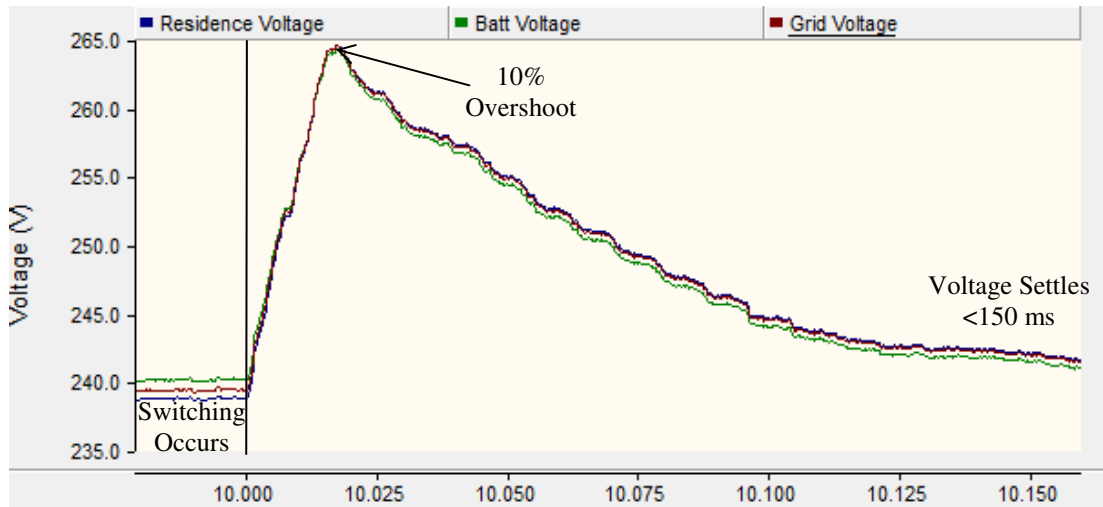


Figure 7.8: Voltage Response during Transition

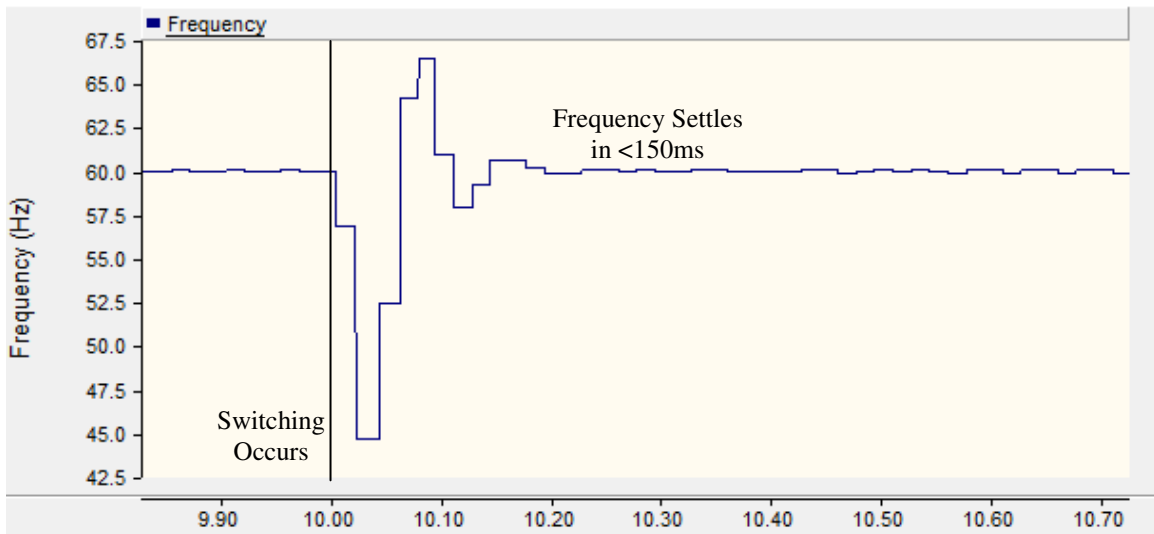


Figure 7.9: Frequency Response during Transition

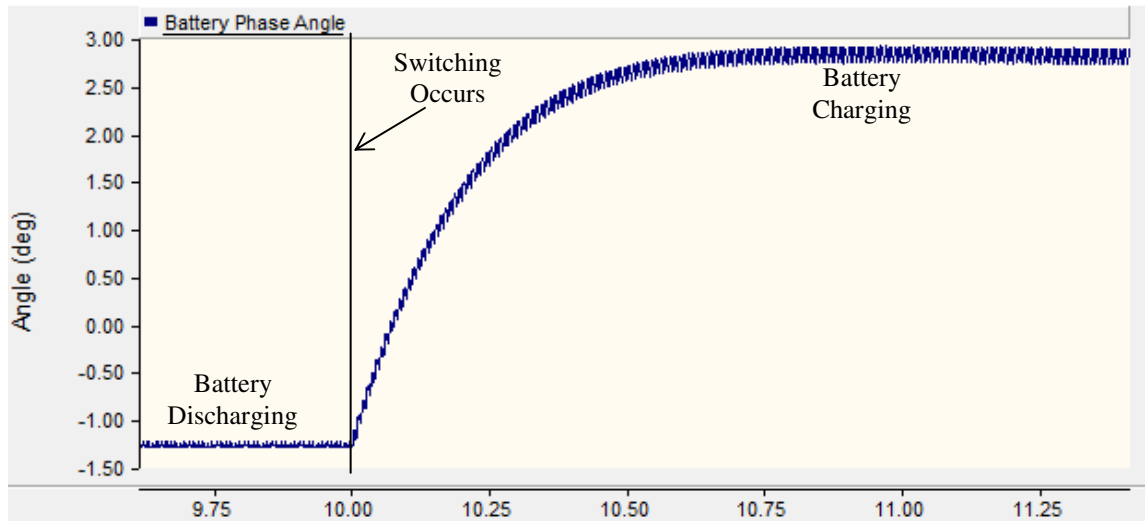


Figure 7.10: Battery Phase Angle (w.r.t. to Load Bus) during Transition

7.3 Scenario 3: Island Mode Operation-Variability of Microsources with a Constant Load

The next scenario to simulate is the impact of varying source output from the PV array and WTG units. In practical application, the output of these units will vary significantly over a relatively short period of time. With the size of the sources and storage properly sized in Chapter 5, the system will still produce enough energy to meet customer need, but the battery inverter will be required to rapidly respond to changes in source output. For this scenario, the irradiance and wind speed are oscillated in a worst case period of 2 seconds and 10 seconds, respectively. While in most cases, the change in resource will occur over a much longer period, this worst case will verify the robustness of the inverter control loop. The full system configuration for this event is given in Table 7.3. During the simulation, the PV array and WTG are varied at their defined intervals. The battery compensates for the variation in output by changing its phase angle with respect to the load. The results of the simulation are given in Figs. 7.11-7.15. It can be seen that

the system remains stable while the sources fluctuate. The battery inverter is able to keep power supply to the load effectively constant as the sources are varying. Since only real power was being varied, only marginal changes in voltage output were observed.

Table 7.3: System Configuration for Scenario 3

	Grid	Battery	PV Arrays	WT Generators	Load
Unit	Offline	Discharging/ Compensation	5 ↔ 9 kW (600-1000 W/m²)	.3 ↔ 4 kW (4-6 m/s)	16 kW 4 kVAR

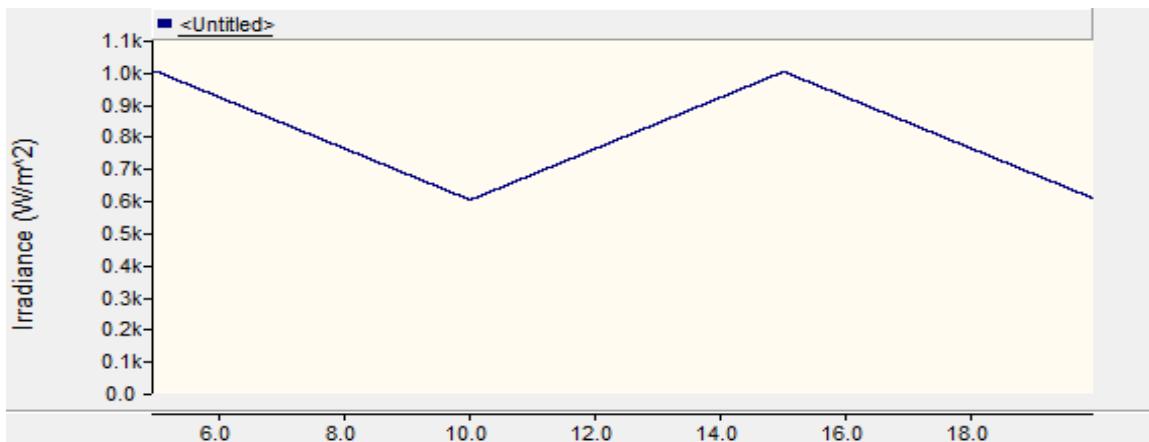


Figure 7.11: Worst Case Solar Irradiance Variation Frequency

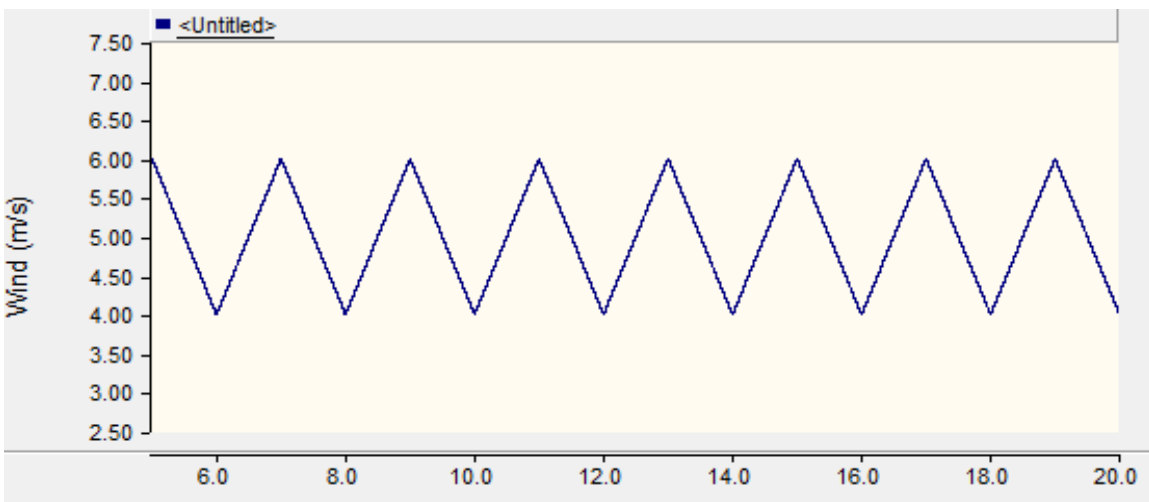


Figure 7.12: Worst Case Wind Speed Variation Frequency

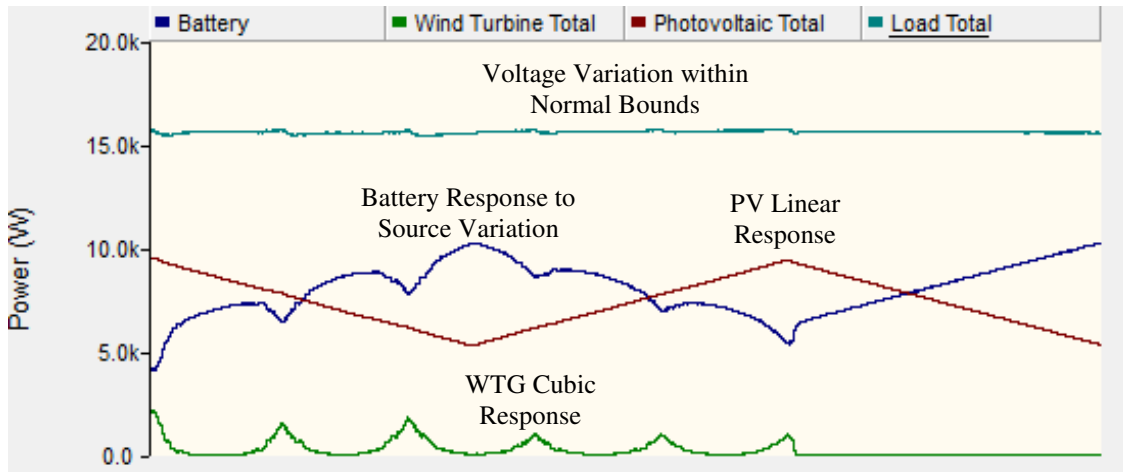


Figure 7.13: Power Output Resulting From Resource Variation

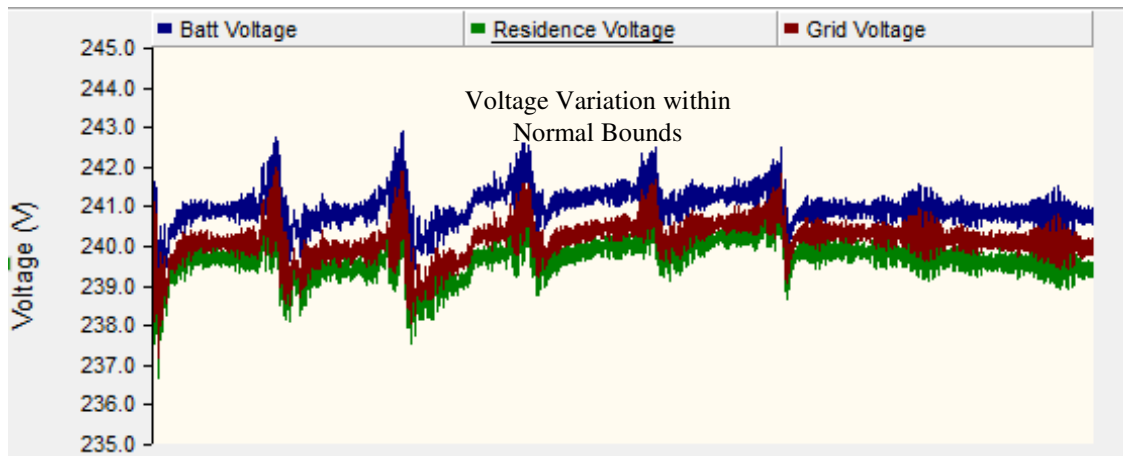


Figure 7.14: Voltage Response to Changing Renewable Sources Variation

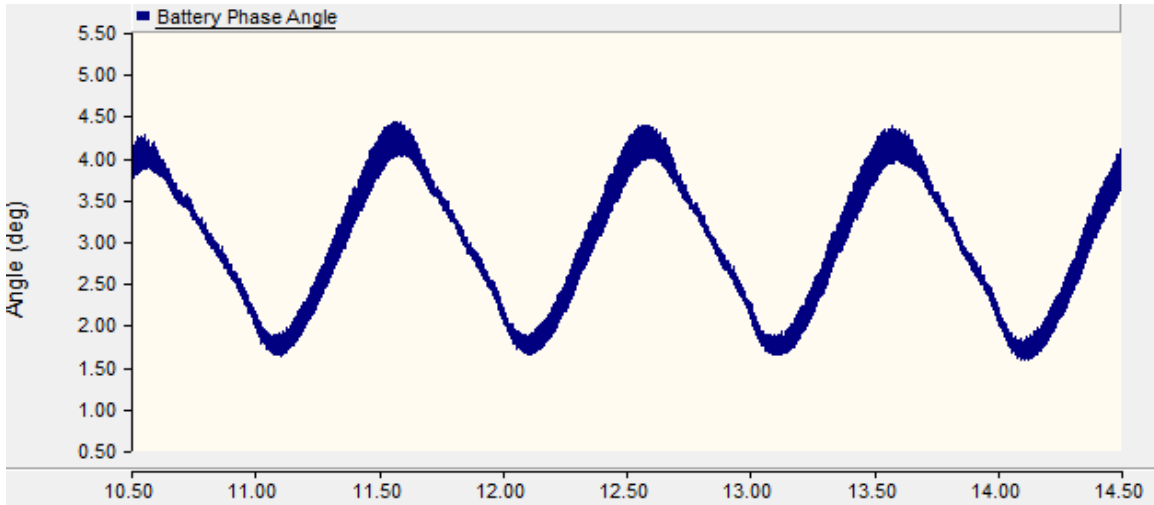


Figure 7.15: Battery Phase Angle Response to Changing Renewable Sources Output

7.4 Scenario 4: Island Mode-Wind Gust Ride Through

Another environmental scenario to analyze is the impact of wind gusts on the system performance. Unlike PV arrays, which have a linear relationship with solar irradiance to power output, wind turbines have a cubic relationship between wind speed and power output. As a result, a doubling of wind speed could result in an eightfold increase in power output. One other factor impacting the cubic relationship is the coefficient of power for the wind turbine which falls significantly as the wind speed increases. As a result, the power output from the wind turbine can be highly variable during a gust event. Since a hurricane produces very strong windgust events, this scenario is a plausible test of the microgrids resiliency to hurricane related events. The full system configuration for this event is given in Table 7.4. The wind gust ramp starts at time equal to 10 seconds. The wind gust performed is a worst case ramp, which would typically be expected to occur over a much longer time period. The PMC is configured such that wind speeds above 20 m/s and below 3 m/s will initiate a trip signal to all WTG breakers. The primary purpose of this scenario is to test the delay in the PMC controller from the time the wind speed exceeds 20 m/s, until the time the unit's trip offline. The results of the simulation are given

in Figures 7.16-7.19. It can be seen that the power output from the WTG unit's increases exponentially at first due to the cubic relationship of wind speed and power, but then quickly flattens at the coefficient of power deteriorates. As a result, the WTG units produce up to a maximum of 35 kW. The battery system compensates for the surge in wind speed by going from a discharge mode of operation to a charging mode very rapidly. When the WTG units finally go offline to protect themselves from over speed, a very large undervoltage condition occurs of about 30% on the system buses, but quickly stabilizes. From this event, it is likely the residential loads may experience a temporary glitch in power supply, but it recovers quickly and normal operation is restored.

Table 7.4: System Configuration for Scenario 4

	Grid	Battery	PV Arrays	WT Generators	Load
Before Event	Offline	Discharge	Offline	4 kW (6 m/s)	9 kW 3 kVAR
After Event	No Change	Charge	No Change	Ramp to 35 kW Ramp to 30 m/s	No Change

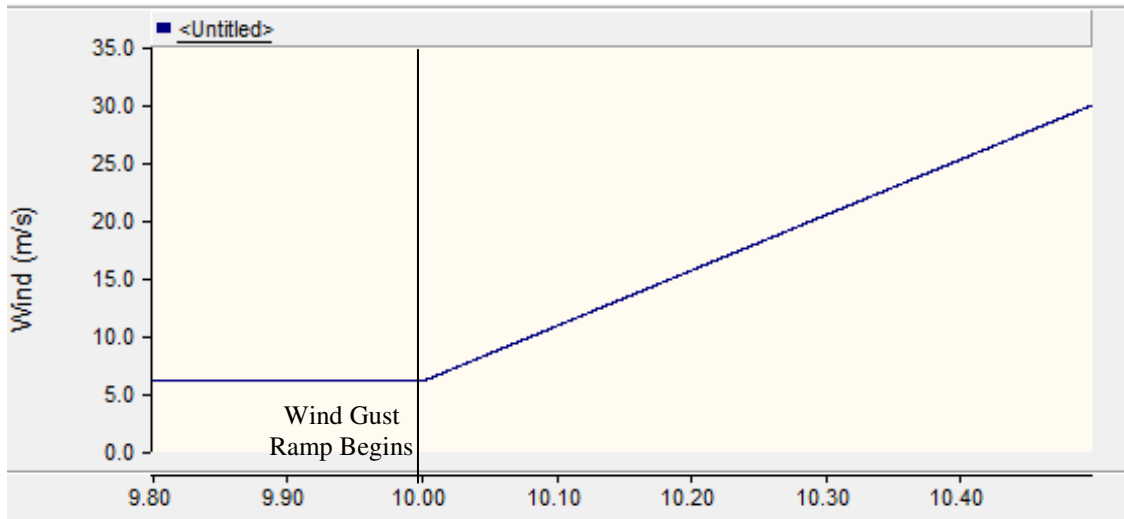


Figure 7.16: Worst Case Wind Gust

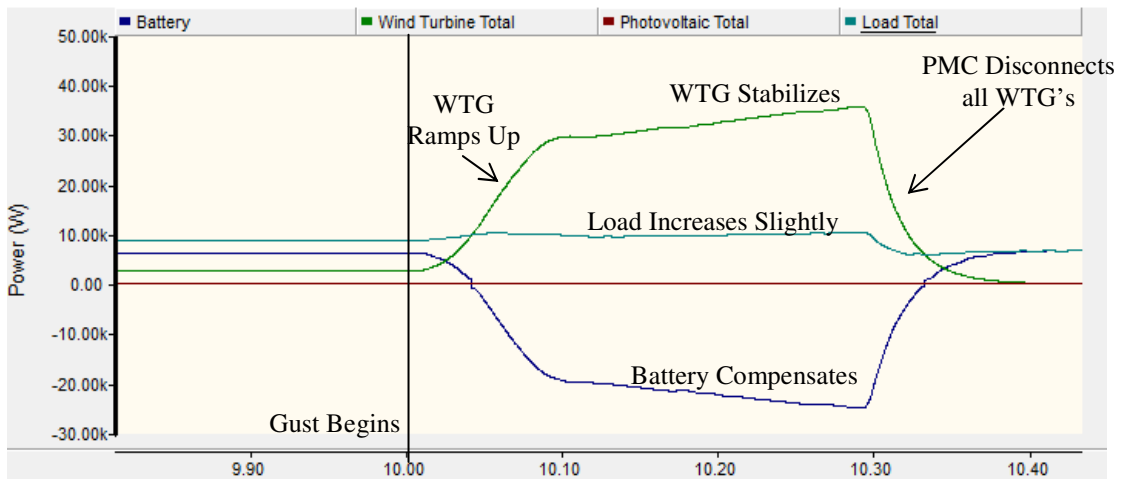


Figure 7.17: Power Output during Wind Gust

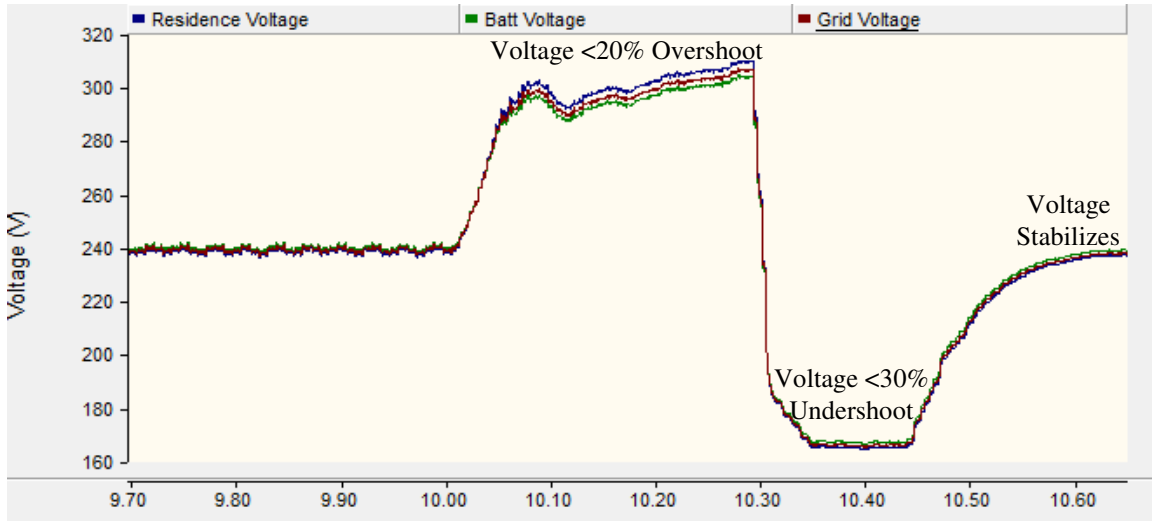


Figure 7.18: Power Output during Wind Gust

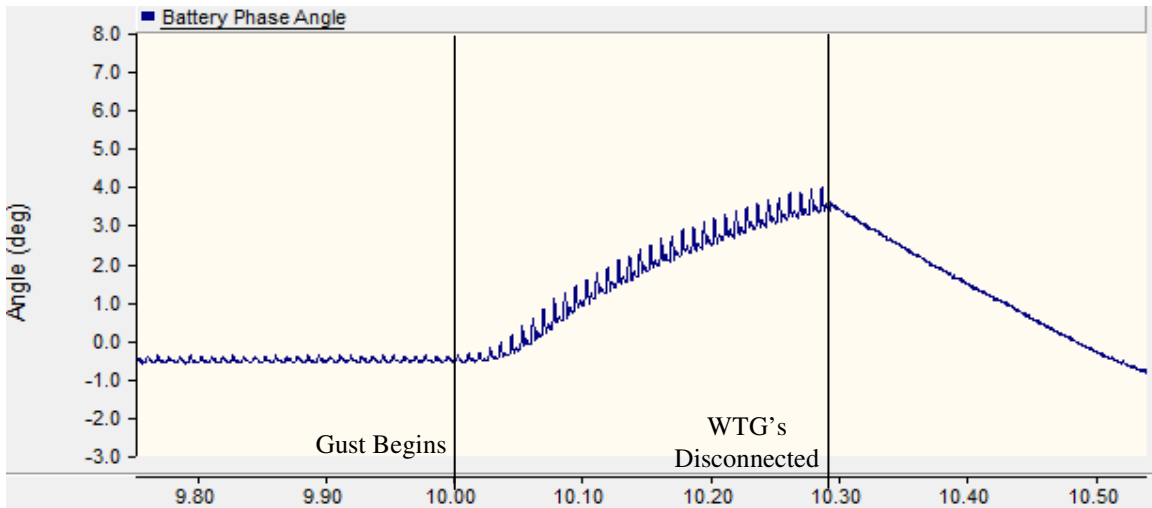


Figure 7.19: Battery Phase Angle Response during Wind Gust

7.5 Scenario 5: Island Mode-PMC Battery Management

For the next two scenarios, the performance of PMC developed in Chapter 5 is analyzed. The PMC serves two primary functions, namely long term source/load balancing and battery charge control. In the following scenario, the load curtailing capability and battery management are investigated. The assumptions are that energy demand is high and renewable generation is

offline. This is consistent with the operation of the microgrid in island mode during or just immediately after a hurricane where the life of the battery is extended as far as possible until the renewable sources can be brought back online. The full system configuration for this event is given in Table 7.5. For this scenario, the battery discharge rate is accelerated to reduce simulation time and test the response rate of the PMC. The discharge rate of the battery begins at time equal 10 seconds. The results of the simulation are given in Figs. 7.20-7.22. It can be seen that the start of curtailment occurs approximately 5 seconds after the battery discharge ramp begins. This is due to the battery SOC crossing the 50% threshold. The curtailment continues when the battery crosses the 25% and 10% threshold as well. The battery phase angle drops while the battery is being discharged, until the load is finally cutoff.

Table 7.5: System Configuration for Scenario 5

	Grid	Battery	PV Arrays	WT Generators	Load
Unit Status	Offline	Rapid Discharge	Offline	Offline	Incrementally Lowered to 0

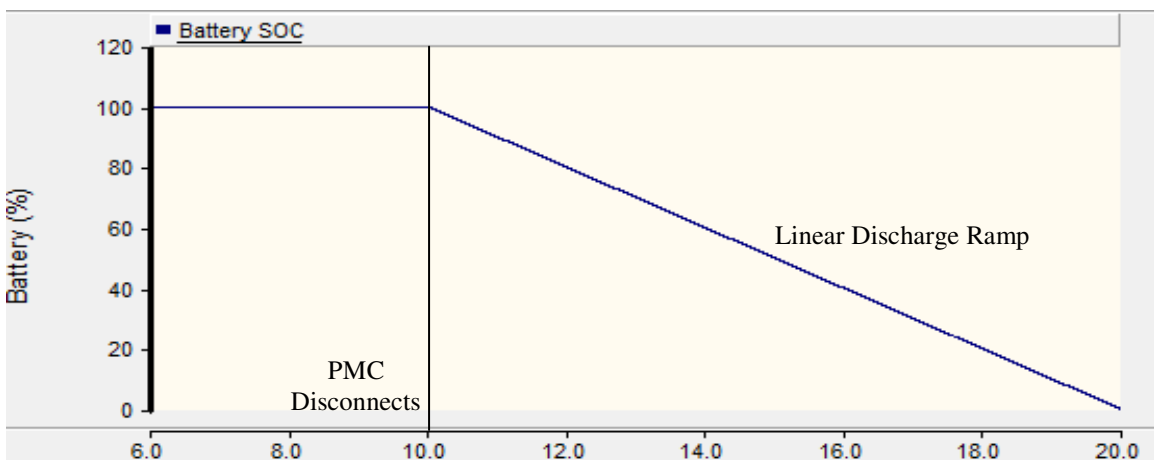


Figure 7.20: Worst Case Battery Discharge Rate

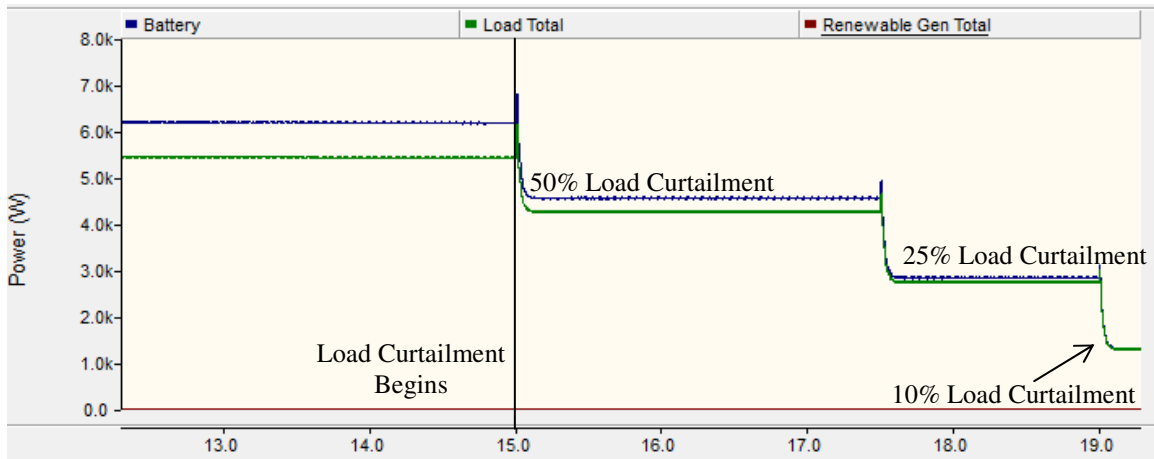


Figure 7.21: PMC Reducing Curtailing Demand from Residences during Battery Discharge

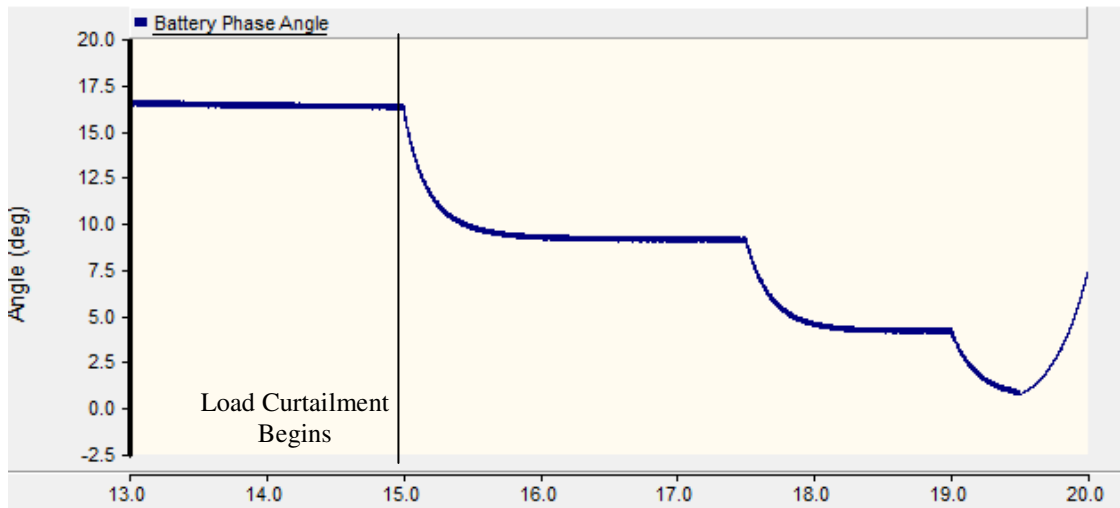


Figure 7.22: Battery Phase Angle Response to Rapid Discharging

7.6 Scenario 6: Island Mode-PMC Source Curtailment

The next verification of the PMC is the curtailment of the generation sources due to low demand and high battery SOC. In this scenario, the PMC will sequentially shutoff generation sources until the demand exceeds generation, so that the battery will begin to discharge from fully charged. Here, the load should be minimally impacted by the switching events taking place. The full system configuration for this event is given in Table 7.6. Starting at time equal to 20

seconds, the units begin switching off with a slight delay in-between to determine the charge level of the battery and the load balance on the system. The assumptions for this scenario are that both the PV array and WTG units are online. To keep the battery from being overcharged, the WTG units are sequentially disconnected from the system. The results of the simulation are given in Figs. 7.23-7.26. It can be seen that the sequential switching of the WTG units off caused the battery charge rate to flatten and balance the demand with the generation from the PV arrays. Although not needed in this scenario, if further curtailment were required, the PV arrays would then be shutoff sequentially as well. The PMC was able to maintain charge on the battery and shutdown unnecessary excess generation from the renewable sources.

Table 7.6: System Configuration for Scenario 6

	Grid	Battery	PV Arrays	WT Generators	Load
Unit Status	Offline	Charging	9.6 kW (1000 W/m²)	7 kW → 0 kW (7 m/s)	9 kW 3 kVAR

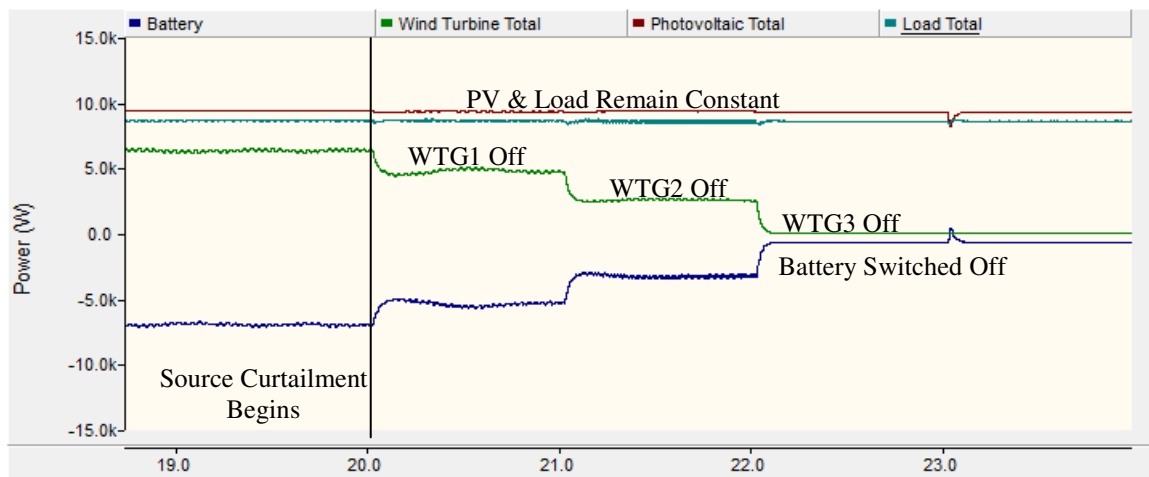


Figure 7.23: PMC Source Curtailment Due to High Battery SOC

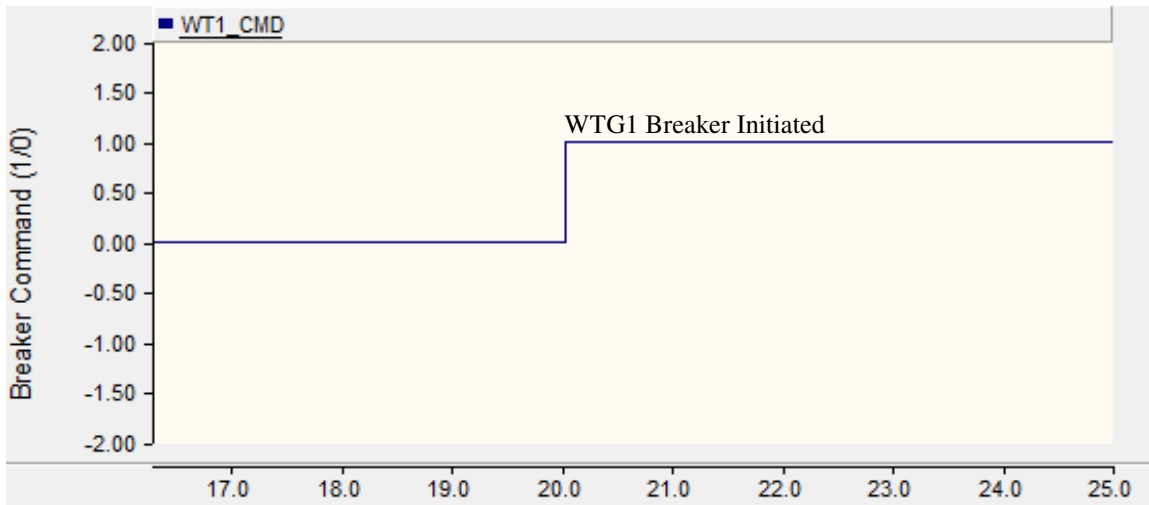


Figure 7.24: WTG 1 Breaker Initialized by PMC

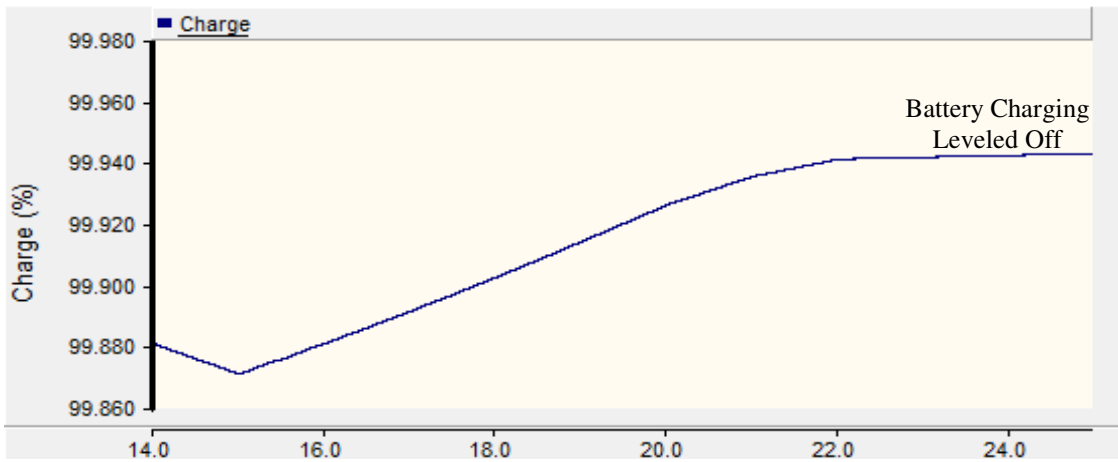


Figure 7.25: Battery SOC Change during Curtailment

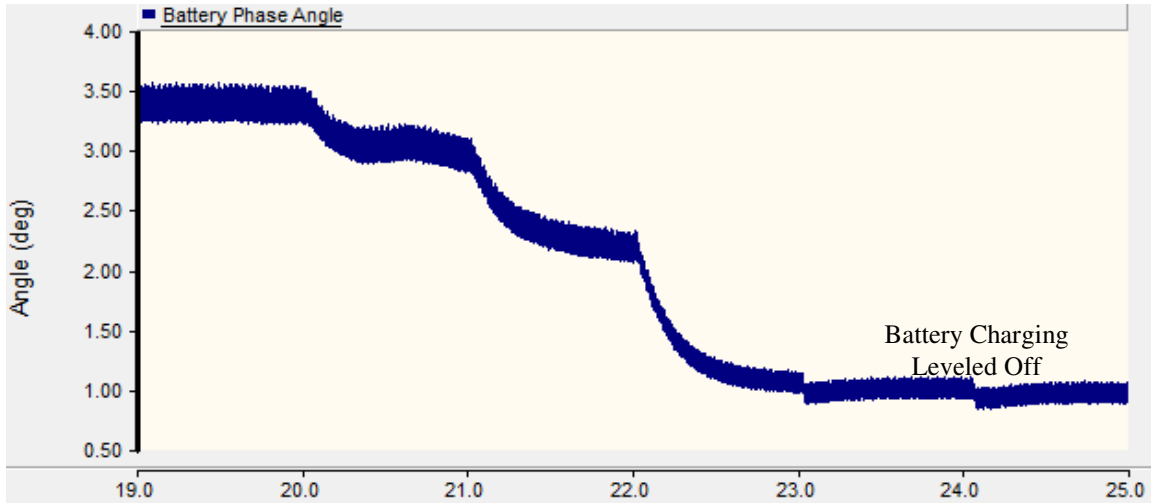


Figure 7.26: Battery SOC Change during Curtailment

7.7 Scenario 7: Island Mode-Wind Turbine Fault Isolation

The next scenario to be investigated is impacted of a fault on the system. The microgrid is designed such that any fault, with exception of the central battery array, can be isolated and allow for continued operation of the remaining system. In this scenario, the terminals of the inverter for WTG1 are faulted to ground, requiring the isolation of the WTG from the rest of microgrid. The full system configuration for this event is given in Table 7.7. The scenario begins at time equal to 10 seconds when the fault occurs. The WTG1 unit and the battery array supply the fault current until the protection initiates and trips the WTG1 breaker. Although not in the scope of this effort, it is assume that all protection devices are tuned for 3 cycle (based of 60 Hz) clearing time. The results of the simulation are given in Figs. 7.27-7.30. It can be seen that a surge in battery and WTG power occurred while the fault was on the line. Once the fault has been isolated, the system returned to normal operating parameters, with one fewer WTG in service. The system voltages drooped momentarily while the fault was active but quickly

stabilized. Since the voltage drop was less than 20% for 3 cycles, most residential loads are able to ride through this momentarily glitch and not experience a visible loss in power.

Table 7.7: System Configuration for Scenario 7

	Grid	Battery	PV Arrays	WT Generators	Load
Before Event	Offline	Discharge	9.6 kW (1000 W/m²)	9 kW (8 m/s)	6 kW 1 kVAR
After Event	Offline	Discharge	No Change	Fault on WTG1	No Change

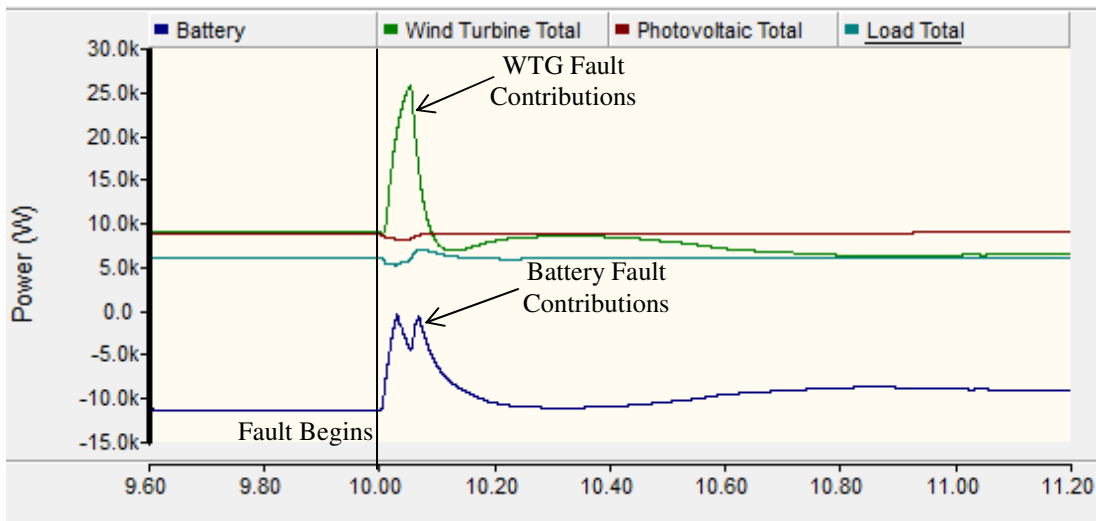


Figure 7.27: Battery and WT Contribution to Fault Event

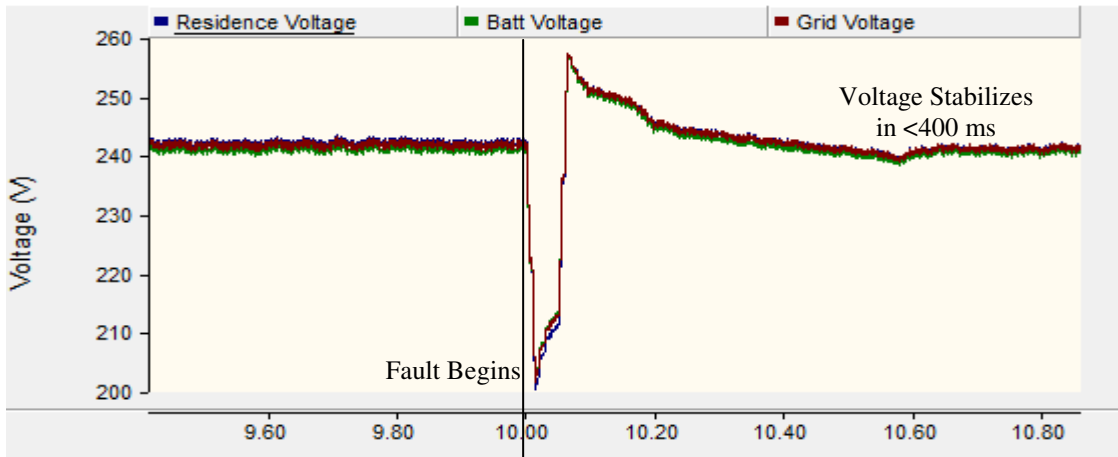


Figure 7.28: System Voltage Response to Fault Event

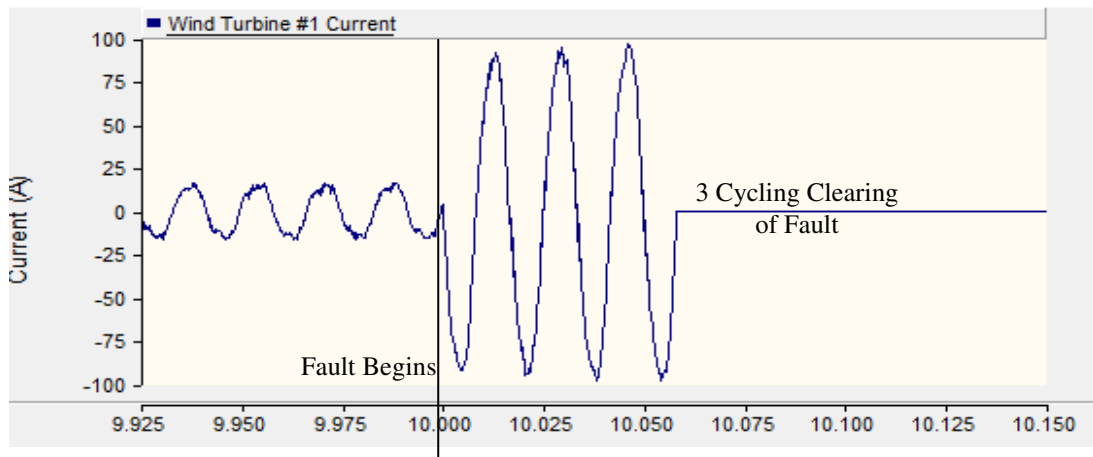


Figure 7.29: WTG Inverter Fault Current Contribution and Isolation (after 3 cycles)

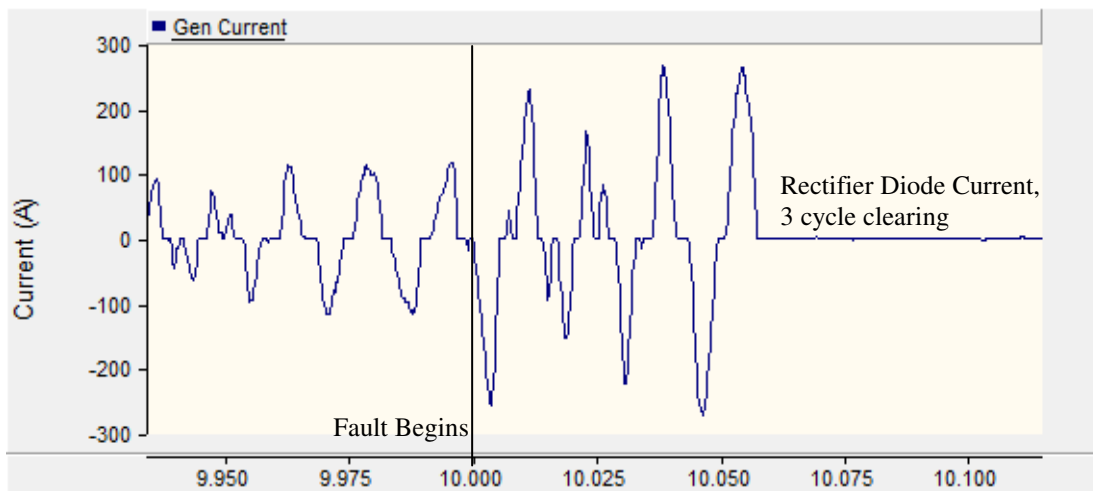


Figure 7.30: WTG PM Generator Fault Current Contribution and Isolation (after 3 cycles)

7.8 Scenario 8: Microgrid Resynchronization with the Grid

With the previous scenarios performed, the last event that needs to be looked at is the interconnection of the microgrid to the macrogrid after an extended outage period. It is assumed for this scenario that in order to prevent a large swing in power generation, only the battery array would be online prior to resynchronization. All other sources are intentionally shut offline. It is possible, but not shown here, that the WTG unit's and PV arrays can come online after grid connection is established and either recharge the battery array or back feed power to the grid. The full system configuration for this event is given in Table 7.8. The PMC will protect from out of phase connection to the grid by not synchronizing until both frequency, voltage, and phase angle are within margin of the grid parameters. With the other sources offline, this is accomplished by varying the output from the battery inverter. Once connected, the battery array will switch back to grid connected mode of operation as discussed in Chapter 5 and reduce its power output to zero. The results of the simulation are given in Figs. 7.31-7.33. It can be seen that with just the battery array online and no other sources, the resynchronization is very direct. The power output and bus voltages experience very negligible impact to the interconnection and the switching offline of the battery array. The addition of metal-oxide varistors (MOVs), helped to reduce the voltage spike experienced by the battery inverter and allow for a safe shutdown.

Table 7.8: System Configuration for Scenario 8

	Grid	Battery	PV Arrays	WT Generators	Load
Before Event	Offline	Discharge	Offline	Offline	9 kW 3 kVAR
After Event	Online	Offline	No Change	No Change	No Change

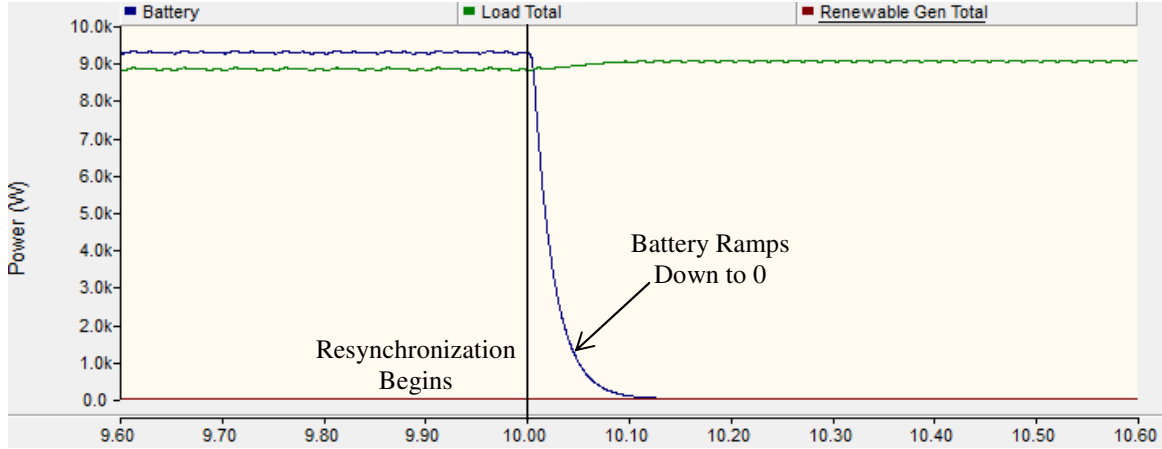


Figure 7.31: Change in Power Output during Resynchronization

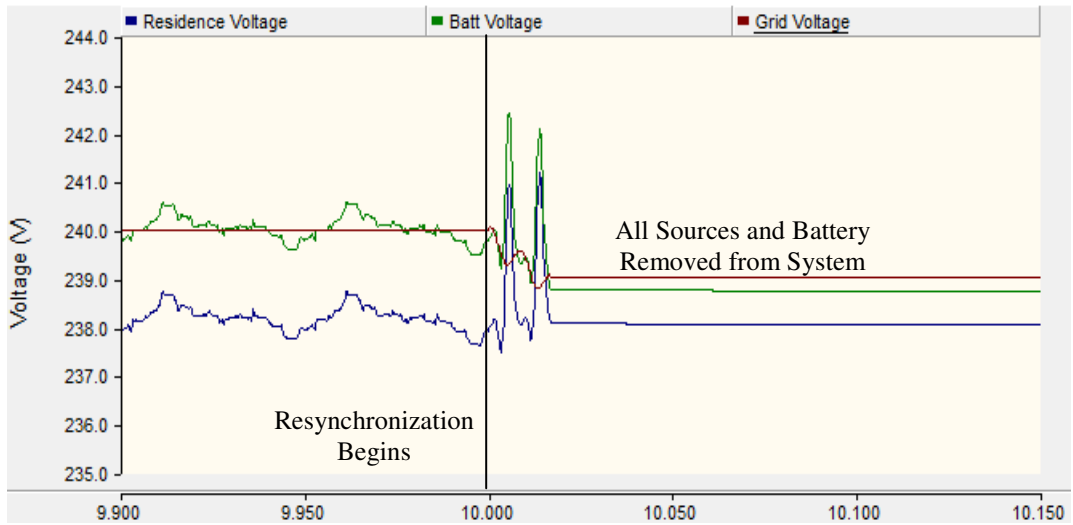


Figure 7.32: System Voltage Change during Resynchronization

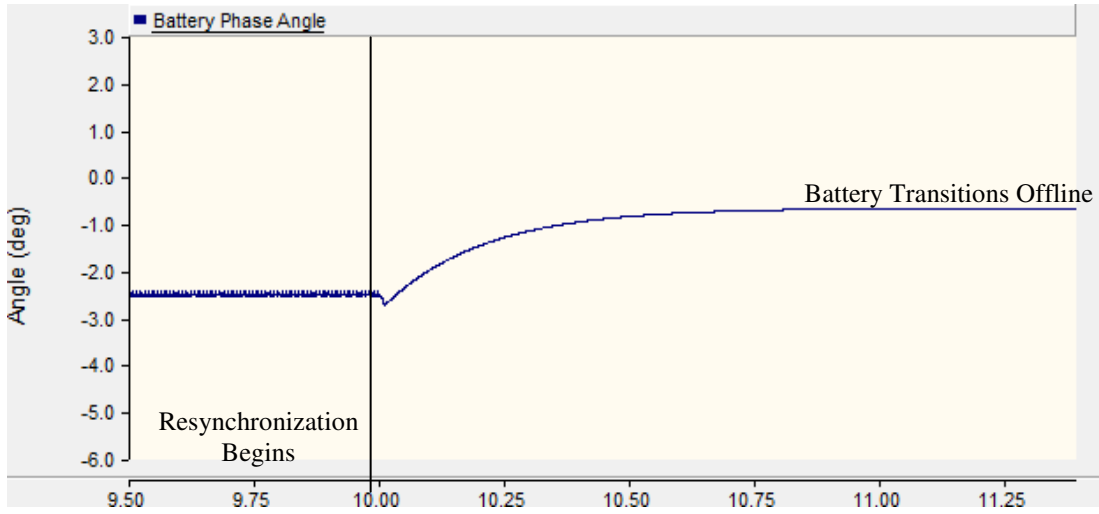


Figure 7.33: Battery Phase Angle Change during Resynchronization

Chapter 8

Conclusions and Future Work

8.1 Research Summary

This thesis researched the design and operation of a residential microgrid for providing a continuous source of power after a major natural disaster. The example natural disaster referenced in this work was a hurricane striking South Florida. The system modeled in PSCAD contained transient models of WTG's, PV arrays, and a central battery array interconnected to an existing distribution system network. The battery array served to act as a voltage/phase angle reference for the renewable sources when operating in island mode. A central power management controller (PMC) was also developed to manage these sources to ensure generation and demand stay balanced along with the SOC of the battery array. Finally, phase-droop control was implemented as a way to rapidly balance power changes due to the low inertia of the inverter based generation. This complete system was simulated for various static and dynamic scenarios where generation, load, and environmental resource were varied. The system performed as expected with all switching related transient events settling in under 500 milliseconds and the battery able to rapidly charge or discharge depending on the system conditions. While frequency and voltage occasionally exceeded the boundaries of a typical grid system, they were acceptable on the microgrid due to its faster ability to respond to transients. Energy models were also developed in MATLAB to ensure that the energy generated by the sources met the demand of the customer throughout the day, with sufficient margin built-in. The energy model was also used to determine the size of the energy storage array such that it could

operate for a sustained period of operation without generation from the renewable sources.

Overall, this thesis provided the basis for research into small microgrids to be used for ensuring power delivery after a natural disaster. Future work can be built off this research to look at further transient scenarios and more in-depth implementation of this proposed microgrid.

8.2 Recommended Future Work

The model developed provided the basis for studying residential microgrid scenarios. There are several areas of study, which can be looked at to expand off this research. Proposed future research involves looking at the communications network, expanded top level control algorithm, and economic analysis.

8.2.1 Communications Future Work

The communications of the microgrid is important for tracking signal measurements and determining what parameters need adjustment based off varying system conditions. Future research in this area should look at the coordination and latency of communication from various sources to a central controller location. This is particularly needed for geographically small microgrids with numerous micro-generation resources. To this effect, future study into residential microgrids should address the design of the communications infrastructure. Given the near instantaneous response of inverter based generation to changes in source or load, the ability to communicate this information to the controllers as quickly as possible is critical for system stability.

8.2.2 Controller Future Work

This thesis provided the basis for centralized power management of a microgrid. Future work on this model should involve expanding the capability of the PMC, particularly in grid-connected mode of operation. There is great potential to expand the PMC to take a more active role in providing localized real and reactive power supply into the macrogrid to help prevent outages before they occur. A further study into the coordination of the top level controller and the integrated communication system is also useful in determining the timing coordination between the central controller and local controls of each inverter and protection device.

Further expanding the fidelity of the inverter controller and harmonic filter are also recommended. The inverter model in this research provides a low fidelity model, with several idealizations made. Revising the inverter control model will produce higher resolution transient results. The design details should include bandwidth constraints, as well as a higher level filter design.

8.2.3 Future Work on Economic Analysis

An economic evaluation for implementing the proposed microgrid is outside the scope of this thesis, but remains a very important topic. Comparing the relative cost of the required hardware for the microgrid and comparing it against the cost of a classical backup system (i.e. gas or diesel generators) will help determine the financial viability of the project. The proposed microgrid in this thesis has the inherent financial advantage of being a fuel-free resource, but this must be weighed against the capital cost and expected maintenance of the hardware required. In addition, the life expectancy of the hardware is also important to evaluating the value of pursuing such an

implementation. A full life-cycle cost model will be needed to understand the financial benefits or pitfalls of such a system. In addition, looking at dual uses for the microgrid such as peak shaving or demand reduction should also be evaluated when assessing the financial viability.

8.2.4 Proposed Pilot Implementation

Implementing the microgrid in an existing residential distribution is relatively easy with respect to hardware that is needed. All of the hardware referenced in this research is commercially available at the time of writing the thesis. The ability to procure some or all of the hardware for physical implementation is very practical. Two potential areas of difficulty are with respect to the top level controls, which requires development, and utility imposed restrictions on distributed generation. Currently the ability to implement a microgrid in a residential community is difficult to impossible in some areas due to precautions taken by the local electric utility to ensure the safety and reliability of electric power to their customers. Likewise, the controller for such a microgrid requires further modeling and development before it is ready to be implemented to scale. For future work on implementing the microgrid, it is important to engage a local utility and encourage their participation into a pilot program to test the viability of the microgrid. If a utility sees a financial advantage in such a system, for example reduced man power needs for line crews after an outage, may encourage their support. The physical implementation of the proposed microgrid could also be applied on an existing microgrid at a research university. Several options are available when this system is ready for implementation.

References

- [1] E. S. Blake, C.W. Landsea, and E.J. Gibney. The Deadliest, Costliest, and Most Intense United States Tropical Cyclones from 1851 to 2010. NOAA Technical Memorandum NWS NHC-6. National Weather Service. Aug 2011.
- [2] P. Hoffman, W. Bryan, and A. Lippert. Comparing the Impacts of the 2005 and 2008 Hurricanes on U.S. Energy Infrastructure. U.S. Department of Energy. Feb 2009.
- [3] J. Buyer. Technology Demonstration of a Prototype Low Carbon Monoxide Emission Portable Generator. Consumer Product Safety Commission. U.S. Page(s): 4. Apr 2012.
- [4] P. Asmus, A. Cornelius, and C. Wheelock. Microgrids Islanded Power Grids and Distributed Generation for Community, Commercial, and Institutional Applications. Pikes Research Group. 4Q'09.
- [5] R. Lasseter, A. Akhil, C. Marnay, J. Stephens, J. Dagle, R. Guttromson, A.S. Meliopoulos, R. Yinger, and J. Eto. The CERTS MicroGrid Concept. Apr 2002.
- [6] E. Strickland. A Microgrid That Wouldn't Quit. <http://spectrum.ieee.org/energy/the-smarter-grid/a-microgrid-that-wouldnt-quit/0>. Oct 2011.
- [7] Smart Meters. Hurricane Irene Shines Spotlight on Microgrids. ["http://www.smartmeters.com/the-news/2581-hurricane-irene-shines-spotlight-on-microgrids.html"](http://www.smartmeters.com/the-news/2581-hurricane-irene-shines-spotlight-on-microgrids.html)
- [8] S.I. Erwin. High-Tech Weapon Makers Set Sights on 'Smart Microgrid' Market. <http://www.nationaldefensemagazine.org/archive/2011/July/Pages/High-TechWeaponMakersSetSightson%E2%80%98SmartMicrogrid%E2%80%99Market.aspx>. Jul 2011.
- [9] H. Lammers. Microgrids: So Much More than Backup Energy. NREL Publication. http://www.nrel.gov/news/features/feature_detail.cfm/feature_id=1980. Aug 2012.
- [10] Y. Yuan, L. Wu, W. Song, and Z. Jiang. Collaborative Control of Microgrid for Emergency Response and Disaster Relief. International Conference on Sustainable Power Generation and Supply, 2009. SUPERGEN '09. Apr 2009.
- [11] Z. Li, Y. Yuan, and F. Li. Evaluating the Reliability of Islanded Microgrid in An Emergency Mode. UPEC 2010. Sep 2010.
- [12] D. Cox. Microgrid Infrastructure Modeling for Residential Microgrids. IEEE Power Engineering Society General Meeting, 2007. IEEE. Jul 2007.

- [13] P. Asmus. Microgrids: Compelling Value Proposition, But Lack of Clear Policy Support. Pike Research. <http://www.pikeresearch.com/blog/articles/microgrids-compelling-value-proposition-but-lack-of-clear-policy-support>. Jan 2011.
- [14] How do hurricanes form? <http://spaceplace.nasa.gov/hurricanes/>.
- [15] Southeast Regional Climate Center. MIAMI WSCMO AIRPORT, FLORIDA
<http://www.sercc.com/cgi-bin/sercc/cliMAIN.pl?f15663>.
- [16] Florida 80-Meter Wind Map and Wind Resource Potential. Wind Powering America.
http://www.windpoweringamerica.gov/wind_resource_maps.asp?stateab=fl.
- [17] FSU-COAPS. Florida's Missing Winds -- New Evidence Supports the Viability of Harnessing Offshore Wind Energy in Florida.
<http://www.ieses.fsu.edu/Archives/Florida-s-Missing-Winds-New-Evidence-Supports-the-Viability-of-Harnessing-Offshore-Wind-Energy-in-Florida>.
- [18] South Florida Wind Resource Time of Day. <http://turfgrass.com/wind/index.html>.
- [19] M.L. Ray, A.L. Rogers, and J.G. McGowan. Analysis of Wind Shear Models and Trends in Different Terrains. Univ. of Massachusetts. Renewable Energy Research Laboratory. 2006.
- [20] Ordinance No. 2012. Land Development Regulations. Brevard County, Florida.
http://ww3.brevardcounty.us/zoning/documents/TowerOrdinanceForWeb_02_12.pdf.
Feb 2012
- [21] Does the "Sunshine" State have a sufficient solar resource to support solar energy applications? Florida Solar Energy Center.
[.http://www.fsec.ucf.edu/en/media/enews/2007/2007-04_Sunshine_state.htm](http://www.fsec.ucf.edu/en/media/enews/2007/2007-04_Sunshine_state.htm). Mar. 2006.
- [22] National Solar Radiation Database. September 2005 average for West Palm Beach, Florida.
http://rredc.nrel.gov/solar/old_data/nsrdb/1991-2005/.
- [23] O. Tremblay, L. Dessaint, and A.I. Dekkiche. A Generic Battery Model for the Dynamic Simulation of Hybrid Electric Vehicles. IEEE Vehicle and Propulsion Conference 2007. Sep 2007.
- [24] H. Zhag and M.Y. Chow. Comprehensive Dynamic Battery modeling for PHEV Applications. IEEE PES General Meeting 2010. Jul 2010.
- [25] F.M. Gonzalez-Longatt. Circuit Based Battery Models: A Review. 2nd Latin American Congress of Electrical Engineering Students. 2006
- [26] Technical Manual for Sun Xtender Batteries. Concord Battery Corporation. Document No. 6-0100. Rev D. Jul 2011.

- [27] F.M. Gonzalez-Longatt. Model of Photovoltaic Module in Matlab. 2nd Latin American Congress of Electrical, Electronics, and Computer Engineering Students. 2005
- [28] 220 Watt Photovoltaic Module BP 3220. Datasheet. BP Solar. 2008
- [29] M.G. Simões, B. Palle, S. Chakraborty, and C. Uriarte. Electrical Model Development and Validation for Distributed Resources. National Renewable Energy Laboratory. Document No. NREL/SR-581-41109. Apr 2007.
- [30] M. Azab. Improved Circuit Model of Photovoltaic Array. International Journal of Electrical Power and Energy Systems Engineering. Mar. 2009
- [31] DC Loading of PV Powered Inverters. Advanced Energy. page 2, 2012
- [32] M. Yin, G. Li, M. Zhou, and C. Zhao. Modeling of the Wind Turbine with a Permanent Magnet Synchronous Generator for Integration. IEEE PES General Meeting 2007. Jun 2007.
- [33] Hummer Wind Power Active Yaw Control Small Wind Turbine Technical Specifications. Datasheet. Hummer Wind Power, LLC. 2009.
- [34] K. Grogg. Harvesting the Wind: The Physics of Wind Turbines. Carleton College. Physics and Astronomy Department. 2005.
- [35] D.S. Parker, J.P. Dunlop, J.R. Sherwin, S.F. Barkaszi Jr., M.P. Anello, S. Durand, D. Metzger, and J.K. Sonne. Florida Solar Energy Center.
<http://www.fsec.ucf.edu/en/publications/html/FSEC-CR-1044-98/index.htm>
- [36] Y. Xue, J. Deng, and S. Ma. Power Flow Control of a Distributed Generation Unit in Microgrid. IEEE Power Electronics and Motion Control Conference, 2009. IPEMC '09 6th International. 2009
- [37] C. Buttay. Switches Domain Map.
http://upload.wikimedia.org/wikipedia/commons/2/24/Switches_domain.svg.
- [38] R.W. Erickson and D. Maksimovic. Fundamentals of Power Electronics. 2nd Edition. Springer Science+Business Media, Inc. page(s): 282-283. 2001.
- [39] H. Cha and T. Vu. Comparative Analysis of Low-pass Output Filter for Single-phase Grid-connected Photovoltaic Inverter. APEC '10. Page(s) 2-3. 2010.
- [40] J. Doucet, D. Eggleston, and J. Shaw. DC/AC Pure Sine Wave Inverter. MQP Terms ABC 20062007. Worcester Polytechnic Institute. 2007.

- [41] R. Majumder, A. Ghosh, G. Ledwich, and F. Zare. Angle Droop versus Frequency Droop in a Voltage Source Converter Based Autonomous Microgrid. Power Engineering Society General Meeting, 2009. Annual IEEE. Jul 2009.
- [42] Building Wire Copper. General Cable. Building Wire & Cable for Commercial and Residential Applications. <http://catalog.proemags.com/publication/1cfe0a62#/1cfe0a62/1>. Jan 2012.
- [43] Voltage Tolerance Boundary. Pacific Gas & Electric. http://www.pge.com/includes/docs/pdfs/mybusiness/customerservice/energystatus/powerquality/voltage_tolerance.pdf. Jan 1999.